PROCEEDINGS OF SCIENCE

The History of High Energy Experiments – from UHURU to IXPE – (a Personal View)

Franco Giovannelli*

INAF - Istituto di Astrofisica e Planetologia Spaziali,
ARTOV - Via Fosso del Cavaliere 100, 00133 Roma, Italy

E-mail: franco.giovannelli@iaps.inaf.it

In this review I will give an overview of astrophysics missions that used rockets, stratospheric balloons and satellites. I will give particular emphasis to those missions that contributed to my scientific results.
Of course I do not claim to be exhaustive both for reasons of space and especially my limited knowledge. However, from this overview of results from multi-frequency measurements carried out by space and ground experiments, my contribution to the knowledge of high-energy cosmic sources can be deduced. I would like also to highlight the use of WISDOM in PHYSICS, in addition, obviously, to its knowledge.
The hope is to be useful to young people so that they learn a way of doing research that is apparently anomalous, but effective.

Content:

Frontier Research in Astrophysics – IV (FRAPWS2024)
9-14 September 2024
Mondello, Palermo, Italy

*Speaker

© Copyright owned by the author(s) under the terms of the Creative Commons Attribution-NonCommercial-NoDerivatives 4.0 International License (CC BY-NC-ND 4.0) All rights for text and data mining, AI training, and similar technologies for commercial purposes, are reserved. ISSN 1824-8039 . Published by SISSA Medialab.

PoS(FRAPWS2024)035

1. Introduction

The astrophysics experiments carried out on board rockets contributed substantially to the advancement of knowledge of cosmic sources: for everyone it is necessary to remember the experiment by Giacconi et al. [1] which detected for the first time X-ray emission from an extrasolar source (Sco X-1) which gave rise to the search for high energy sources through the preparation of experiments on board satellites with instruments sensitive to the UV. This is the period around the beginning of the 1970s which can be defined as the advent of the space age. From then on, a myriad of experiments sensitive to the bands of the electromagnetic spectrum not accessible from the ground due to the atmospheric barrier became the source of an immense quantity of data which in the space of just fifty years far exceeded the amount of data acquired until then with ground-based optical telescopes.

Figure 1 shows schematically the amount of data acquired along the electromagnetic spectrum versus time (updated from [2], after [3]).

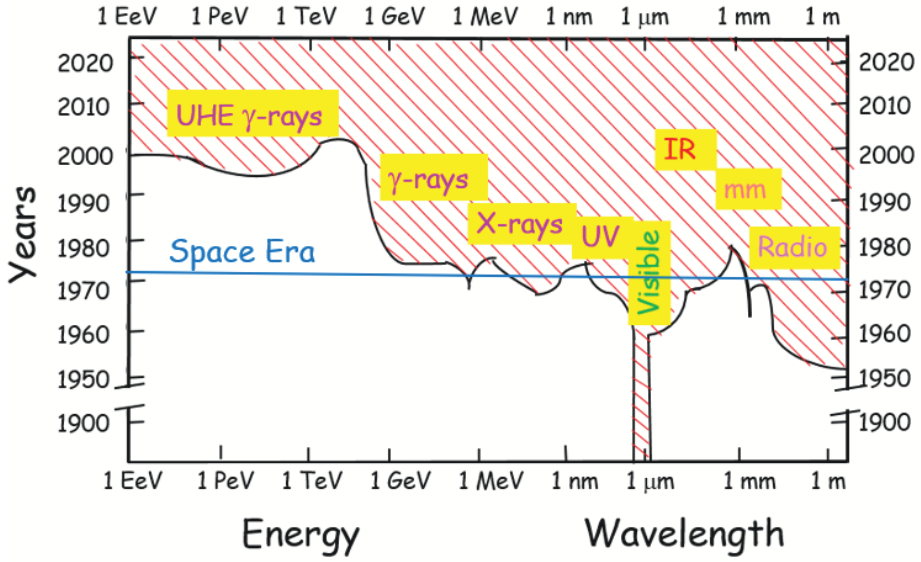

Figure 1: Sketch of the multifrequency data acquired after the beginning of the "Space Era" (updated from [2], after [3]).

It is therefore quite evident that the claim to illustrate the history of space experiments in a complete form can only be satisfied through an encyclopedia. And this is not our case. However, among the various attempts to expose the history of space experiments, the paper *A Chronological History of X-Ray Astronomy Missions* by Santangelo, Madonia & Piraino [4] deserves to be taken into consideration. I will make an excursion into this history privileging those experiments that directly or indirectly have marketed my scientific career.

1.1 Historical Introduction

The origin of the concept of neutron stars can be found in a publication of Landau [5] in which he arrived at the notion of a collapsed star with the density of a nucleus (really a "nucleus star") and demonstrated – independent of Chandrasekhar – that there is an upper mass limit for dense

PoS(FRAPWS2024)035

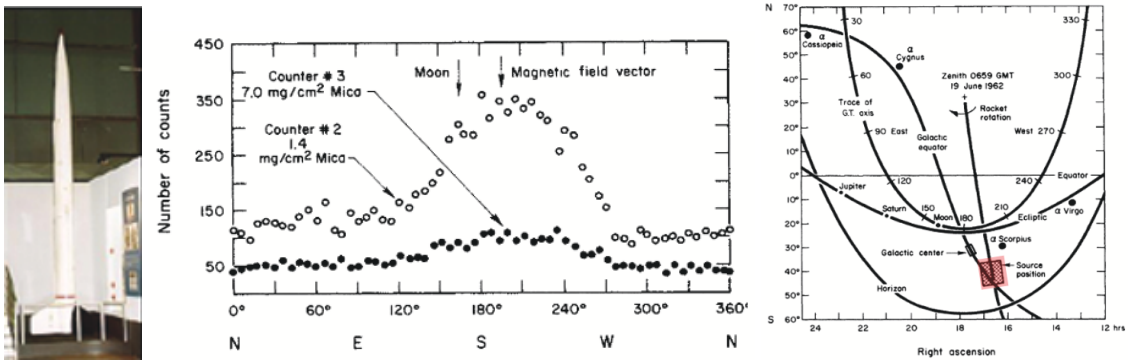

Figure 2: Left panel: Aerobee rocket (credit: USAF Museum). Central panel: Number of counts versus azimuth angle. Right panel: Position of the source (Sco X-1) (adopted from [1]).

stellar objects of about 1.5 $M_{\odot}$. Even more important short abstract of their talk presented at the December 1933 meeting of the American Physical Society, Baade & Zwicky [6] first suggested that the supernova was the result of the transition from a normal star to a neutron star. The essential point [7,8] being that the energy release in such a process is comparable to the change in gravitational potential energy of a star, which collapses from its "normal" size of $\sim 10^6$ Km down to the size of a neutron star of $\sim$ 10 Km.

As underlined in the summary of Brecher's talk *Origin of Neutron Stars* [9], the abstract by Baade & Zwicky [6] probably contains the highest density of new, important (and correct) ideas in high energy astrophysics ever published in a single paper.

The discovery of the first X-ray source (Sco X-1) [1] accelerated the studies on neutron stars, until that Zel'dovich, Ya, B. & Guseinov, O.Kh. [10] and Guseinov & Zel'dovich [11] suggested the presence of an unseen massive companion in a binary system.

In the meantime, experiments of various kinds were being developed to be carried on rockets, exploiting the experience gained by von Braun during the Second World War on propulsion. NASA undertook the development of a series of rockets called AEROBEE. The Aerobee name, given by Van Allen, is a contraction of AEROjet and BumbleBEE, the latter referring to the early rocket family of Van Allen's. Aerojet had supplied propulsion for both the WAC-Corporal and the Bumblebee according to an Aerojet 1948 brochure. The largest of the Aerobee family is the Aerobee 350 (i.e. 100 lb payload to 350 miles) sponsored by NASA. It is 50 ft long, 22 inches diameter and over 3 tons gross weight. Most Aerobees included a payload recovery system employing a parachute and using telemetry to release the payload and the parachute. Most Aerobees were launched from towers over 100 ft high designed by Aerojet's AETRON Division. The towers allow for a nearly vertical launch. Figure 2 (left panel) shows an Aerobee rocket.

The experiment – equipped with proportional counters in the energy range 2-10 keV – that gave birth to X-ray astronomy was launched aboard an Aerobee rocket from the White Sands Missile Range, New Mexico, at 23:59 MST on June 18, 1962. The moon was one day past full and was in the sky about 20' east of south and 35' above the horizon. The rocket reached a maximum altitude of 225 km and was above 80 km for a total of 350 seconds [1]. The authors believed that the data can best be explained by identifying the bulk of the radiation as soft X-rays from sources outside the solar system. Synchrotron radiation by cosmic electrons is a possible mechanism for

PoS(FRAPWS2024)035

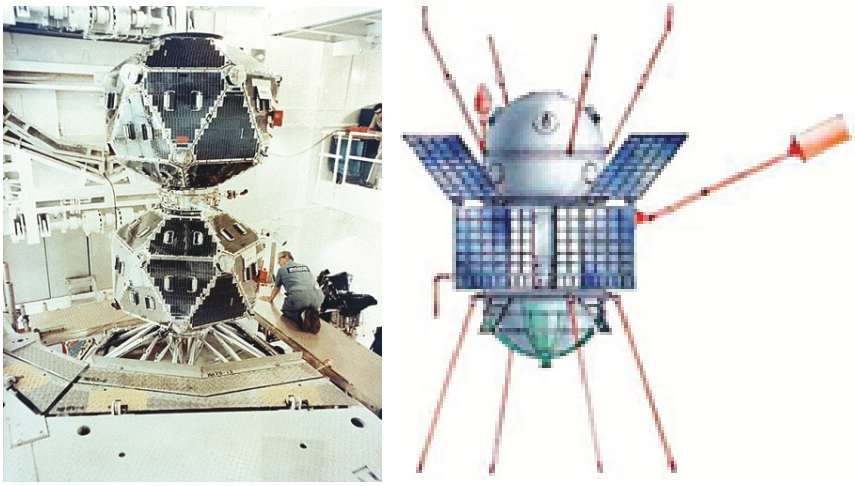

Figure 3: Left panel: Vela 5A/B in its cleanroom. The two satellites, A and B, were separated after launch (Credit: NASA-EPDC). Right panel: Cosmos 461 (Credit: Soviet Space Program).

the production of these X-rays. Figure 2 (central panel) shows the number of counts versus azimuth angle. The numbers represent counts accumulated in 350 s in each 6° angular interval. Figure 2 (right panel) shows the portion of sky explored by the counters, and the position of the source (Sco X-1) is indicated with a red rectangle [1].

This paper [1] *Evidence for X-Rays from Sources Outside the Solar System* gave rise to the 2002 Nobel Price of Riccardo Giacconi.

Another milestone in the history of high energy astrophysics was the discovery of gamma-ray bursts (GRBs). These have caused a revolution, giving rise to thousands of papers in search of an explanation of their origin and the physics that govern them. Even today, not everything is clear. Numerous reviews have been published on the subject, so much so that it is almost impossible to cite them all. I will limit myself to citing a recent review of mine "*Gamma-Ray Bursts: The Energy Monsters of the Universe*" [12] which contains a vast bibliography useful for navigating the stormy ocean of GRBs.

During the "cold war" epoch, the U.S.A. started a program for the construction of a group of satellites, named Vela, to detect nuclear detonations and monitor Soviet Union compliance with the 1963 Partial Test Ban Treaty.

Figure 3 (left panel) shows the Vela-5A/B Satellite in its cleanroom. The two satellites, A and B, were separated after launch.

The first detection of a gamma-ray burst (GRB) occurred on July 2, 1967, by the U.S. Vela-3 and Vela-4 satellites. However, since the data were coming from a military investigation and for this classified, the official announcement of the detection of a GRB with the origin outside the solar system to the scientific community occurred in 1973 (Klebesadel, Strong & Olson [13]). This first event is named now GRB 670702. The fundamental characteristics – duration of $\approx$ 10 s, two-pulse light curve and peak emission around the MeV energy band – were very different from the properties expected for a nuclear test in space – short-duration, hard X-ray burst, non-structured.

Analysing the data – acquired from July 1969 to July 1972 by the four Vela spacecrafts, Vela

PoS(FRAPWS2024)035

5A, 5B, 6A, and 6B, which were arranged almost equally spaced in a circular orbit with a geocentric radius of $\sim 1.2 \times 10^5$ km – an unexpected result arrived: sixteen short bursts of photons in the energy range 0.2-1.5 MeV was observed. Burst durations ranged from less than 0.1 s to $\sim$ 30 s, and the time-integrated flux density in the measured energy interval ranged from the minimum identifiable level of $\sim 10^{-5}$ ergs cm^{-2} to more than 2×10^{-4} ergs cm^{-2}. Significant time structure within bursts was observed. Directional information eliminates the Earth and Sun as sources [13]. This article marked the beginning of a new era for the understanding of our Universe characterized by sudden events with phantasmagoric luminosities ($\approx 10^{51}$ erg s^{-1}), the origin of which remained uncertain for decades.

Within the Cosmos series of Soviet satellites, Cosmos 461 (shown in the right panel of Fig 3) became famous because observed at least one GRB observed by the VELA satellites (Mazets, Golenetskij & Il'Inskij [14]) and for measuring the diffuse γ-ray background (Mazets et al. [15,16]).

After the discovery of these rapid and highly energetic events in the gamma-ray energy band, research into their origin was unleashed. The name "Gamma-Ray Burst" was the official denomination of such events.

Bodan Paczyński – Vilnius 8th February 1940 - Princeton 19th April 2007 –, the youngest Polish Academician of Sciences, emigrated in the USA at Princeton in 1982, gave a fundamental impulse to astrophysics with his pioneering efforts to develop the technique called gravitational lensing that permitted the discovery of the first terrestrial planet found outside our solar system. Despite widespread skepticism from the astrophysics community, he also championed the idea that the still-mysterious events known as GRBs originated billions of light years away rather than within our own Milky Way galaxy. With his paper *Gamma-Ray Bursters at Cosmological Distances* [17] he suggested that GRBs can be originated at z = 1-2: a theory that was ultimately confirmed by observations.

I had the honor of meeting him personally in 1978 in Warsaw, during my 40-days stay as guest of the Polish Academy of Sciences at the newborn N. Copernicus Center, directed by Joe Smak.

Although big progress has been obtained in the last few years, GRBs theory needs further investigation in the light of the experimental data coming from old and new satellites, often coordinated, such as BeppoSAX or BATSE/RXTE or ASM/RXTE or IPN or HETE or INTEGRAL or SWIFT or AGILE or Fermi or MAXI. All these satellites are schematically reproduced in Fig. 4 where the main past, present, and future space-based missions for GRB science are shown [18]. All these satellites are described in details in the paper by Tsvetkova et al. [19].

Figure 5 shows some of the ground- and space-based facilities that observe GRBs, which are detected across the whole electromagnetic spectrum [19].

In spite of thousands papers appeared in the literature since the discovery of GRBs, the problem of their energy emission is still elusive: i) what is jet's composition? (kinetic or magnetic?); ii) where is dissipation occurring? (photosphere? deceleration radius?); iii) how is radiation generated? (synchrotron, Inverse Compton, hadronic?) [20,21].

2. From UHURU to IXPE

In this section I will briefly describe the main characteristics of the satellites or payloads aboard balloon borne, and the most significative results obtained, following my personal choose,

PoS(FRAPWS2024)035

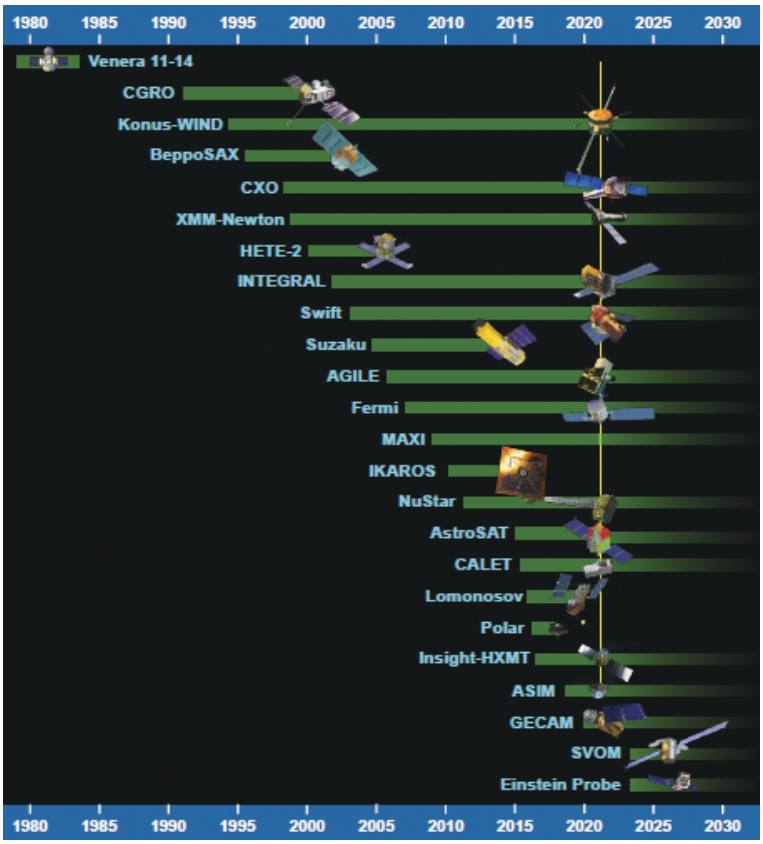

Figure 4: Main past, present, and future space-based missions for GRB science (Adopted from [18]).

starting from the first satellite completely devoted to X-ray astronomy, until IXPE (Imaging X-ray Polarimetry Explorer) mission.

2.1 The UHURU satellite

The UHURU satellite – the Small Astronomical Satellite 1 (SAS-1) –, whose name in Swahili language means "Freedom", was the first X-ray satellite. Figure 6 shows its main characteristics (https://heasarc.gsfc.nasa.gov/docs/uhuru/uhuru.html). The main result obtained during the operations over two years was the catalog of 339 X-ray sources in the range 2-6 keV, shown in Fig. 7 [22].

2.2 The Small Astronomy Satellite 2 (SAS-2)

The second NASA Small Astronomy Satellite (SAS-2) was dedicated to γ-ray astronomy in the energy range above 35 MeV. Figure 8 shows the main characteristics and science highlights of this satellite (https://heasarc.gsfc.nasa.gov/docs/sas2/sas2.html).

The salient results obtained were the measurement of γ-ray emission from several radio pulsars: Crab, Vela, PSR 1818-04, and PSR 1747-46 [23] and the emissivity of the Milky Way: $N_{\gamma SAS-2} = 1.3 \times 10^{42}$ photons s^{-1} [24].

PoS(FRAPWS2024)035

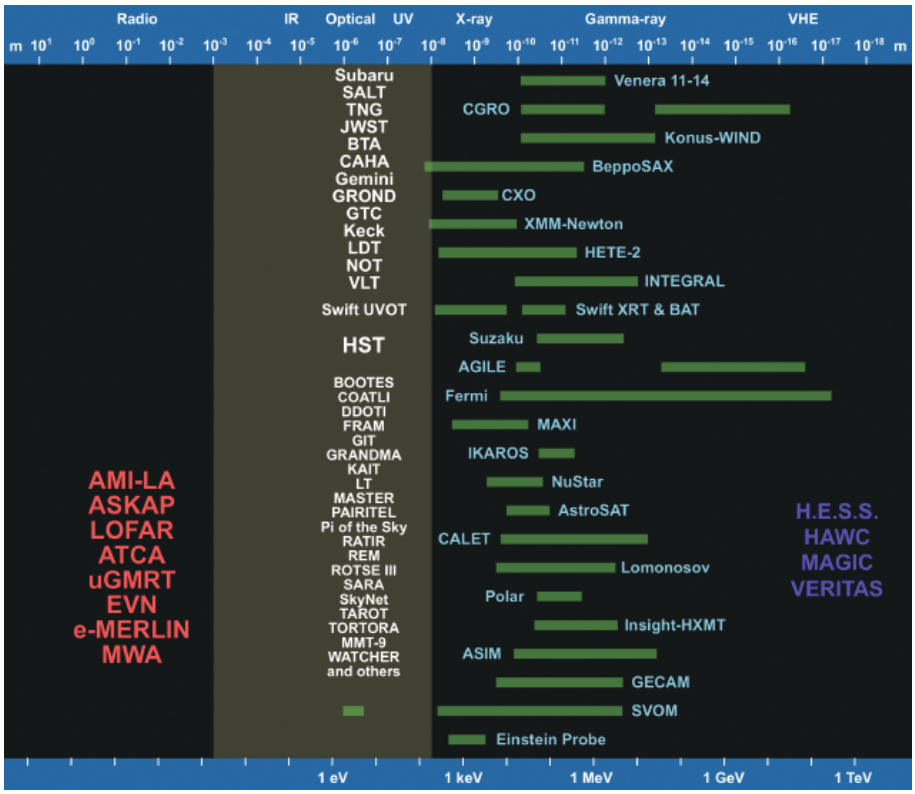

Figure 5: Some of the ground- and space-based facilities that observe GRBs, which are detected across the whole electromagnetic spectrum (adopted from [19]).

The Uhuru Satellite

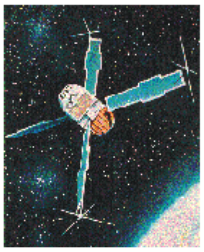

Uhuru, also known as the Small Astronomical Satellite 1 (SAS-1) was the first earth-orbiting mission dedicated entirely to celestial X-ray astronomy. It was launched on 12 December 1970 from the San Marco platform in Kenya. December 12 was the seventh anniversary of the Kenyan independence and in recognition of the hospitality of the Kenyan people, the operating satellite was named *Uhuru,* which is the Swahili word for *freedom.* The mission operated over two years and ended in March 1973.

Mission Characteristics

- Lifetime : 12 Dec 1970 - March 1973
- Energy Range : 2-20 keV
- Payload : Two sets of proportional counters: 2-20 keV 0.084 m^2
- Science Highlights:
  - First comprehensive and uniform all sky survey with a sensitivity of 10^{-3} the Crab intensity.
  - The 339 X-ray sources detected are binaries, supernova remnants, Seyfert galaxies and cluster of galaxies
  - Discovery of the diffuse X-ray emission from clusters of galaxies
- Archive : HEASARC hosts the 4th Uhuru Catalog

Photograph of ***Uhuru*** satellite courtesy of SAO.

Figure 6: Main characteristics of the UHURU satellite. Page authors: Lorella Angelini & Jesse Allen (adopted from https://heasarc.gsfc.nasa.gov/docs/uhuru/uhuru.html).

PoS(FRAPWS2024)035

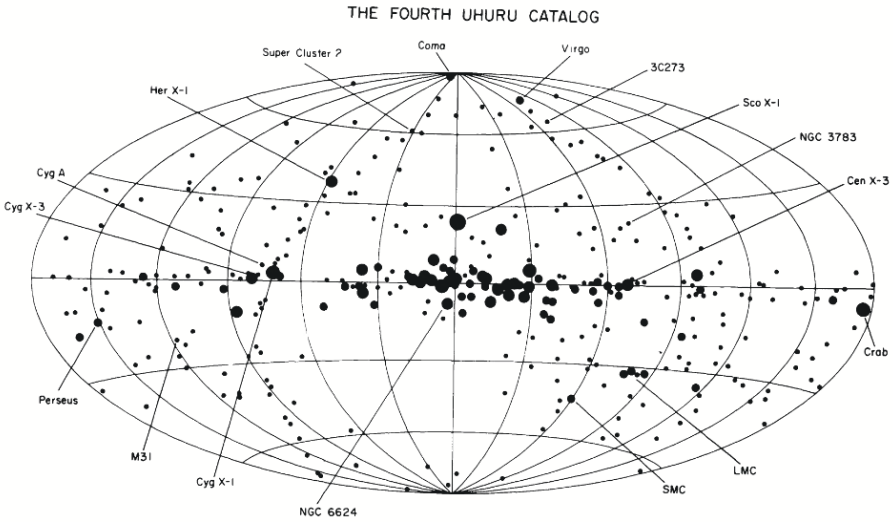

Figure 7: The sources are displayed in galactic coordinates. The size of the symbols representing the sources is proportional to the logarithm of the peak source intensity (adopted from [22]).

The Small Astronomy Satellite 2 (SAS-2)

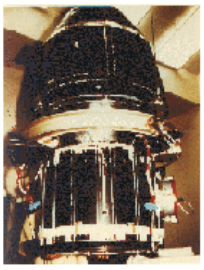

The second NASA Small Astronomy Satellite (SAS-2) was dedicated to gamma-ray astronomy in the energy range above 35 MeV. SAS-2 was launched on 1972 November 15 and began operations on 1972 November 19. On 1973 June 8, a failure of the low-voltage power supply ended the collection of data.

Mission Characteristics

- **Lifetime** : 19 November 1972 - 8 June 1973
- **Energy Range** : 20 MeV - 1 GeV
- **Payload** :
  - 32-level wire spark-chamber aligned with satellite spin axis (20 MeV-1 GeV), eff. area 540 cm^2
- **Science Highlights**:
  - The first detailed look at the gamma-ray sky.
  - Established the high energy component of diffuse celestial radiation.
  - Correlated the gamma-ray background with galactic structural features.
- **Archive** : HEASARC hosts Raw data, image and exposure maps

Figure 8: Main characteristics and science highlights of the SAS-2 satellite. Page authors: Lorella Angelini & Jesse Allen
(https://heasarc.gsfc.nasa.gov/docs/sas2/sas2.html).

PoS(FRAPWS2024)035

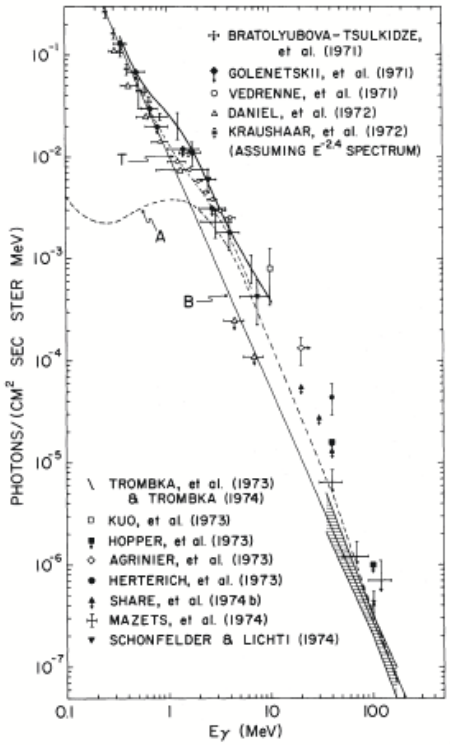

Figure 9: The diffuse celestial radiation observed by several experiments. The shaded area represents the SAS-2 data unfolded from the detector response, together with its uncertainty. The symbols for other results are explained in the Figure (adopted from [25]).

Figure 9 shows the diffuse celestial radiation observed by several experiments [25]. The shaded area represents the SAS-2 data unfolded from the detector response, together with its uncertainty. The symbols for other results are explained in the Figure.

Giovannelli [26] discussing the origin of low energy cosmic rays estimated the emissivity in the γ-ray band of possible cosmic ray sources, with the following results:

- **Young Open Clusters (YOC)**: the EGRET flux from the Berk 87 open cluster, place at distance of 0.9 kpc to the Earth, corresponds to a total γ-ray emissivity $N_\gamma \cong 10^{38}$ ph s^{-1} above 100 MeV [27,28].

  Taking account of the total number of open clusters in the Galaxy $\sim (0.5-1)\times 10^5$, of its decline with age with an approximate exponential law with a characteristic time scale of $\sim 10^8$ yr, very few open clusters are more than a few hundred million years in age [29]. Then, about 90% of them are younger than 10^7 yr. A reasonable simple extrapolation of the number of YOCs containing early type stars ith velocity of the stellar wind greater than 2,500 km s^{-1}, and then γ-ray emitters [30], which are contained within 2.5 kpc from the Sun, to the whole Galaxy leads to an upper limit of $\sim 10^3$. Therefore, the γ-ray emissivity of γ-ray emitter-like YOCs, above 100 MeV, could reach the value $N_{\gamma YOC} \cong 10^{41}$ ph s^{-1}.

- **Radio Pulsars and Recycled Pulsars**: there are $\sim$ 600 radio pulsars observed (in the 1990-

PoS(FRAPWS2024)035

ies) in the Galaxy [31]. Among them, only seven radio pulsars were detected as γ-ray emitters: Crab, Vela, PSRB1055-52, PSRB1706-44, PSRB1951+32, PSRB1509-58 (only detected at low energy) and the radio quiet Geminga [32,33]. However, 42 millisecond pulsars – most of them in binary systems – ere masured with EGRET and only upper limits of order 10^{-7} cm^{-2} s^{-1} on steady emission were established [34]. Taking account of the possible steady emission from recycled pulsars and of consistent predictions of Lipunov [35] on their emissivity, the contribution of the recycled pulsars to the totl emissivity of the Galaxy ($N_{\gamma RecPs} \sim 10^{39}$ ph s^{-1}) is negligible with respect to that of the radio pulsars. Indeed, taking account of the average emissivity of a radio pulsar [35], the contribution of the class of radio pulsars to the total emissivity of the Galaxy is $N_{\gamma RPs} \cong 10^{40}$ ph s^{-1}.

- **Isolated Black Holes**: in the matter spherically and adiabatically accreting onto a Schwarzschild black hole, inelastic collisions of protons produce π°s which decay into γ-rays. Giovannelli, Karakuła & Tkaczyk [36,37] calculated the expected γ-ray spectra from that process in the case of a galactic black hole of $10M_{\odot}$. The luminosity and emissivity of such a black hole, accreting 10^{-8} $M_{\odot}$ yr^{-1}, are 6.3 $\times 10^{33}$ erg s^{-1} and 2.1 $\times 10^{37}$ ph s^{-1} for Mach's number equal 1 or 2.8 $\times 10^{32}$ erg s^{-1} and 7.3 $\times 10^{35}$ ph s^{-1} for Mach's number equal 2. (*) Under the hypothesis that all the Galaxy γ-ray emissivity ($N_{\gamma SAS-2} = 1.3 \times 10^{42}$ photons s^{-1}), measured by SAS-2 [24], is coming from these collapsed objects, the upper limits to the number of black holes in the Galaxy is 10^5 or 10^6 for Mach's number equal 1 or 2, respectively. Assuming as reasonable number of black hole in the Galaxy ($\sim 2 \times 10^4$), and the emissivity of each black hole equal to 2.1 $\times 10^{37}$ ph s^{-1}, the contribution of isolated black holes to the Galaxy emissivity is $N_{\gamma IBH} \sim 4 \times 10^{41}$ ph s^{-1}.

(*) The Mach number is given by the ratio of the velocity of the gas to the local sound speed. In order to evaluate the temperature, concentration and velocity of the plasma near the black hole it is necessary to solve the system of equations describing the plasma motion (Michel, 1972) taking into account the distance from the black hole in units of gravitational radius and the u = R-component of four velocity. Mach's number 1 and 2 correspond to different values of u_0^2 (1.0266 and 2.1213, respectively) at a distance r_0 from the black hole [36,37].

- **Supernova (SN) Explosions**: statistical properties of radio pulsars in our Galaxy implies a formation rate of neutron stars of about one per each 30 years in the present cosmological epoch. Taking into account the Evolutionary Scenario Machine, developed by Lipunov & Postnov [38], which showed a dramatic evolution of the SN explosion rates during during the first 5-7 billion years of the galactic life, the contribution of the SN explosions to the present Galaxy emissivity is $N_{\gamma SN} \cong 6 \times 10^{41}$ ph s^{-1}.

- **Black Holes and Neutron Stars in Binary Systems**: in the Evolutionary Scenario Machine [38], the matrix of binary systems states gives a number of black holes and neutron stars of the order of few units $\times 10^4$; then the contribution of these systems to the total Galay emissivity is $N_{\gamma BH,NS-BSs} \cong 2 \times 10^{41}$ ph s^{-1}.

Therefore, it is tentatively possible to evaluate the total Galaxy γ-ray emissivity as the sum of the former contributions:

PoS(FRAPWS2024)035

$$N_{\gamma Tot} = N_{\gamma YOC} + N_{\gamma RPs} + N_{\gamma IBH} + N_{\gamma SN} + N_{\gamma BH,NS-BSs} \cong 1.3 \times 10^{42} \text{ ph s}^{-1} = N_{\gamma SAS-2}$$

This result is amazing!.

2.3 The COS-B satellite

The ESA mission COS-B, along with NASA's SAS-2, provided the first detailed views of the Universe in Gamma-rays. Figure 10 shows the main characteristics of this satellite (https://heasarc.gsfc.nasa.gov/docs/cosb/cosb.html).

The COS-B Satellite

The ESA mission COS-B, along with NASA's SAS-2, provided the first detailed views of the Universe in Gamma-rays. COS-B carried a single large experiment, the Gamma-Ray Telescope, which was responsibility of a group of European research laboratories know as the *Caravane Collaboration*. Launched on the 9 August 1975, COS-B was originally projected to last two years, but it operated successfully for 6 years and 8 months. It provided the first complete map of the Galaxy in gamma-rays.

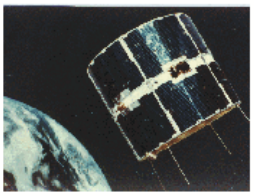

Mission Characteristics

- **Lifetime** : 9 Aug 1975 - 25 April 1982
- **Energy Range** : 2 keV - 5 GeV
- **Payload** :
  - Magnetic-core, wire-matrix, spark chamber gamma-ray detector (~30 MeV-5 GeV), eff. area 50 cm^2 at 400 MeV
  - a 2-12 keV proportional counter mounted on the side of the gamma-ray detector
- **Science Highlights**:
  - Observations of gamma-ray pulsars, binary systems.
  - Gamma-ray map of the Galaxy.
  - Detailed observations of the GEMINGA gamma-ray pulsar.
- **Archive** : HEASARC hosts raw data, image and exposure maps from the gamma-ray detector

Figure 10: Main characteristics and science highlights of the COS-B satellite. Page authors: Lorella Angelini & Jesse Allen (https://heasarc.gsfc.nasa.gov/docs/cosb/cosb.html).

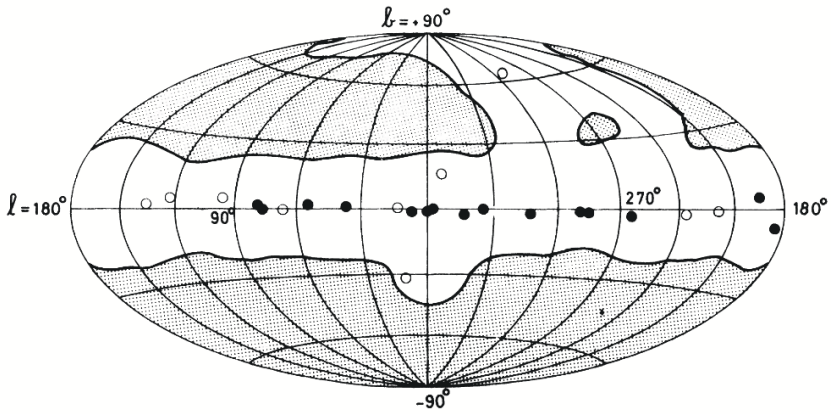

Figure 11: The COS-B 2CG Catalog. The filled circles denote sources with measured fluxes 1.3×10^{-4} photons cm^{-2} s^{-1}. Open circles denote sources below this threshold (adopted from [39]).

PoS(FRAPWS2024)035

The 37-hour orbit of Cos-B was an eccentric orbit that ensured that the satellite was outside the Earth's radiation belts for most of the time. During the seven years of operation (9 August 1975 - 25 April 1982) the most important result was the detection of 25 γ-ray sources out of 30 observations made during the first 3-years and a complete γ-ray map of the disc of the Milky Way [39]. Figure 11 shows the region of the sky searched for γ-ray sources (unshaded) and sources detected above 100 MeV by spatial analysis. The filled circles denote sources with measured fluxes 1.3×10^{-4} photons cm^{-2} s^{-1}. Open circles denote sources below this threshold.

2.4 Stratospheric Balloons

A multitude of experiments launched aboard stratospheric balloons can be consulted at https://stratocat.com.ar > globos. A paper by Ubertini [40] reports historical notes on scientific balloons and in particular lists those numerous experiments in which there was the participation of our old institute of astrophysics and cosmic physics (IAPS) of the INAF (Istituto Nazionale di Astrofisica).

In the 1970s, numerous stratospheric balloons were launched with various types of astronomy experiments on board. Among these, I would like to mention the High Energy X-Ray Experiment (HEXE) which was built and operated in close collaboration of MPE and the Institut für Astronomie und Astrophysik der Universität Tübingen.

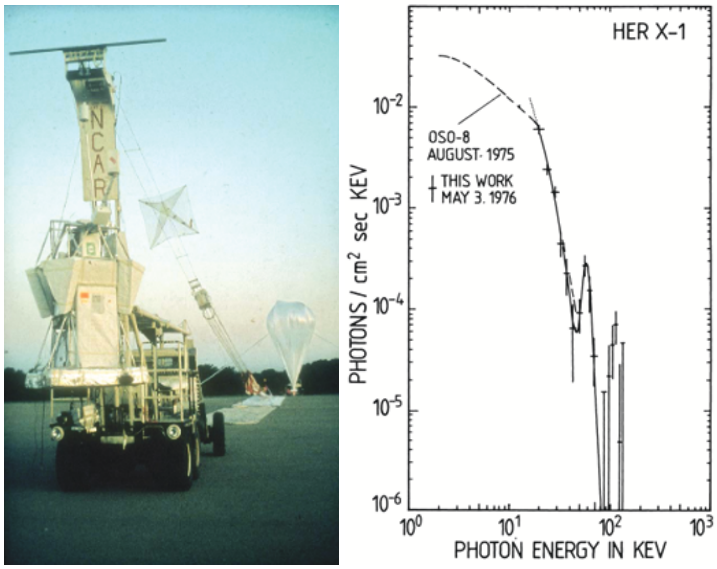

Figure 12: Left panel: HEXE-1 payload ready for the launch (adopted from [41]). Right panel: Her X-1 cyclotron line (adopted from [42]).

Left panel of Fig. 12 shows the payload of HEXE-I ready to be launched from the base of Palestine, Texas, USA on 1976 May 3 [41]. Her X-1 was observed from 06:12 to 10:12 UT during a 10 hour balloon flight and the result was one of the most important obtained in the field of X-ray astronomy: Historical detection of a cyclotron line in at $\sim$ 58 keV [42]. The energy of the cyclotron line is connected with the magnetic field intensity of the neutron star, as:

PoS(FRAPWS2024)035

Figure 13: Left panel: a multi-instrumented gondola with several X-ray experiments from Italian Universities and CNR-LAS. Right panel: the million cubic meter balloon just inflated and ready for launch (credit: Franco Giovannelli).

$$E_c = 11.6 \times (B/10^{12}G) \times (1+z)^{-1} \text{ keV}$$

Thus the magnetic field intensity in Her X-1 is B $\approx 5 \times 10^{12}$ G [42]. Right panel of Fig. 12 shows this historical measure.

Since the very beginning of the scientific research with stratospheric balloons, Italian scientists were among the pioneers in their use.

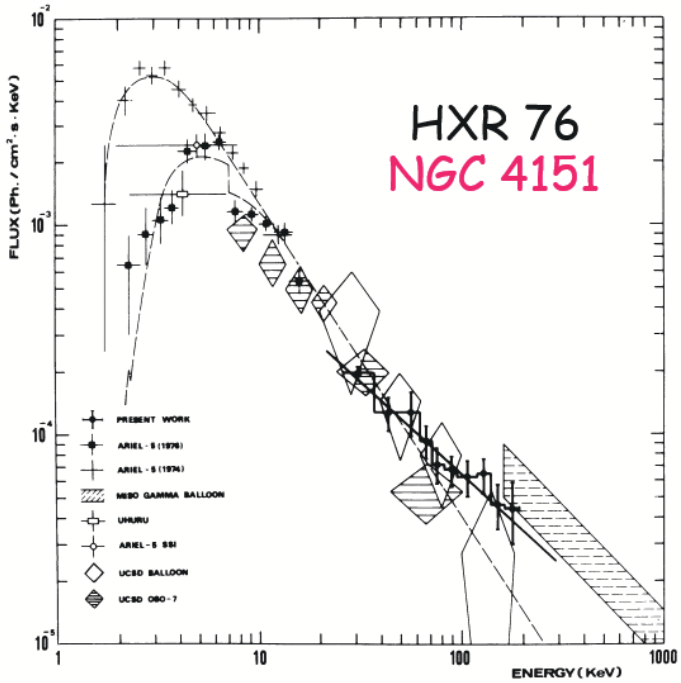

Figure 14: Photon spectrum of NGC 4151. HXR-76 data are compared with those from previous experiments (adopted from [44]).

From the Milo Base (Luigi Broglio Base), Trapani, Italy on 29 July 1976, a 10^6 m^3 balloon carried a multi-instrumented gondola with several X-ray experiments from Italian Universities and CNR-LAS (Consiglio Nazionale delle Ricerche-Laboratorio di Astrofisica) di Frascati (HXR 76).

PoS(FRAPWS2024)035

That mission made history because by chance during the flight was detected for the first time a radio frequency gamma-ray burst of non-solar origin [43].

The left panel of Fig. 13 shows the gondola carrying several X-ray experiments. The right panel of Fig. 13 shows the million cubic meter balloon just inflated and ready for launch (credit: Franco Giovannelli).

The main result obtained with the HXR-76 experiment was the measurement of the X-ray source 4U 1206+39 associated with the Seyfert galaxy NGC 4151. It was observed with the high-pressure proportional chamber on board the Transatlantic Balloon Facility. The spectrum in the 25-190 keV range may be fitted with a power law with spectral slope a = 0.9 ± 0.2 [44]. (*)

(*) This was the topic of my seminar in Warsaw (May 1978) at the newborn N. Copernicus Center (Joe Smak as Director), where I stayed as guest of the Polish Academy of Sciences for 40 days during which Joseph (Joe) Patterson (Guest) was working on his PhD thesis.

2.5 The HEAO-1 satellite

Beginning in 1977, NASA launched a series of very large scientific payloads called High Energy Astronomy Observatories (HEAO). The first of these observed the sky in the energy range 0.2 keV - 10 MeV and provided nearly constant monitorig of X-ray sources producing a catalog of 842 sources with a limiting flux of 0.25 μJy at 5 keV, or ~ 0.25 UFU, assuming a Crab-like spectrum (1.1 μJy at 5 keV = 1 UFU (Uhuru Flux Unit).

Figure 15 shows the main characteristics and science highlights of the HEAO-1 satellite (https://heasarc.gsfc.nasa.gov/docs/heao-1/heao-1.html). Figure 16 shows the HEAO-1 all-sky X-ray catalog (NASA at https://heasarc.gsfc.nasa.gov/docs/heao-1/heao-1.html).

2.6 The Ariel V satellite

Ariel V satellite was launched on 15 October 1974 from the San Marco Malindi base and operated until 14 March 1980 for monitoring the X-ray sky in the energy range 0.3 - 40 keV. Figure 17 shows the main characteristics and science highlights of this satellite (https://heasarc.gsfc.nasa.gov/docs/ariel5/ariel5.html).

The advent of the Ariel V satellite has significantly marked my scientific trajectory. In fact, with the discovery of an X-ray source, called A 0535+26, the hunt began to find its optical counterpart and therefore the behavior of this system along the entire electromagnetic spectrum. And this is what I intend to tell for the benefit of readers, especially young ones.

In the Ariel V error box of the A 0535+26 source were contained 11 stars up to 23rd magnitude. A ~ 9 mag star (HDE 245770) was inside the error box (see Fig. 18 [46]). The a priori probability of finding a 9 mag star in such a field is 0.004. HDE 245770 shows H_α and H_β in emission, H_γ filled in with emission, and H_δ, H_ϵ,....,H_{10} in absorption. HDE 245770 was then considered the probable optical counterpart of the X-ray source A0535+26. But to be certain, a direct link between the optical behavior and X-rays had to be found.

The optical measurements of HDE 245770 during December 1977 were not obtained by chance, but thanks to a prediction made by myself under the hypothesis that the few X-ray outbursts detected

PoS(FRAPWS2024)035

The HEAO-1 Satellite

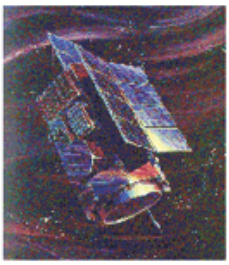

Beginning in 1977, NASA launched a series of very large scientific payloads called **High Energy Astronomy Observatories** (HEAO). The first of these missions, **HEAO-1** surveyed the X-ray sky almost three times over the 0.2 keV - 10 MeV energy band, provided nearly constant monitoring of X-ray sources near the ecliptic poles. More detailed studies of a number of objects were made through pointed observations lasting typically 3-6 hours.

Mission Characteristics

- Lifetime : 12 August 1977 - 9 January 1979
- Energy Range : 0.2 keV - 10 MeV
- Payload :
  - A1 - Large Area Sky Survey experiment (LASS) :
    0.25-25 keV, eff. area 7 modules each of 1350 - 1900 cm^2, FOV varied between 1° X 4° to 1° x 0.5° for finest collimators.
  - A2 - Cosmic X-ray Experiment (CXE) :
    six separate proportional counters
    - Low Energy Detectors (LED) 0.15-3.0 keV, eff. area 2 detectors of 400 cm^2 each
    - Medium Energy Detector (MED) 1.5-20 keV, eff. area 1 detector at 800 cm^2
    - High Energy Detector (HED) 2.5-60 keV, eff. area 3 detectors at 800 cm^2 each

    MED and HEDs had various FOV settings, 1.5° x 3°, 3° x 3° and 3° x 6°
  - A3 - Modulation Collimator (MC) :
    0.9-13.3 keV, eff. area 2 collimators 400 cm^2 (MC1) & 300 cm^2 (MC2), FOV 4° X 4°
  - A4 - Hard X-Ray / Low Energy Gamma Ray Experiment :
    seven inorganic phoswich scintillator detectors
    - Low Energy Detectors 15-200 keV, eff. area 2 detectors 100 cm^2 each, FOV 1.7° x 20°
    - Medium Energy Detectors 80 keV - 2 MeV, eff. area 4 detectors 45 cm^2 each, FOV 17°
    - High Energy Detector 120 keV - 10 MeV, eff. area 1 detector 100 cm^2, FOV 37°
- Science Highlights:
  - Complete flux-limited High Galactic Latitude Survey (Piccinotti et al. 1982).
  - Measurement of X-ray background from 3-50 keV (Marshall et al. 1980, ApJ, 235, 4.)
  - Comprehensive catalog of X-ray sources (one for each experiment).
  - Several hundred optical companions and source classifications based on X-ray source positions.
  - Monitored variability of a variety of objects from AGNs to X-ray binaries.
  - Studied aperiodic variability in Cyg X-1 on timescales on a few milliseconds
  - Discovered the first eclipse seen in a low-mass X-ray binary.
- Archive: HEASARC hosts catalogs, spectra, lightcurves, maps and raw data.

Not all are available for all experiments.

Figure 15: Main characteristics and science highlights of the HEAO-1 satellite. Page authors: Lorella Angelini & Jesse Allen (https://heasarc.gsfc.nasa.gov/docs/heao-1/heao-1.html).

were roughly periodic. This is clearly reported in Fig. 19 [47], where the first two detected X-ray outbursts are reported in red as well as the few measurements during the "rise" of the third outburst.

And here there was my intuition: since the slope of the rise was similar to that of the first outburst, I made the hypothesis that a similar outburst would have occurred (the third) and then a fourth one, similar to the second, would have occurred simply with a same delay of the second with respect to the first outburst. In this way I predicted a possible X-ray outburst of the A 0535+26 pulsar in the period ranging from December 3, 1977 to January 9, 1978, with a maximum around December 10-15. On December 17, Bartolini et al. [48] measured a decay from an outburst of HDE 245770. The X-ray outburst was announced a few days later by Chartres & Li [49] thanks to SAS 3 measurements (maximum in 2-10 KeV on December 23.5), and much later the entire 1977 December X-ray outburst at different energies was reconstructed (see Table 1 of the review

PoS(FRAPWS2024)035

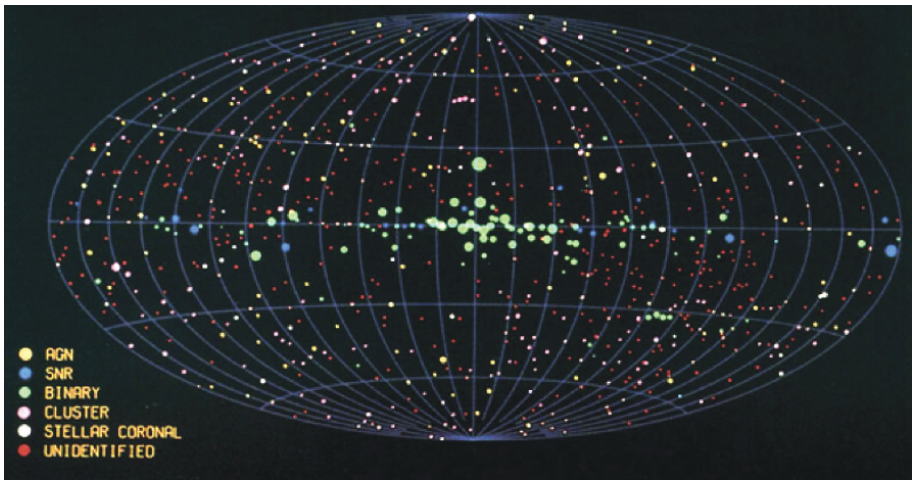

Figure 16: HEAO-1 all-sky X-ray catalog (adopted from NASA at https://heasarc.gsfc.nasa.gov/docs/heao-1/heao-1.html).

The Ariel V Satellite

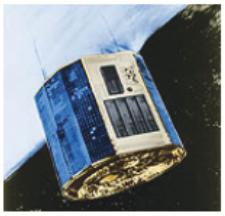

Ariel V was launched into a low inclination (2.8 degrees) orbit from the San Marco launch platform in the Indian Ocean on 15 October 1974. The mission was a British-USA collaboration. The Science Research Council managed the project for the UK and GSFC/NASA for the USA. Ariel V was dedicated to monitoring the X-ray sky with a comprehensive payload. The mission ended in the spring of 1980.
+Read more

Mission Characteristics

- **Lifetime:** 15 October 1974 - 14 March 1980
- **Energy Range:** 0.3-40 keV
- **Payload:**

Experiments aligned with the spin axis.

- Rotation Modulation Collimator (RMC) (0.3-30 keV).
- High resolution proportional counter spectrometer.
- Polarimeter/spectrometer.
- Scintillation telescope.
- All-Sky Monitor (ASM) a small (~1 cm^2) pinhole camera (3-6 keV).
- Sky Survey Instrument (SSI) composite of two proportional counters with 290 cm^2 effective area each (1.5-20 keV).

- **Science Highlights:**

- Long-term monitoring of numerous X-ray sources.
- Discovery of several long period (minutes) X-ray pulsars.
- Discovery of several bright X-ray transients probably containing a Black Hole (*e.g.* A0620-00=Nova Mon 1975).
- Establishing that Seyfert I galaxies (AGN) are a class of X-ray emitters.
- Discovery of iron line emission in extragalactic sources.

+Read more

- **Archive:** HEASARC hosts lightcurves from the ASM and the Raw data and the 3rd Ariel V catalog from the SSI.

Figure 17: Main characteristics and science highlights of the Ariel V satellite. Page authors: Lorella Angelini & Jesse Allen (https://heasarc.gsfc.nasa.gov/docs/ariel5/ariel5.html).

PoS(FRAPWS2024)035

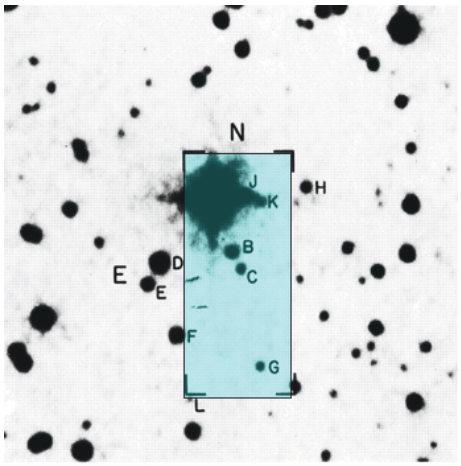

Figure 18: An enlargement of the red Palomar Observatory Sky Survey plate in the region of A0535+26, whose error box is marked by the light blue rectangle; the bright star is HDE 245770 (Adapted from [46]).

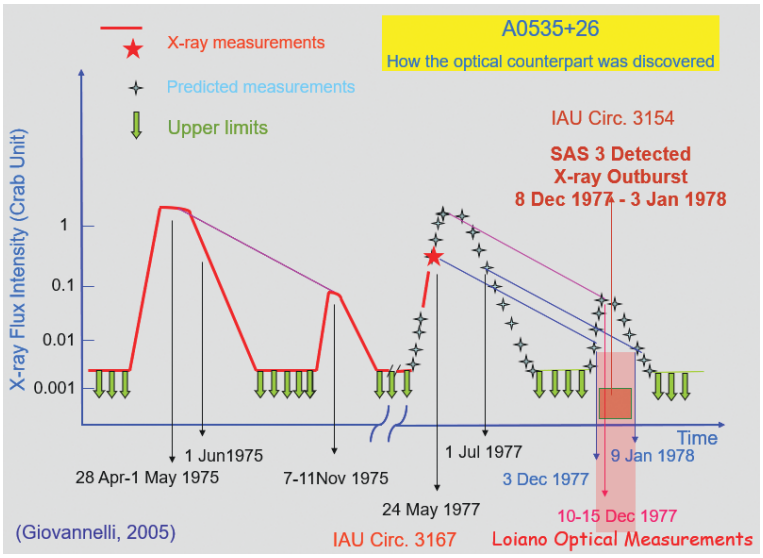

Figure 19: Schematic of how the optical counterpart of A0535+26 was discovered (adopted from [47]).

by Giovannelli & Sabau- Graziati [2]). The outburst started on December 8, 1977 and was still strong on January 3, 1978. After this date no measurements are available. Then, the "hazardous" prediction of Giovannelli was awarded by the first direct evidence about the association of the star HDE 245770 with the X-ray pulsar A 0535+26 [48].

Once the association between A 0535+26 and HDE 245770 was established, the problem of its classification arose. Giangrande et al. [50] by using – at the 152 cm Loiano telescope – a Boller & Chivens 26767 grating spectrograph: 831 grooves/mm II-order grating: 39 Å/mm and Kodak 103 aO plates, classified HDE 245770 as O9.IIIe. This classification, although obtained "with antediluvian means" typical of the 1980s, is still valid after 45 years!

PoS(FRAPWS2024)035

2.7 The Einstein Observatory (HEAO-2)

The HEAO-2 satellite – renamed Einstein after launch – was launched on 12 November 1978 and operated until April 1981. It was the first fully imaging X-ray telescope put into space, and with its spatial resolution of ~ 2 arcsec completely changed the view of the X-ray sky. Figure 20 shows the main characteristics and science highlights of this satellite (https://heasarc.gsfc.nasa.gov/docs/einstein/heao2.html).

The Einstein Observatory (HEAO-2)

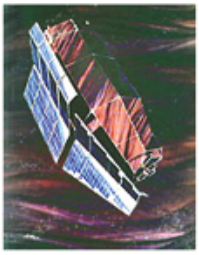

The second of NASA's three High Energy Astrophysical Observatories, HEAO-2, renamed Einstein after launch, was the first fully imaging X-ray telescope put into space. The few arcsecond angular resolution, the field-of-view of tens of arcminutes, and a sensitivity several 100 times greater than any mission before it provided, for the first time, the capability to image extended objects, diffuse emission, and to detect faint sources. It was also the first X-ray NASA mission to have a Guest Observer program.
Overall, it was a key mission in X-ray astronomy and its scientific outcome completely changed the view of the X-ray sky.

Mission Characteristics

- Lifetime : 12 November 1978 - April 1981
- Energy Range : 0.2 - 20 keV
- Special Features : First imaging X-ray telescope in space
- Payload :
  - A Wolter Type I grazing incidence telescope (0.1-4 keV).
    Four instruments could be rotated, one at a time, into the focal plane:
    - Imaging Proportional Counter (IPC; 0.4-4.0 keV)
      eff. area 100 cm^2, FOV 75′, ~1 arcmin spatial resolution.
    - High Resolution Imager (HRI; 0.15-3.0 keV)
      eff. area 5 - 20 cm^2, FOV 25′, ~2 arcsec spatial resolution.
    - Solid State Spectrometer (SSS; 0.5-4.5 keV)
      eff. area 200 cm^2, FOV 6′, E/delta E of 3-25
    - Focal Plane Crystal Spectrometer (FPCS; 0.42-2.6 keV)
      eff. area 0.1 - 1.0 cm^2, FOV 6′, 1′x20′, 2′x20′, 3′x30′, E/delta E of 50-100 for E < 0.4 keV, E/delta E of 100-1000 for E > 0.4 keV
  - Monitor Proportional Counter (MPC; 1.5-20 keV)
    eff. area 667 cm^2, FOV 1.5°, energy resolution ~20% at 6 keV. Co-aligned with the X-ray telescope.
  - Objective Grating Spectrometer (OGS) : 500 mm^{-1} & 1000 mm^{-1}, energy resolution dE/E ~ 50. Used in conjunction with HRI.
- Science Highlights:
  - First high resolution spectroscopy and morphological studies of supernova remnants.
  - Recognized that coronal emissions in normal stars are stronger than expected.
  - Resolved numerous X-ray sources in the Andromeda Galaxy and the Magellanic Clouds.
  - First study of the X-ray emitting gas in galaxies and clusters of galaxies revealing cooling inflow and cluster evolution.
  - Detected X-ray jets from Cen A and M87 aligned with radio jets.
  - First medium and Deep X-ray surveys
  - Discovery of thousands of "serendipitous" sources
- Archive : HEASARC hosts Catalogs, Spectra, Lightcurves, Images and Raw data

Figure 20: The main characteristics and science highlights of Einstein satellite. Page authors: Lorella Angelini & Jesse Allen (https://heasarc.gsfc.nasa.gov/docs/einstein/heao2.html).

HEAO-2 Observatory detected 191 extragalactic X-ray sources – with z known – of different classes (QSOs, Seyfert Galaxies, BL Lac, elliptical and SO, spiral and irregular galaxies).

Looking at the plot of Fig. 21 [51], Giovannelli & Polcaro [52] had the idea, now very popular, that the the *engine* producing high energy radiation is of the same kind for all extragalactic emitters. Mass and mass accretion rates are the unique parameters which differentiate extragalactic emitters containing central black holes from the galactic black holes.

PoS(FRAPWS2024)035

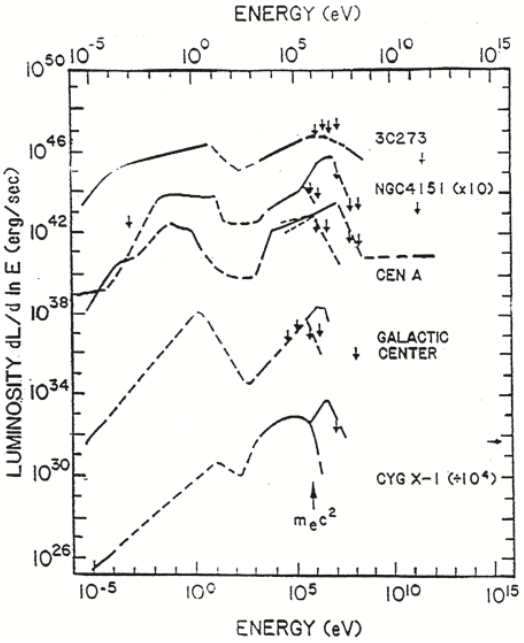

Figure 21: Energy spectra of several accreting black hole candidates (adapted from [51]).

The emission of the extragalactic X-ray sources can be expressed as $L_{TOT} = L_{NUC} + L_{HG}$, where, L_{NUC} is the nuclear luminosity and L_{HG} is the host galaxy luminosity, formed by the integrated emission of its discrete sources. Such components can be derived by using the Giovannelli & Polcaro [52] diagram (here after GP86).

Thus a general relationship between log z and the logarithm of the 2 keV equivalent monochromatic luminosity of the brightest object in a given redshift interval (regardless of the class of the object) was found [52](*). This function is almost constant for $z < 0.001$; it has a continuous inflection of about two orders of magnitude between $z = 0.001$ and $z = 0.01$, and at $z > 0.01$, where only AGNs are present, it matches with a straight line, with slope equal to 1.6. They suggested that such a smooth function implies a physical continuity of these objects.

(*) The embryo of this idea was born during a weekend at the Warsaw Observatory in May 1978 in a conversation with Bodhan Paczyński, to whom I asked whether it would be possible to find the equivalent of the HR diagram for extragalactic sources, that I was dreaming. He replied, "**Why not! Good luck!**".

Later, with the advent of higher sensitivity X-ray experiments, different samples of extragalactic X-ray emitters were discovered [53 and the references therein] and [54]. Top panel of Fig. 22 shows all these samples with the maximum X-ray luminosity function found by GP86 (red line). This figure report also the position – marked with a blue star – of the QSO J 1148+5251 at $z = 6.42$ [55] whose predicted X-ray luminosity is 7×10^{47} erg s^{-1} by using the GP86 diagram.

For the weaker sources, the luminosity functions are parallel to the GP86 function (blue, green, and fuchsia lines). For $z < 0.001$, there is a substantial constancy of the functions. In other words this means that the contribution to the luminosity is mostly coming from the discrete sources of the host galaxies (middle panel of Fig. 22). This is in complete agreement with the results obtained

PoS(FRAPWS2024)035

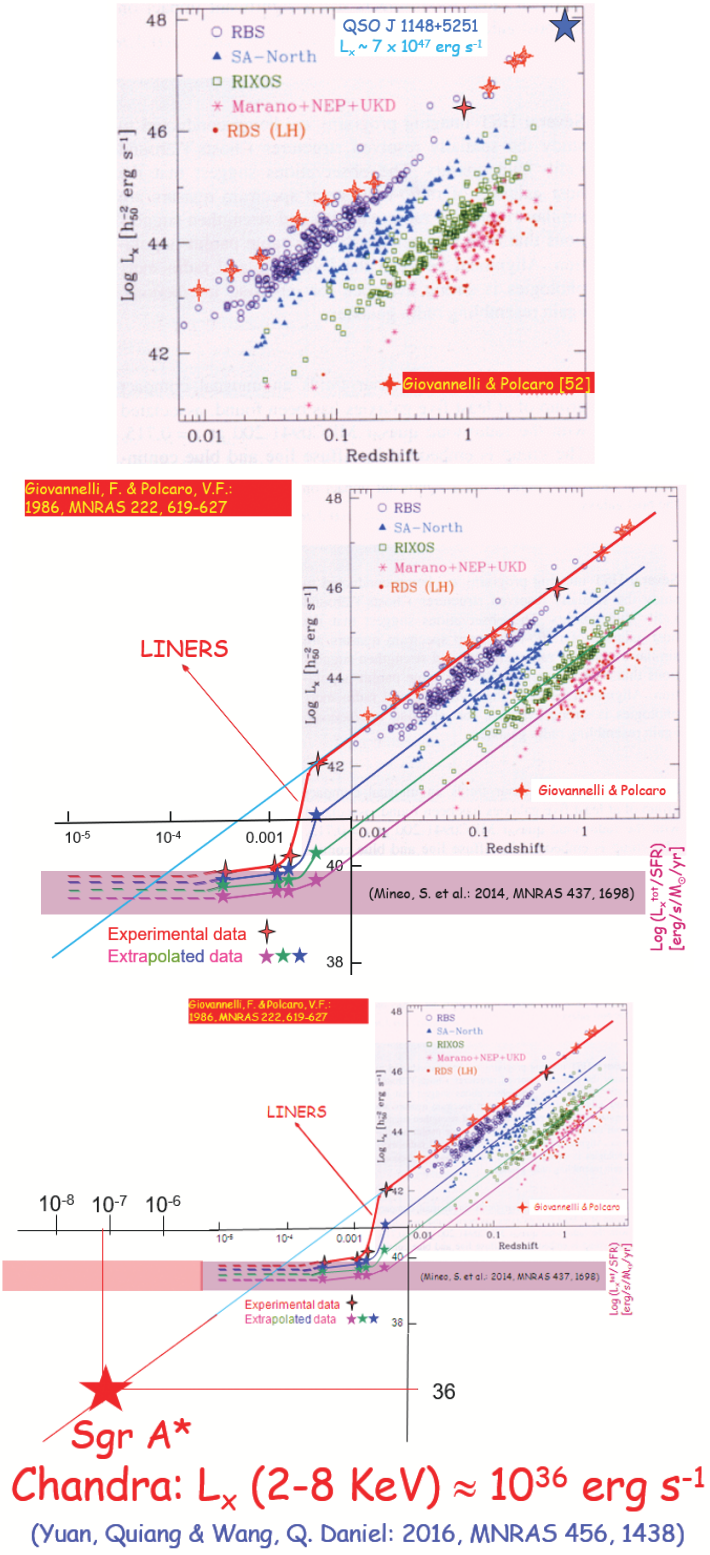

Figure 22: Top panel: L_{xmax} versus z for extragalactic X-ray emitters. Red crosses represent the upper part of the GP86 diagram [52]. The deeper surveys [53,54] shown in the diagram are indicated with different colors. Middle panel: The entire GP86 diagram superimposed on that of Hasinger et al. [53,54]. The light plum-colored band indicates the range of Mineo et al. [56] results. The bottom panel shows the same but with extrapolation to Bottom panel: the same but with extrapolation to 10^{36} h_{50}^{-2} erg s^{-1} [57].

PoS(FRAPWS2024)035

by Mineo et al. [56] (light plum-colored band). The light blue line in continuation of the red line indicates the contribution of the nucleus (L_{NUC}) to the total luminosity of galaxies with $z \leq 0.002$. The bottom panel shows the same, but with extrapolation to $10^{36}\ h_{50}^{-2}$ erg s^{-1}, the value of the X-ray luminosity of Sgr A^*, measured by Chandra satellite [57].

2.8 The International Ultraviolet Explorer (IUE)

The International Ultraviolet Explorer (IUE) satellite was launched on January 26, 1978 and during its long operational life (~ 18 yr) has made a fundamental contribution to ultraviolet astrophysics(*). Figure 23 shows its main characteristics (https://science.nasa.gov > iue).

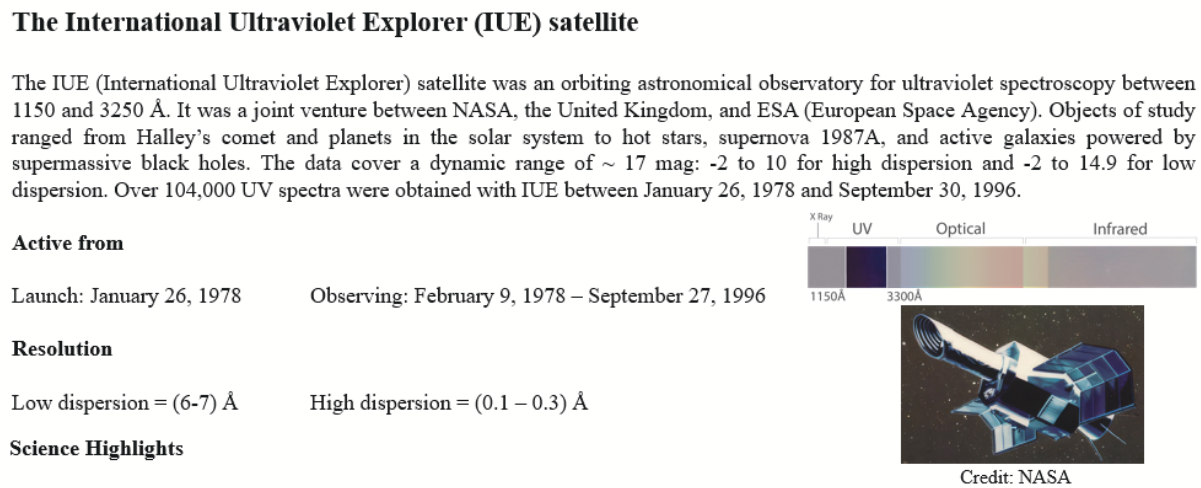

Figure 23: Main characteristics and science highlights of the International Ultraviolet Explorer (IUE) satellite (adapted from https://science.nasa.gov > iue).

(*) As coordinator of several groups of scientists, I was one of the most frequent users of the IUE, conducting research mainly on X-ray binary systems, cataclysmic variables and T Tauri stars. The measurements from the IUE were part of the mosaic completed by infrared, optical and X-ray measurements.

2.8.1 The X-ray/Be system A 0535+26/HDE 245770

From the numerous IUE spectra both in low- and high-resolution it was possible to detect interstellar, symmetrical and asymmetrical lines.

- Filling the 2200 bump it was possible to determine the E(B-V) = 0.75 [58,59];
- From the HeII broadening it was possible to determine the rotational velocity of the O9.7 IIIe star as $v_{rot} \times \sin i = 230$ km s−1 [60], and later the inclination angle $i = 37° \pm 2°$ [61];

PoS(FRAPWS2024)035

- From CIV and SiIV asymmetrical lines it was possible to determine the velocity of the stellar wind as $v_{terminal}$ = 630 km s^{-1} [60,62];
- The mass loss rate of the system in quiescence is $\dot{M} \simeq 10^{-8}$ $M_\odot$ yr−1 [60,62], and in strong outburst $\dot{M} \simeq 7.7 \times 10^{-7}$ $M_\odot$ yr−1 [63].

The spectral energy distribution from UV to IR of the X-ray/Be system A 0535+26/HDE 245770 is shown in Fig. 24 [62].

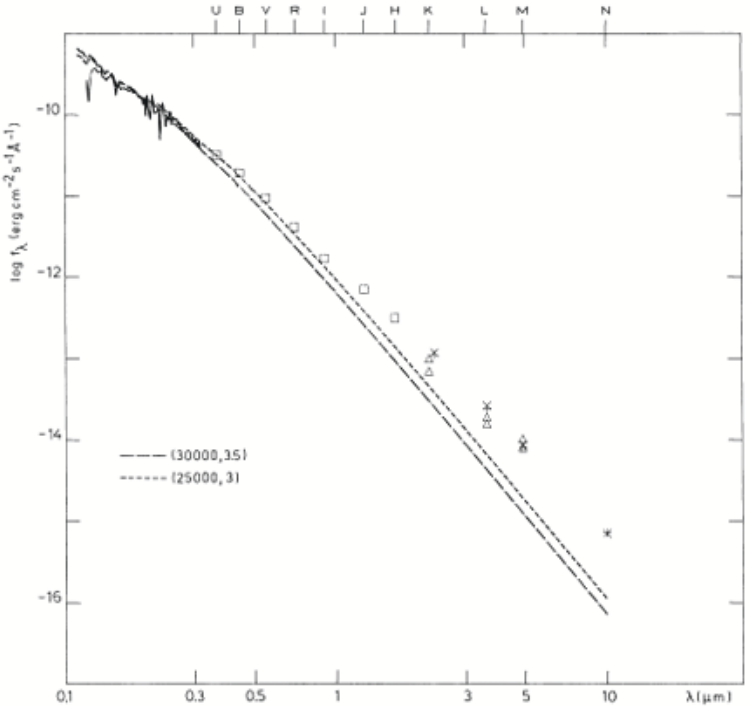

Figure 24: Spectral energy distribution of the A 0535+26/HDE 245770 system from UV to IR (adopted from [62].

2.8.2 The cataclysmic variable SS Cyg

SS Cyg has been the target of many observations proposed by my group and accepted by the IUE commission for allocation time. Figure 25 shows typical short wavelength (SW) spectra of SS Cyg in quiescence ($M_V \approx 12$) and in outburst ($M_V \approx 8$), and a composite spectrum SW + long wavelength (LW) (SW + LW: 1200-3200 Å) [64].

The UV flux is $F_\lambda \propto \lambda^\alpha$, with α = -4 for $\lambda \leq 1450$ Å, and α = -1.2 for $\lambda \geq 1450$ Å. The value α = -4.0 is consistent with a tail of a Rayleigh-Jeans emission from a black body (BB) with T ≃ 15 keV. This slope is the same of that of AM Her: the prototype of POLARS [64]. At this point the obvious idea arises that SS Cyg is a cataclysmic variable with a magnetic field such as to make it an intermediate polar or even a polar.

Since the reddening of SS Cyg reported in the literature vary significantly from one another, Gaudenzi et al. [65] decided to understand the origin of such discrepancies. Thus, by using the

PoS(FRAPWS2024)035

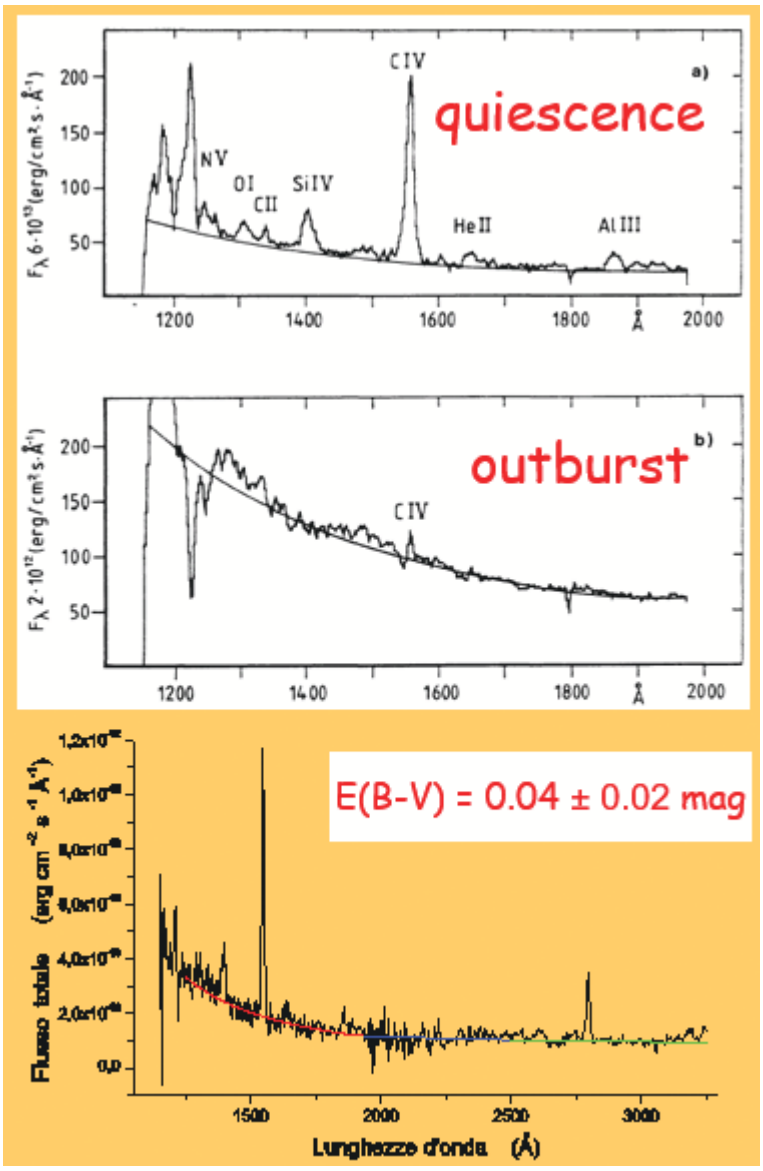

Figure 25: Typical IUE SW spectra of SS Cyg in quiescence and in outburst and a composite (SW+LW) spectrum in quiescence (adopted from [64].

INES archive of the IUE satellite, they analyzed the spectra of SS Cygni in quiescence in order to determine the value of the reddening of the binary system. The results demonstrated that the reddening is comprised by two components: the first, interstellar in origin, with a value E(B-V) = 0.04 ± 0.02 mag, and the second, intrinsic to the binary system, with values up to E(B-V) = 0.16 ± 0.02 mag. The intrinsic value of the reddening is variable along the quiescent phase (t%) and with orbital phase, as shown in Fig. 26.

Lombardi, Giovannelli & Gaudenzi [66] found orbital modulations in the UV continuum at 1700 after long and short outbursts of SS Cyg, as well as at 2700 after short outburst and in the UV emission lines of NV, SiIV and CIV both after short an long outbursts. Optical line fluxes

PoS(FRAPWS2024)035

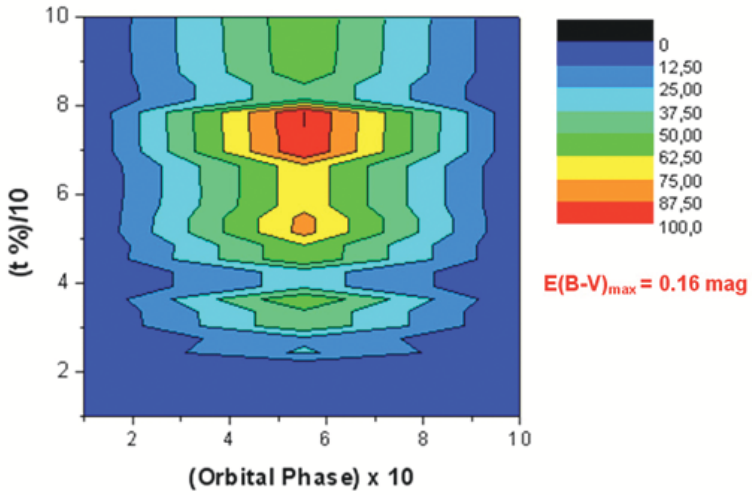

Figure 26: E(B-V) contour in the Orbital phase - t% plane. The maximum value $E(B\text{-}V)_{max}$ = 0.16 mag corresponds to 100% of E(B-V) depicted in red (adopted from [65].

modulations with the orbital period have been detected in H_α, H_β, H_γ, H_δ, HeI 4471 and HeI 6678 [67]. Orbital modulations of emission lines and continuum are typical of intermediate polars (IPs). Figure 27 shows some of the UV and optical modulations just mentioned.

Furthermore, INTEGRAL satellite detected a set of magnetic cataclysmic variables (MCVs), all of the intermediate polar type except one, SS Cyg, reported as a dwarf nova (DN), that means non magnetic CV (NMCV) [68] (see Fig. 28). Then a spontaneous question arises: if SS Cyg is an NMCV, why did INTEGRAL not detect other NMCVs? Alternatively, SS Cyg is also an MCV like all the others detected by INTEGRAL.

So that it is important to determine the magnetic field intensity in the white dwarf of SS Cyg by using all information available. A critical point for this purpose is coming from the indetermination of the distance of SS Cyg: The distance, measured with the Hubble Space Telescope (HST), is D_H = 166 ± 12 pc [69], or using very long baseline interferometric radio observations the distance is D_M = 114 ± 2 pc [70], or D_P = 114.6 ± 0.6 pc [71]. Howell et al. [72] found a correlation between the strength of the high-state UV emission lines and the strength of the white dwarf magnetic field, B. By using such a relationships and the luminosity of CII and CIV derived for SS Cyg placed at distance of 166 pc or 114 pc from the fluxes measured with the IUE [73]), it is possible to derive the magnetic field intensity of order $2^{+0.5}_{-0.6}$ MG or 6^{+3}_{-2} MG depending on the distance. Figure 29 shows the luminosity of: CII vs B (left panel) and CIV vs B (right panel).

Körding et al. [74] showed the hardness intensity diagram (HID) for X-ray binaries (XRBs) and SS Cyg. The analogy among black holes, neutron stars and SS Cyg appears evident (left panel of Fig. 30). They detected also a radio jet from SS Cyg (right panel of Fig. 30), and upper limits for linear and circular polarization of 3.2 ± 2.7% and -3.2 ± 2.7%, respectively. They have some difficulties in explaining the behaviour of SS Cyg under the hypothesis that SS Cyg is a dwarf nova. Everything would be better explained if instead SS Cyg were an intermediate polar, as suggested earlier by the analysis of Fig. 29, especially if the distance of SS Cyg was 114 pc instead of 166 pc,

PoS(FRAPWS2024)035

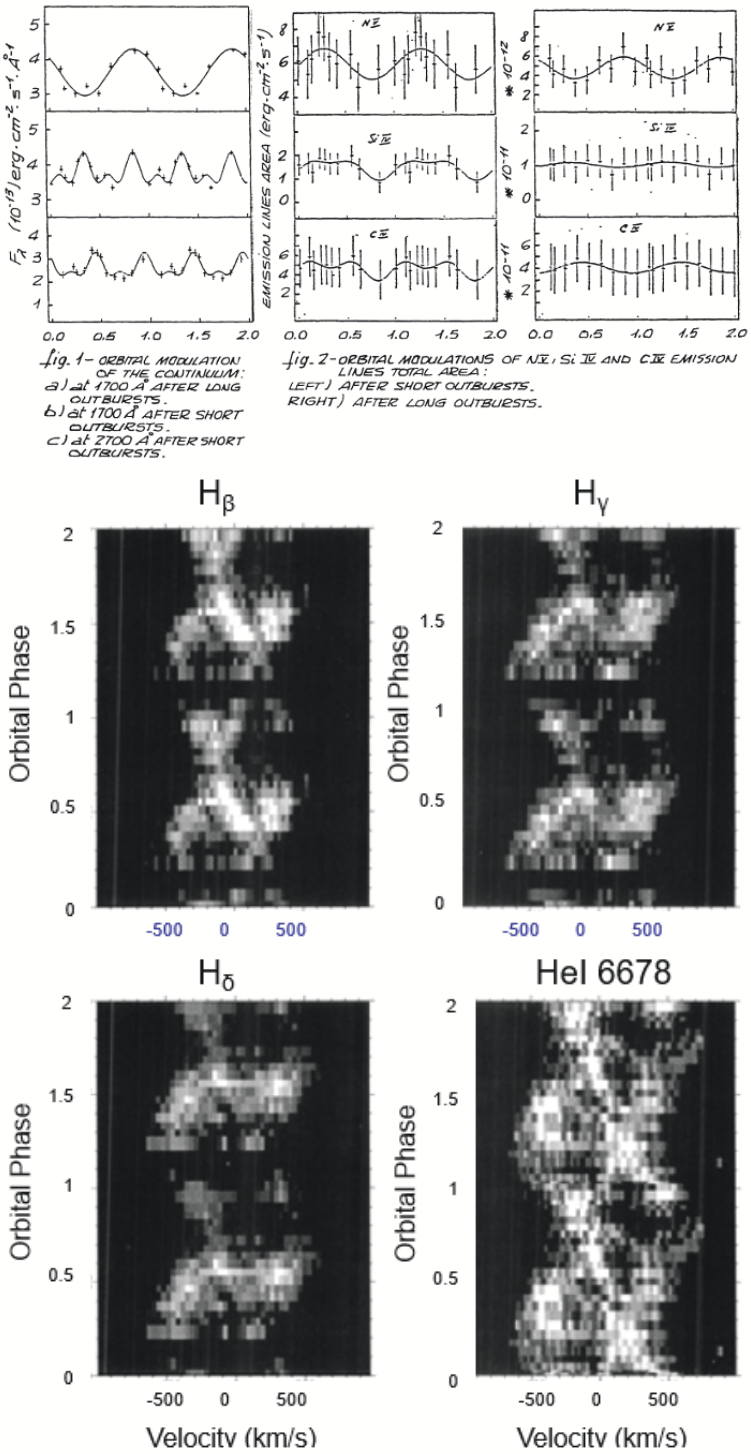

Figure 27: Upper panel: Orbital UV modulations of continuum at 1700 and 2700 and of NV, SiIV and CIV emission lines [66]. Lower panel: Trailed spectrograms of H_β, H_γ, H_δ and HeI 6678; the black band at phase ~ 0.2 in the Balmer lines are due to the lack of observations during this phase [67].

PoS(FRAPWS2024)035

Name[a]	α, δ[b] (IBIS position)	type[c]	offset[d] (′)	Map code[e]	Count rate[f] (ct s^{-1})	Exposure (ks)	Flux[g] 20-100 keV	P_{orb} (min)	P_{spin} (s)	Distance[h] (pc)	Refs
1RXS J002258.3+614111	5.739,61.714	IP	1.7	B4(8.7)	0.15 ± 0.01	3767	0.81	241.98	563.53	510	[1,2,3,4]
V709 Cas	7.207,59.303	IP	0.8	B5(54.3)	1.03 ± 0.01	3562	5.53	320.4	312.77	300	[1,2,5]
XY Ari⋆	44.047,19.457	IP	1.1	B5(5.5)	0.53 ± 0.12	119	2.85	363.884	206.298	610	[1,2,6]
GK Per	52.777,43.928	IP/DN	1.7	B5(4.7)	0.26 ± 0.07	277	1.4	2875.4	351.34	-	[1,2]
TV Col⋆	82.357,-32.819	IP	0.1	B4(11.6)	0.68 ± 0.08	248	0.37	329.181	1911	330	[1,2,7,8]
TW Pic⋆	83.766,-57.998	IP?/VY Scl?••	2.5	B1(5.8)	0.3 ± 0.07	363	1.61	-	-	-	[1,2,9,10,11]
BY Cam	85.728,60.842	AP	1.2	B5(5.1)	0.69 ± 0.11	162	3.7	201.298	11846.4	140	[1,2]
MU Cam	96.316,73.567	IP	0.6	B4(5.4)	0.24 ± 0.06	548	1.29	283.104	1187.24	440	[1,2,12]
SWIFT J0732.5−1331⋆	113.13,-13.513	IP	1.6	B3(6.1)	0.39 ± 0.06	409	2.09	336.24	512.42	-	[1,2,13]
V834 Cen	212.260,-45.290	P	0.9	B1(5.4)	0.16 ± 0.03	1675	0.86	101.51712	6091.0272	70	[1,2]
IGR J14536−5522	223.421,-55.394	P	2.0	B4 (11.9)	0.27 ± 0.03	2658	1.45	189.36	11361.6	140	[1,2,14]
NY Lup	237.052,-45.481	IP	0.5	B5(49.1)	1.17 ± 0.03	3141	6.28	591.84	693.01	-	[1,2,15]
V2400 Oph	258.173,-24.279	IP	2.2	B1(33.4)	0.68 ± 0.02	4453	3.65	204.48	927.6	180	[1,2,16]
1H 1726−058	262.606,-5.984	IP	0.7	B5(22.8)	0.85 ± 0.04	1449	4.56	925.27	128	-	[1,2,17]
V2487 Oph	262.960,-19.244	IP/N••	2.3	B3(9.1)	0.18 ± 0.02	4562	0.97	-	-	-	[1,2,18]
AX J1832.3−0840⋆	278.083,-8.721	?	3.1	B4(5.5)	0.07 ± 0.03	3090	0.38	-	-	-	[1,2,19,20]
V1223 Sgr	283.753,-31.153	IP	0.8	B5(52.2)	1.45 ± 0.03	2358	7.79	201.951	746	150	[1,2]
V1432 Aql	295.052,-10.421	AP	0.2	B5(10.8)	0.69 ± 0.07	429	3.7	201.938	12150.4	240	[1,2,21,22]
V2069 Cyg	320.906,42.279	IP•	1.8	B5(6.2)	0.21 ± 0.03	1648	1.13	448.824	743.2	-	[1,2,23,24]
1RXS J213344.1+510725	323.446,51.122	IP	0.3	B5(25.8)	0.65 ± 0.03	2207	3.49	431.568	570.82	-	[1,2,25]
SS Cyg	325.698,43.582	DN	0.6	B5(23.0)	0.7 ± 0.03	1674	3.76	396.1872	-	-	[1,2,26]
FO Aqr	334.514,-8.354	IP	1.7	B4(6.1)	0.65 ± 0.2	54	3.49	290.966	1254.45	250	[1,2,27]
AO Psc⋆	343.815,-3.194	IP	1.3	B4(4.8)	0.43 ± 0.11	108	2.31	215.461	805.2	200	[1,2,28,29]

Figure 28: List of Cataclysmic Variables detected by the INTEGRAL satellite (adopted from [68]. Light red rectangle marks SS Cyg.

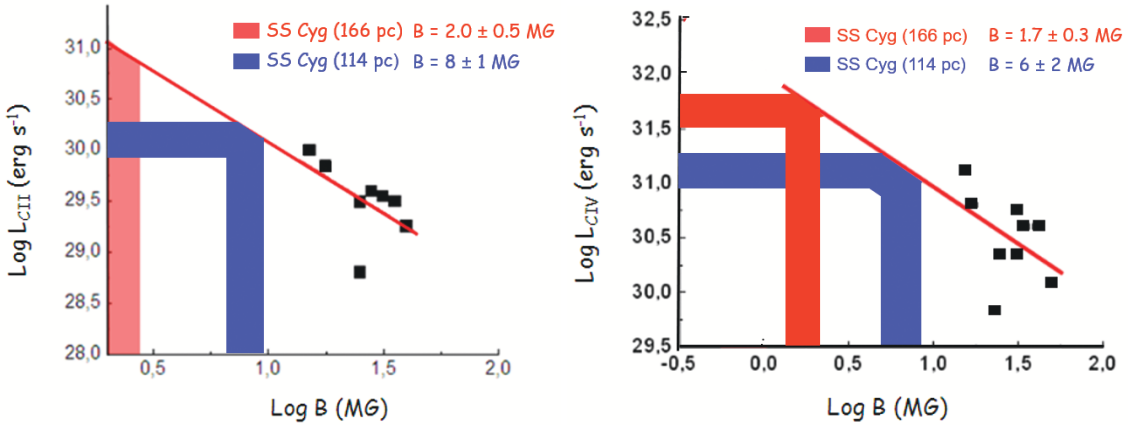

Figure 29: Left panel: CII luminosity vs B (from [72] black squares). Right panel: CIV luminosity vs B (from [72] black squares). The luminosities of CII and CIV of SS Cyg are coming from [73].

so the intensity of the magnetic field would be approximately 6 MG. This value of B would support the expectation of Dubus et al. [75] to explain the variations in the mid-IR (11.7 μm) emission.

A complete discussion about the controversial nature of the cataclysmic variable SS Cygni is reported in the recent paper by Giovannelli et al. [76].

2.9 The Astron satellite

The N. Copernicus Center opened in May 1978 and began to play an important role as a meeting place for scientists from the Soviet bloc (Warsaw Pact) and the West bloc (Atlantic Pact). In 1979, during my second stay at the N. Copernicus Center as guest of the Polish Academy of Sciences, I met Gennady Bisnovatyi-Kogan with whom I laid the foundations for scientific collaboration and friendship over a bottle of Vodka Wyborowa. Gennady and his PhD student Sergey Lamzin had just published "The chromosphere, corona, and X-ray emission of the T Tauri star RU Lupi" [77] in

PoS(FRAPWS2024)035

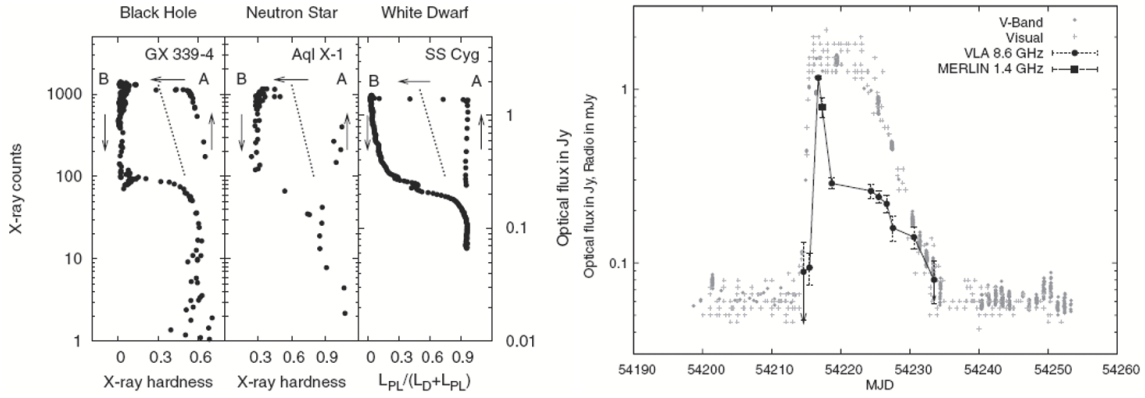

Figure 30: Left panel: Hardness intensity diagrams (HID) for a black hole, a neutron star and the dwarf nova SS Cyg. The arrows indicate the temporal evolution of an outburst. The dotted line indicates the "jet line" observed in black hole and neutron star XRBs: on its right side one generally observes a compact jet; the crossing of this line usually coincides with a radio flare. The hardness ratio for XRBs is defined as the ratio of the counts in the 6.3-10.5 keV range to 3.8–6.3 keV range, and the X-ray counts represent the 3.8–21.2 keV counts of the Rossi X-ray Timing Explorer. For SS Cyg L_D is the disc/boundary layer luminosity derived from the extreme ultra-violet counts. The X-ray luminosity L_{PL} is for the 3-18 keV energy range. Right panel: Radio and optical light-curve of SS Cyg (adopted from [74]).

which they proposed models (developed in 1979) that would need experimental data in the UV and X-ray bands to be validated. So the game was up: the recently launched IUE satellite, as well as all ESO telescopes for optical and infrared measurements (accessible to me) and the Astron satellite (accessible to him) would be the ideal tools to test the models. And so a fruitful collaboration was born.

Figure 31 shows the main characteristics of the Astron satellite (https://imagine.gsfc.nasa.gov/science/toolbox/missions/astron.html). I was the only foreign guest observer to use this satellite.

The Astron satellite was designed for ultraviolet and X-ray astrophysical observations in the 2-25 keV energy range.

2.9.1 The X-ray pulsar Her X-1

One of the most important results was the monitor of Hercules X-1 (1983-1987), providing data during its low state in 1983 and from when it turned back on in 1984 [78]. Figure 32 shows the configuration of the inner edge of the disk and the neutron star (a); neutron star and the disk in the "low-on" state (b); neutron star and the disk in the "high-on" state.

Sheffer et al. [78] suggested a geometrical model to explain the structure of the main pulse and the variations in its profile with the phase of the 35-day cycle.

2.9.2 The Classical T Tauri Star RU Lupi

A long-term (1982-1988) multifrequency program on Classical T Tauri Stars (CTTSs) was developed by the international group leaded by Franco Giovannelli. The facilities used for such a campaign were the International Ultraviolet Explorer (IUE), the ASTRON X-ray/UV Soviet satellite, and the ESO 0.6-m UBVRI telescope, 1-m IR telescope, 1.5-m telescope for low resolution optical spectroscopy, and 3.6-m telescope for Echelle high resolution spectroscopy.

PoS(FRAPWS2024)035

Astron

Lifetime: March 1983 – June 1989

Country (primary): Soviet Union

Primary Science

The Astron satellite was designed for ultraviolet and X-ray astrophysical observations (2-25 keV)

Science Highlights

- Monitored Hercules X-1, providing data during its low state in 1983 and from when it turned back on in 1984
- Investigation of accretion of material from red giants onto neutron stars

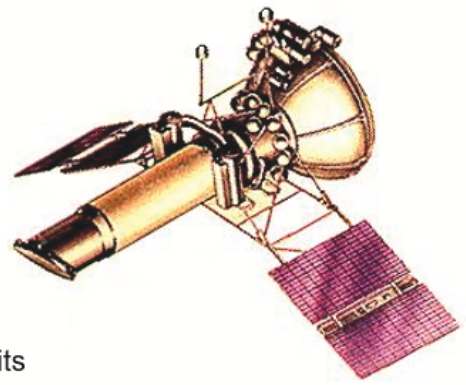

An artist's impression of the Astron spacecraft (Credit: Soviet Space Program)

Figure 31: Main characteristics and science highlights of the Astron satellite (adapted from https://imagine.gsfc.nasa.gov/science/toolbox/missions/astron.html).

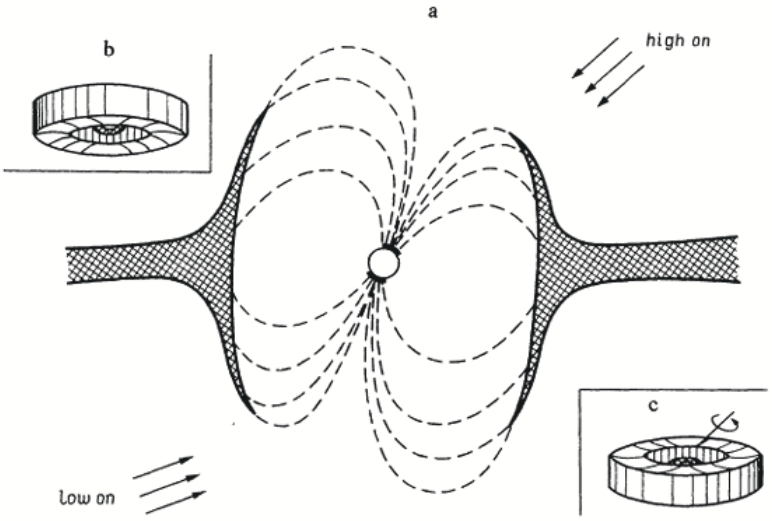

Figure 32: Configuration of the inner edge of the disk and the neutron star (a); neutron star and the disk in the "low-on" state (b); neutron star and the disk in the "high-on" state (adopted from [77]).

PoS(FRAPWS2024)035

The results were published in two main papers, the first with the experimental results (Giovannelli et al. [79]), the second with the interpretation of data and modeling (Lamzin et al. [80]). A review paper about RU Lupi was published by Giovannelli [81].

One of the main results obtained during the long-term multifrequency program was the simultaneous detection of emissions in different energy bands that allowed to construct the Spectral Energy Distribution (SED) of RU Lupi, as shown in the upper panel of Fig. 33.

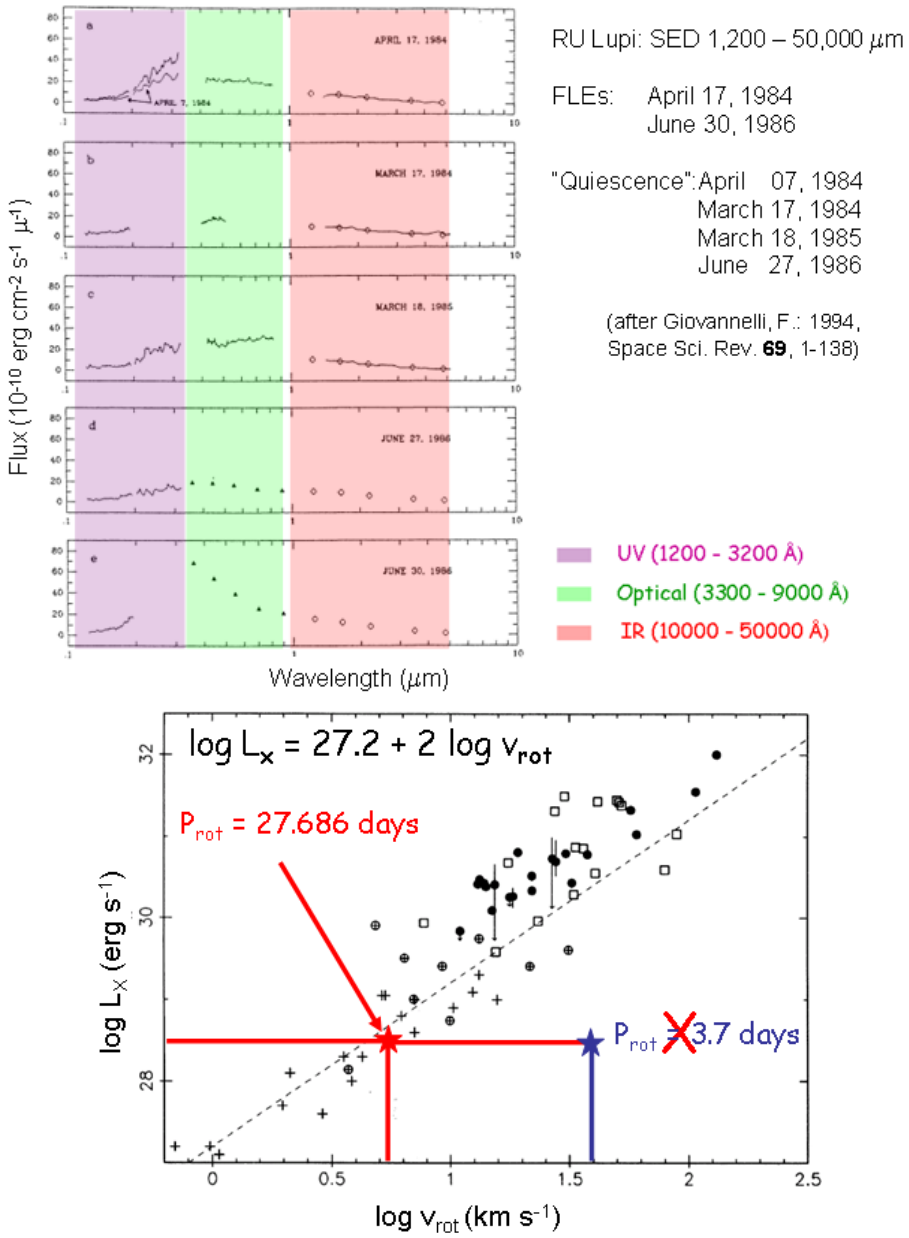

Figure 33: Left panel: SED (1,200-50,000 μm) of RU Lupi in different epochs (adapted from [81]). Right panel: X-ray luminosity vs stellar equatorial velocity for TTS (•), late-type dwarfs (+), dKe-dMe stars (⊕), and RS CVn systems (square). The right position of RU Lupi is marked with a red star, and the wrong position is marked with a blue star (adopted from [81] after [82]).

PoS(FRAPWS2024)035

In two occasions, RU Lupi showed a strong activity (Flare-Like Events: FLEs), much higher than that in "quiescence". Together with the FLEs reported in the literature, these two FLEs allowed to determine their periodicity: P_{FLEs} = 27.686 ± 0.002 days [81]. This could be the rotational period of RU Lupi. Indeed, if we use the relationship between the X-ray luminosity (L_X) versus the rotational velocity (v_{rot}) for T Tauri stars, late-type dwarfs, dKe-dMe stars, and RS CVn systems (Bouvier [82]), the position of RU Lupi fits the relationship $\log L_X = 27.2 + 2 \log v_{rot}$ if P_{FLEs} = 27.686 ± 0.002 days is used, instead of using the "wrong" value reported in the literature of 3.7 days – that simply does not exist (Giovannelli et al. [83]) – whose wrong origin is largely commented in [81]. Lower panel of Fig. 33 shows the diagram of the X-ray luminosity (L_X) versus the rotational velocity (v_{rot}) where the "correct" position of RU Lupi is overlapped with a red star, and the "wrong" position with the blue star.

With the 27.7-day periodicity at which FLEs repeat, one can explain the positive detection of RU Lupi in the X range (2-25 KeV) made with the ASTRON satellite (Giovannelli, F. et al. [84]): this detection occurred in phase with this period, while some observations made with other satellites, including ASTRON, provided only upper limits on the emission, with measurements obtained in anti-phase.

2.9.3 Orbital Period of A 0535+26/HDE 245770 and Spin Period of the X-ray Pulsar

As discussed by Bartolini et al. [85] two very similar events in optical occurred on February 24, 1976 and December 20, 1977 (see Fig. 34). The slope of these growths in V magnitude of HDE 245770 was the same and such events were associated to X-ray flares [86,87]. The time elapsed between the two events is 665.137 ± 0.002 days, close to six times the suggested period of 110-111 days [86,88,89]. Thus a period of 110.856 ± 0.002 days has been deduced.

Giovannelli et al. [90] published the history of the spin period of the pulsar A 0535+26 from its discovery in 1975 with the Ariel V satellite [91] until 1990, as shown in Fig. 35. A value of $\dot{P}/P$ = -6.8 $\times 10^{-4}$ yr^{-1} was deduced by Giovannelli et al. [92].

Since the X-ray flares of A 0535+26 occurred regularly in phase with the orbital period (~ 111 days), we expected to detect with the Astron satellite X-ray outbursts at periastron passage on April 19, 1985 and March 17, 1986. ASTRON did not detect such X-ray outbursts, but measured X-ray fluxes of ~ 6.5 mCrab and < 5 mCrab, respectively in the energy range 2-25 keV. The probable reason of the lack of X-ray outbursts was that the pulsar A 0535+26 was rotating at equilibrium period, too fast for material to enter [93].

By analyzing the data related to the X-ray flare of December 1977-January 1978 from various experiments reported by Violes et al. [94], it is possible to relate the optical event of December 20, 1977 reported by Bartolini et al. [85] and Rōssiger [95] with the X-ray flare reported in [94]. The delay of about 8 days of the X-ray flare with respect to the optical flare is evident (see Fig. 36). And this delay will be extensively commented in the next section 2.10. The flux was still quite weak on 1977 December 20.5, when Chartres & Li [87] observed a soft X-ray flare-up in the 2-10 keV energy range. The flux was equal to that from the Crab on December 25 and reached a maximum (1.5 times that of the Crab) on December 28. Four periods were defined in the time history (A, B, C, and D) shown in Fig.36 and commented in [94].

PoS(FRAPWS2024)035

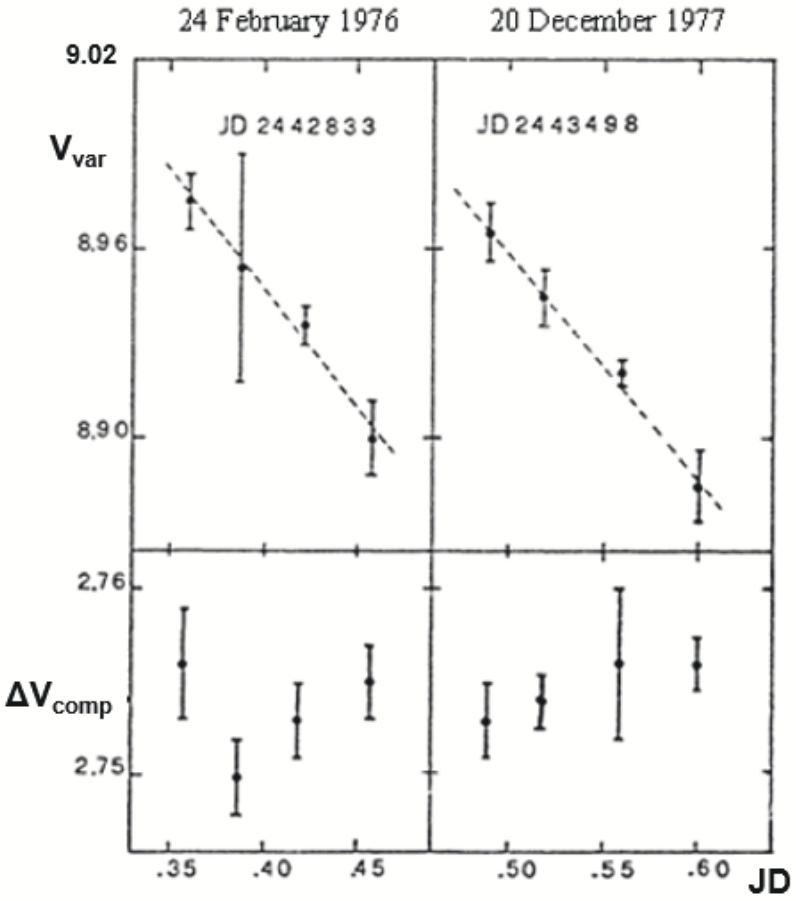

Figure 34: Up: V magnitude of HDE 245770 on the JD 2442833 and JD 2443498 deduced from both comparison stars BD 26°876 and 125 Tau. Down: differences of magnitude between the two comparison stars during the same night (adapted from [85]).

2.10 The Hakucho [CORSA-B] satellite

CORSA-B satellite – renamed Hakucho (Japanese for swan) – was launched on 21 February 1979. It was dedicated to study and monitor transient phenomena in the energy range 0.1-100 keV. Figure 37 shows its main characteristics (https://heasarc.gsfc.nasa.gov/docs/hakucho/hakucho.html).

The importance of the Hakucho satellite in my research comes from a suggestion that a member of my group, Adriano Guarnieri, made to the Hakucho group by telegram in which he suggested to make an observation of A 0535+26 around 13 December 1981 because our group had detected an optical flare on 5 December 1981 – named 811205E. The Hakucho team detected a short X-ray flare just at the predicted date (December 13, 1981) [96]. This amazing prediction was published by Giovannelli & Sabau-Graziati [97]. Fig. 38 shows the optical measurements of HDE 245770 made at the telescope of Loiano (Guarnieri et al. [98]). Superimposed are two vertical lines, a red one indicating the maximum of the optical event and a blue one indicating the X-ray event. The separation between the two events is 8 days.

And this event of December 5, 1981 (JD 2444944) is exactly 13 orbital cycles distant from the

PoS(FRAPWS2024)035

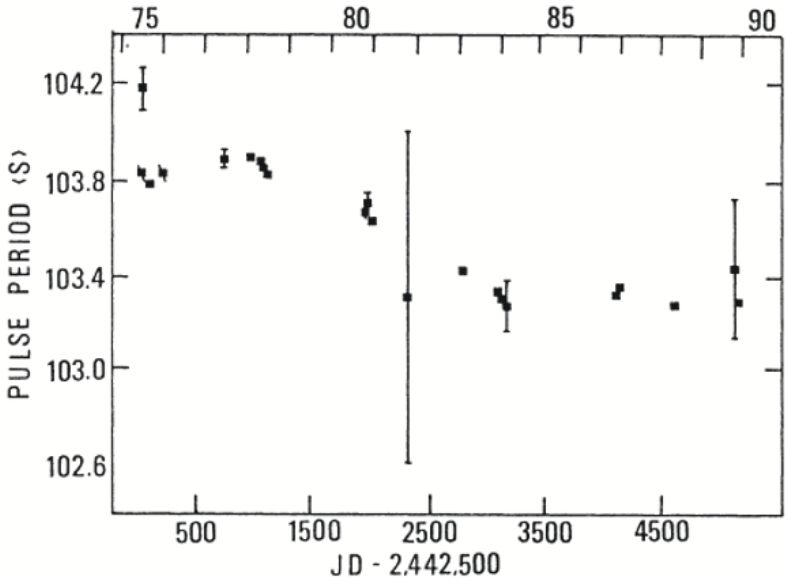

Figure 35: The history of spin period of the X-ray pulsar A 0535+26 (adopted from [90]).

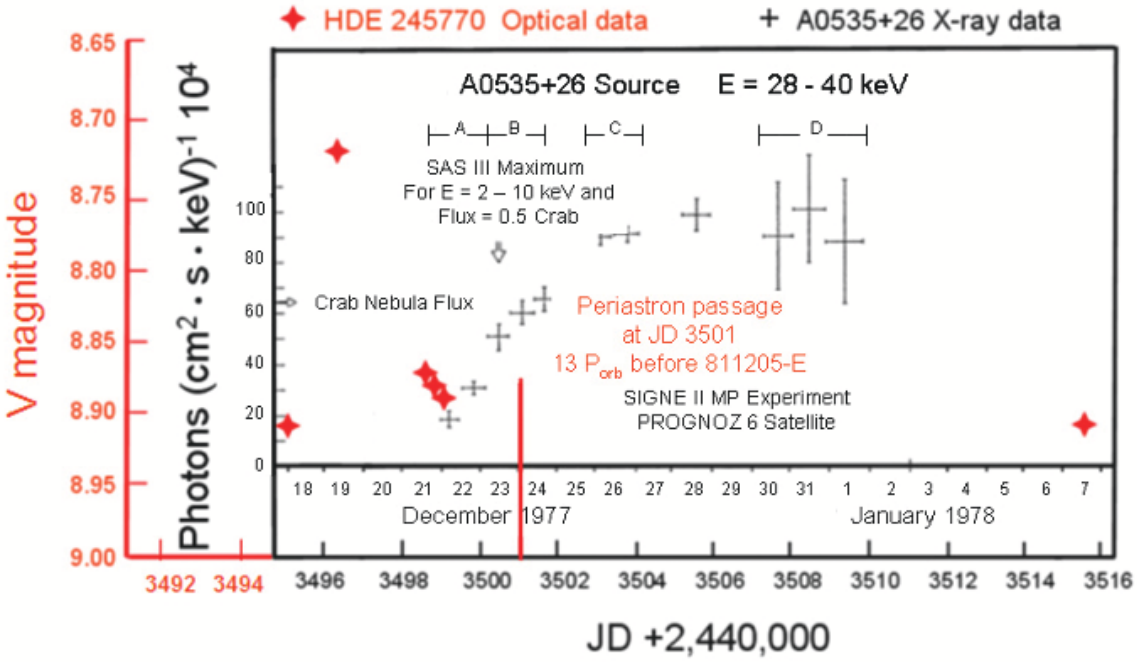

Figure 36: The 28-40 keV light curve of A 0535+26 for the 1977 December flare-up. For comparison, the 28-40 keV Crab Nebula flux is indicated by a horizontal arrow. The vertical arrow indicates the moment of the maximum 2-10 keV flux observed by SAS 3. Four periods for the energy spectra – discussed in [94] – are designated A, B, C, and D. (adapted from [94]). Optical flare of HDE 245770 [85,95] (red stars) preceding the X-ray outburst of A 0535+26. The red line marks the periastron passage at the thirteenth cycle before 811205-E (adapted from [99]).

PoS(FRAPWS2024)035

The Hakucho [CORSA-B] Satellite

Corsa-B was the first X-ray astronomy Japanese satellite. Launched on 21 February 1979, it was renamed Hakucho (Japanese for swan) symbolizing one of the most interesting X-ray objects, Cyg X-1. As many other X-ray satellite launched in that period, Hakucho was designed to study and monitor transient phenomena with particular emphasis on X-ray bursts. It was still operating when the second X-ray Japanese satellite Tenma launched in 1983.

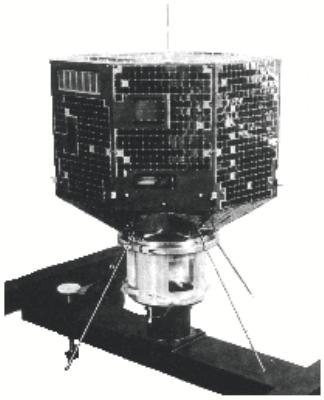

Mission Characteristics

- **Lifetime** : 21 February 1979 - 16 Aprile 1985
- **Energy Range** : 0.1 - 100 keV
- **Payload** :
  - Very Soft X-ray (VSX) experiment 0.1-0.2 keV
    Four units of proportional counters
    each with eff area ~ 78 cm^2
    Two parallel to the spin axis FOV = 6.3° X 2.9° FWHM
    two offset FOV = 24.9° X 2.9° FWHM
  - Soft X-ray (SFX) 1.5-30 keV Six units of proportinal counters
    Parallel to the spin axis :
    - Two FOV 17.6 deg FWHM; eff area=69 cm^2 each
    - Two FOV 5.8 deg FWHM; eff area=40&83 cm^2

    Two offset FOV = 50.3° X 1.7° FWHM eff area =32 cm^2 each
  - Hard X-ray (HDX) 10-100 keV scintillator
    FOV 4.4° X 10.0° FWHM eff area =45 cm^2

- **Science Highlights**:
  - Discovery of soft X-ray transient Cen X-4 and Apl X-1
  - Discovery of many burst sources
  - Long-term monitoring of X-ray pulsar (e.g. Vela X-1)
  - Discovery of 2 Hz variability in the Rapid Burster later named Quasi Period Oscillation.

- **Archive** : No data available at HEASARC

Figure 37: The main characteristics of the Hakucho [CORSA-B] satellite (https://heasarc.gsfc.nasa.gov /docs/hakucho/hakucho.html).

event of December 20, 1977 (JD 2443498), assuming the orbital period of 111.0 ± 0.4 days; this value is in agreement with all optical and X-ray determinations.

Giovannelli, Bisnovatyi-Kogan & Klepnev [99] (here after GBK13) used the 811205E for constructing the ephemerides of the system A 053526/HDE 245770 as $JD_{opt-outb} = JD_0(2{,}444{,}944) \pm n(111.0 \pm 0.4)$ d. So, going back 22 orbital periods we get what is shown in Fig. 39: the periastron passage of the neutron star occurred about 14 days before the discovery of the X-ray pulsar by the satellite Ariel V [91]. There are no previous X-ray data and therefore it cannot be excluded that the X-ray event could have started a few days earlier, exactly 8 days after the periastron passage.

In conclusion GBK13 [99] showed that the optical behavior of the Be star in the high-mass X-ray transient A0535+26/HDE245770 shows that at periastron the luminosity is typically enhanced by 0.02 to a few tenths mag, and the X-ray outburst occurs eight days after the periastron. They constructed a quantitative model for this event based on a nonstationary accretion disk behavior, connected with a high ellipticity of the orbital motion. They explained the observed time delay between the peaks of the optical and X-ray outbursts in this system by the time of radial motion of the matter in the accretion disk, after an increase of the mass flux in the vicinity of a periastral point in the binary. This time is determined by the turbulent viscosity with a parameter of α = 0.1-0.3. The increase of the mass flux is a sort of flush that reaches the external part of the accretion disk

PoS(FRAPWS2024)035

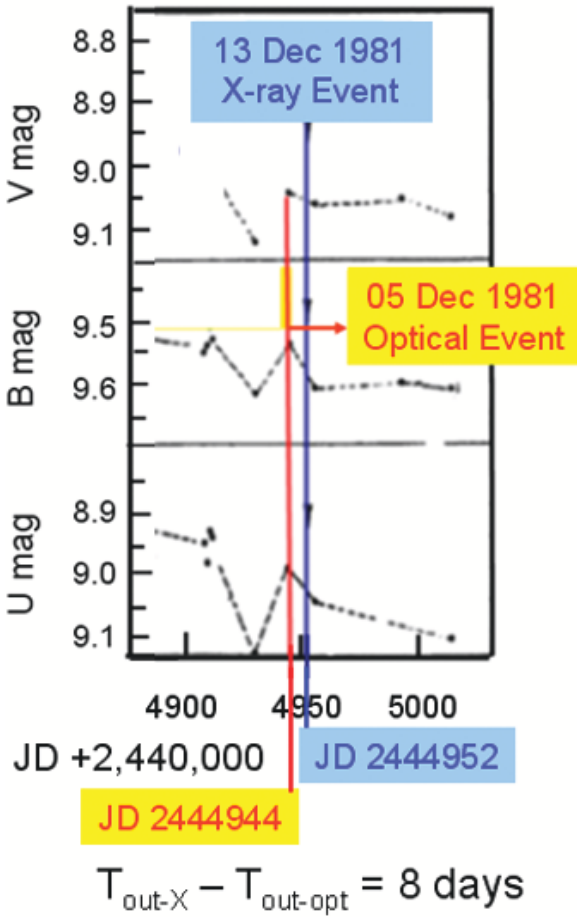

Figure 38: UBV measurements of HDE 245770 on December 1981. Red vertical line shows the maximum of the optical flare occurred on December 5, 1981 (JD 2444944) and the blue one indicating the time (December 13, 1981 = JD 2444952) when the X-ray flares occurred (adapted from [97], with the data from [98]).

around the neutron star, which enhances the optical luminosity. The subsequent X-ray flare occurs when the matter reaches the hot central parts of the accretion disk and the neutron star' surface.

Their model may be valid also for AGNs. Indeed, Nandra et al. [100] found a delay of ~ four days between UV and X-ray emissions in NGC 7469; Maoz, Edelson & Nandra [101] found a delay of ~ 100 days between optical and X-ray emissions in the Seyfert galaxy NGC 3516; Marshall, Ryle & Miller [102] found a delay of ~ 15 days between optical and X-ray emissions in Mkr 509, and Doroshenko et al. [103] found a delay of ~ ten days between R, I and X-ray luminosities in the Seyfert galaxy 3C 120. It is interesting that a short qualitative explanation of these lags in AGNs, very similar to their quantitative model, was suggested by Marshall et al. [102].

Giovannelli et al. [104] planned optical measurements mainly around the periastral passages of the neutron star with the aim of verifying the validity of the model developed in [99]. Their observations – planned around the 108th orbital periods after 811205E (JD2456932 ≡ October 1, 2014) – showed an optical enhancement of ~ 0.03 mag that enabled them to announce the subsequent X-ray outburst with intensity of 10-100 mCrab (Giovannelli et al. [105,106]), that indeed was detected and culminated on JD 2456940 with a ~ 50 mCrab intensity (Nakajima et al.

PoS(FRAPWS2024)035

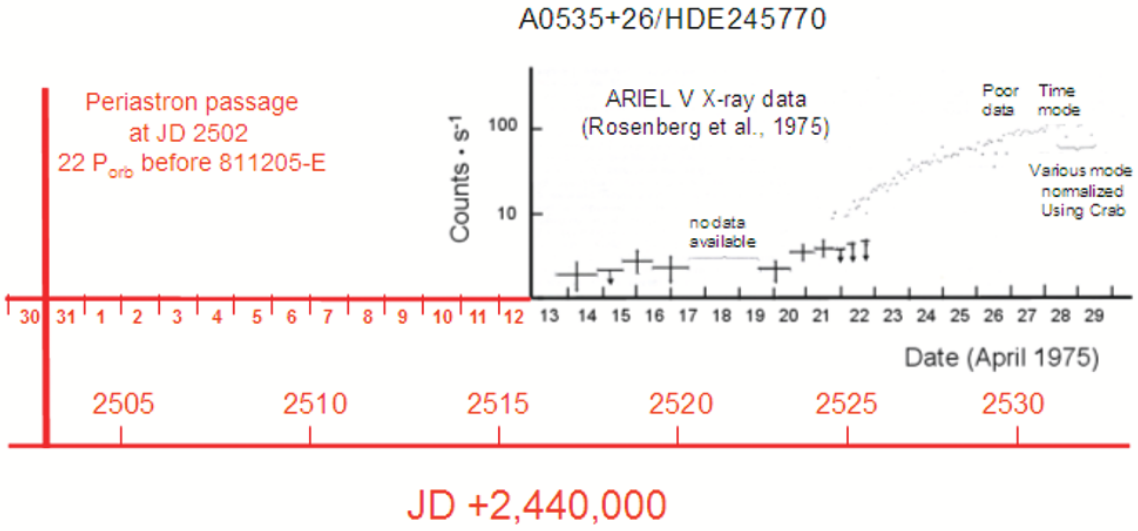

Figure 39: The periastron passage of the neutron star 22 orbital periods before 811205E and the data of the discovery of A 0535+26 taken from [91] adapted from [99]).

[107]). This is an astonishing confirmation of the time-delay model developed by GBK13 [99].

It is right to remind that the mechanism proposed by GBK13 for explaining the X-ray-optical delay in A 0535+26/HDE 245770 is based on an enhanced mass flux propagation through the viscous accretion disk. This mechanism, known as UV-optical delay (the delay of the EUV flash with respect to the optical flash) was observed and modeled for cataclysmic variables (e.g. Smak [108]; Lasota [109]). Time delays have been detected also in several other X-ray transient binaries. This is the reason that urged Bisnovatyi-Kogan & Giovannelli [110] to generalize the aforementioned model, developed for the particular case of A 0535+26/HDE 245770 (Flavia' star). This general model provides the formula (1) of the time delay between the optical and X-ray flashes appearance in transient cosmic accreting sources:

$$\tau = 6.9 \frac{m^{2/3} \dot{m}^{1/15}}{\alpha^{4/5} (T_4)^{28/15}} \qquad (1)$$

where:

$m = M/M_\odot$; $\dot{m} = \dot{M}/(10^{-8}\ M_\odot/\mathrm{yr})$; $T_4 = T_0/10^4$ K ;

α = viscosity , and T_0 = maximum temperature in optics.

By using this formula it is possible to obtain an excellent agreement between the experimental and theoretical delays found in:

- X-ray/Be system A0535+26/HDE245770: $\tau_{exp} \simeq 8$ days (GBK13); $\tau_{th} \simeq 8$ days;
- Cataclysmic variable SS Cygni; $\tau_{exp} = 0.9$–1.4 days [111]; $\tau_{th} \simeq 1.35$ days;
- Low-mass X-ray binary Aql X-1/V1333 Aql: $\tau_{exp} \sim 3$ days [112]; $\tau_{th} \simeq 3.2$days
- Black hole X-ray transient GRO J1655-40: $\tau_{exp} \sim 6$ days [113]; $\tau_{th} \simeq 6.5$ days.

PoS(FRAPWS2024)035

In this general formula the α-viscosity parameter plays an important role, and usually it is hard to be determined. However, if the other parameters are known, because experimentally determined, the formula (1) can be used for determining α, taking into account the experimental delay measured in a certain source.

In [110] the authors quantitatively also discuss a model for time-lag formation in active galactic nuclei (AGNs).

2.11 ROSAT - The Roentgen Satellite

The Roentgen Satellite, ROSAT, a Germany/US/UK collaboration, was launched on June 1, 1990 and operated for almost 9 years. The first 6 months of the mission were dedicated to the all sky-survey (using the Position Sensitive Proportional Counter detector), followed by the pointed phase. The survey obtained by ROSAT was the first X-ray (0.1 - 2.5 keV) and EUV (62-206 eV) all-sky survey using an imaging telescope with an X-ray sensitivity of about a factor of 1000 better than that of UHURU.

Figure 40 shows its main characteristics (https://heasarc.gsfc.nasa.gov/docs/rosat/rosat.html).

The Roentgen Satellite, ROSAT, a Germany/US/UK collaboration, was launched on June 1, 1990 and operated for almost 9 years. The first 6 months of the mission were dedicated to the all sky-survey (using the Position Sensitive Proportional Counter detector), followed by the pointed phase. The survey obtained by ROSAT was the first X-ray and XUV all-sky survey using an imaging telescope with an X-ray sensitivity of about a factor of 1000 better than that of UHURU. During the pointed phase ROSAT made deep observations of a wide variety of objects.

Mission Characteristics

- **Lifetime** : 1 June 1990 - 12 February 1999
- **Energy Range** : X-ray 0.1 - 2.5 keV , EUV 62-206 eV
- **Special Feature** : All sky-survey in the soft X-ray band
- **Payload** :
  - An X-ray telescope used in conjunction with one of the following instruments (0.1-2.5 keV)
    - Position Sensitive Proportional Counter
      (PSPC) 2 units : detector B, used for the pointed phase, & detector C ,used for the survey
      FOV 2 ° diameter eff area 240 cm^2 at 1 keV
      energy resolution of deltaE/E=0.43 $(E/0.93)^{-0.5}$
    - High Resolution Imager (HRI)
      FOV 38 ' square ; eff area 80 cm^2 at 1 keV
      ~ 2 arcsec spatial resolution (FWHM)
  - A Wide Field Camera with its own mirror system
    (62-206 eV) FOV 5 ° diameter

- **Science Highlights**:
  - X-ray all-sky survey catalog, more than 150000 objects
  - XUV all-sky survey catalog (479 objects)
  - Source catalogs from the pointed phase (PSPC and HRI) containing ~ 100000 serendipitous sources
  - Detailed morphology of supernova remnants and clusters of galaxies.
  - Detection of shadowing of diffuse X-ray emission by molecular clouds.
  - Detection (Finally!) of pulsations from Geminga.
  - Detection of isolated neutron stars.
  - Discovery of X-ray emission from comets.
  - Observation of X-ray emission from the collision of Comet Shoemaker-Levy with Jupiter.

- **Archive** : HEASARC hosts Catalogs, Spectra, Lightcurves, Images and Raw data

Figure 40: The main characteristics of the ROSAT satellite (https://heasarc.gsfc.nasa.gov/docs/rosat/rosat.html).

PoS(FRAPWS2024)035

I was in Garching in the early 1990s for looking at ROSAT observations around A 0535+26. I noted that the soft spectrum had a shape similar to that of a Supernova Remnant (SNR).

I then hypothesized that A 0535+26 was "immersed" in a SNR. So, Giovannelli et al. [114, 115] suggested that the SNR S 147 could have been originated by an asymmetric supernova explosion in a moderate massive B-type binary system which produced the A 0535+26 pulsar, eccentrically orbiting around the O9.7 IIIe star HDE 245770.

Looking at the catalog of SNRs I discovered that the pulsar was placed at the border of the SNR S147. Minkowski [116] discussed about "*Cygnus Loop and Some Related Nebulosities*". Figure 41 shows the R. Minkowski's 48 inch Schmidt photograph of S147, exposed 2 hours on 103a-E with an OR 1 filter and reproduced in [117]. The red star indicates the position of A 0535+26/HDE 245770 system.

But it was necessary to verify if the distance of the SNR S147 were the same of the pulsar A 0535+26, as well as the age and position.

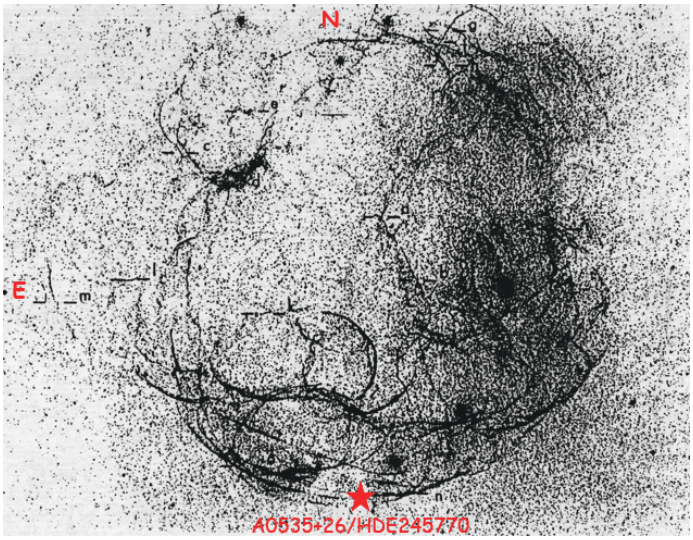

Figure 41: Minkowski's 48 inch Schmidt photograph of S147, exposed 2 hours on 103a-E with an OR 1 filter. The red star indicates the position of A 0535+26/HDE 245770 system.

- **Age**: following the rotational history of the pulsars in massive X-ray binaries [118] and relationship between the pulse period and the time since the SN explosion, which originated the binary system [119], a 104-s X-ray pulsar can be the collapsed remnant of a SN explosion occurred roughly 2×10^5 years ago. Figure 42, adapted from [119], shows the suggested phases in the rotational evolution of a pulsar that was born in a massive binary system (HMXB) and superimposed the representative points of the X-ray/Be systems A 0535+26/HDE 245770, GPS 1722-36, and the accreting neutron star 1E 2259+586, probably in a low mass X-ray binary (LMXB). The ages of the three X-ray pulsars are roughly in agreement with the ages of the correspondent SNRs, derived from radio measurements. For example, the derived age of S 147 is ~ 110,000 years [120], compatible with that derived by using the curve reported in Fig. 42. The value of S 147 distance of 2×10^5 yr is in perfect agreement with Sofue, Fürst & Hirth [121].

PoS(FRAPWS2024)035

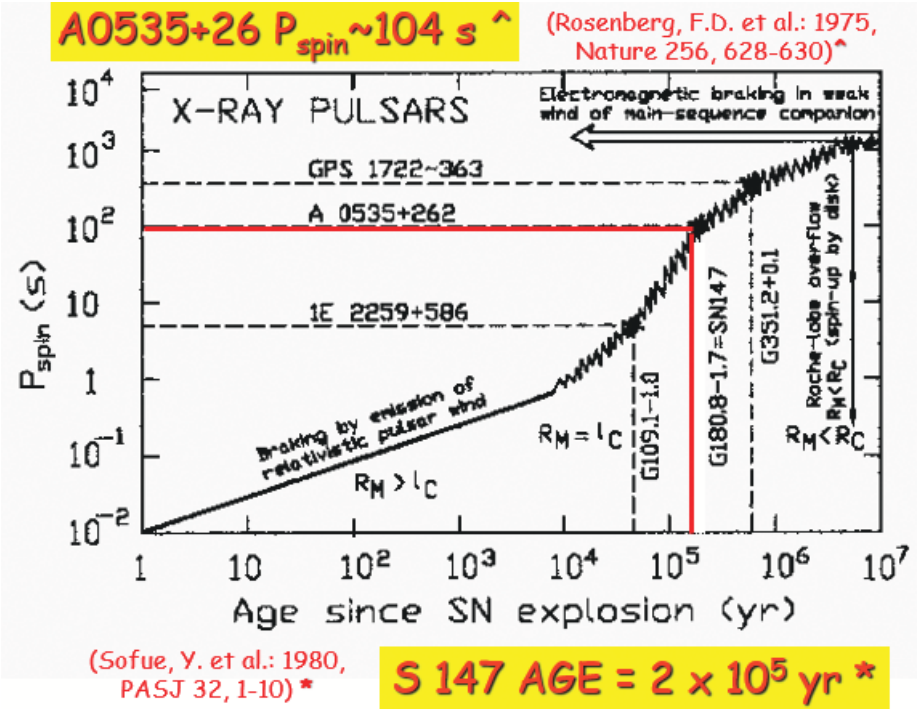

Figure 42: Suggested phases in the rotational evolution of a pulsar that was born in a massive close binary system. R_M, R_c and l_c are the radius of the magnetosphere, of co-rotation and of the light cylinder, respectively. The positions of the X-ray/Be systems A 0535+26/HDE 245770, GPS 1722-36, and the accreting neutron star 1E 2259+586 are reported together with the correspondent SNRs G 180.8-1.7 ≡ SN147, G 351.2+0.1 and G 109.1-1.0, respectively (adapted from [122]).

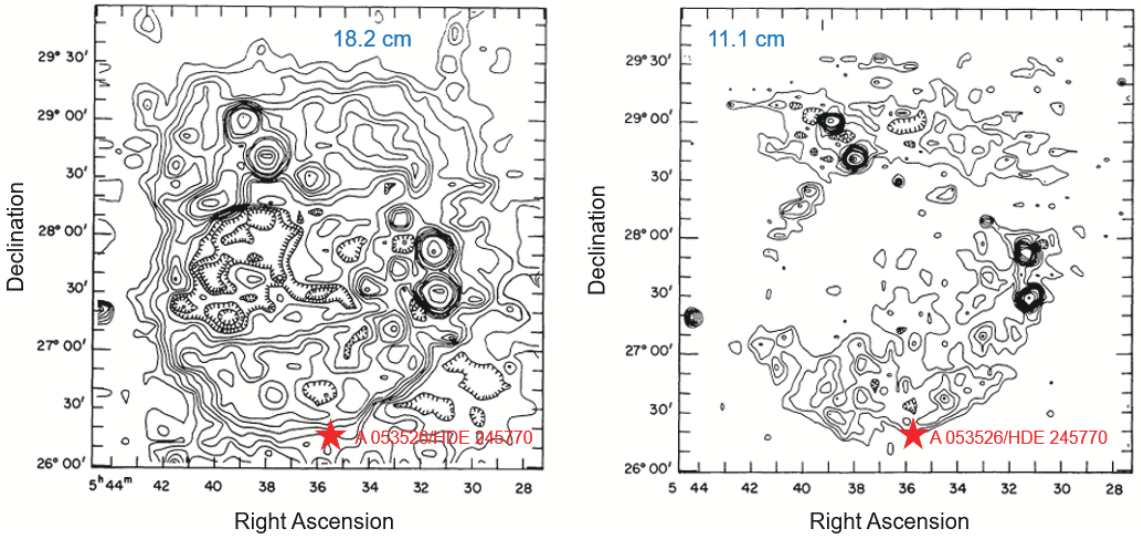

Figure 43: Radio maps at 18.2 cm (left panel) and at 11.1 cm (right panel) of the SNR S 147 (adapted from [120]). The red stars indicate the position of the binary system A 0535+26/HDE 245770.

PoS(FRAPWS2024)035

- **Distance**: the SNR S 147 is placed at 1.4 ± 0.3 kpc [123, 124] and HDE 245770 is placed at 1.8 ± 0.6 kpc [50]. The SNR S 147 southern rim raches the position of A 0535+26. This fact is supported by the radio maps of the SNR made at 18.2 cm and 11.1 cm [120], as shown in Fig. 43. Therefore, the distances of the X-ray/O9.7 IIIe system and SNR S 147 are fully compatible.

- **Position**: the proper motion of HDE 245770 is poorly determined (SAO catalog) and only upper limits of 2×10^{-2} arcsec yr^{-1} in right ascension and declination are given. Assuming these upper limits as the components of the proper motion of the O9.7 IIIe star, at a distance of 1.8 kpc, the HDE 245770/A 0535+26 system has traveled ~ 33 pc in ~ 2×10^5 yr. This figure is compatible with the estimated radius of the SNR S 147, from radio measurements [120]. Thus, the X-ray/O9.7 IIIe system in order to cross 33 pc in 2×10^5 yr (the age of S 147 derived from Fig. 42) would have had a velocity of ~ 160 km s^{-1}, which is a value compatible with the possible kick velocity in an asymmetric SN explosion [123-125], and lower than the tangential orbital velocity of the system, which is ~ 210 km s^{-1} [126].

Once the association between the system A 0535+26/HDE 245770 and the supernova remnant S 147 was established, Giovannelli & Sabau-Graziati [122] looked for the association between the sample of HMXB transient sources (HMXBTSs) – reported in Table 1 of Giovannelli et al. [127] – containing 51 objects, known at that time. Among these, 38 systems were recognized as containing X-ray pulsars. A list of galactic X-ray pulsars, updated to 2001, contained 88 of them [127]. All these binary systems are concentrated on the galactic plane in a narrow band of galactic latitude (3°.9) and uniformly distributed in galactic longitude [128]. Therefore, their spatial density is:

$$D = 88/(360 \times 3.9) = 0.0627 \text{ Deg}^{-2}$$

Supposing, in the first approximation, that the distribution is gaussian, the standard deviation is $\sigma = 7.9 \times 10^{-3}$ Deg^{-2}.

In the same band of 3°.9 around the galactic plane, the 220 SNRs of the Green's catalog [129] are concentrated on the galactic plane [130], with the exception of few objects. Taking into account the dimensions of each SNR [129], all the SNRs in such a band keep occupied ~ 100 Deg^2. Supposing the two distributions independent, the casual coincidence between the X-ray pulsars and SNRs is:

$$N = (62.7 \pm 7.9) \times 10{-}3 \times 100 \simeq 6.3 \pm 0.8$$

Figure 44 shows 41 X-ray pulsars which lie within SNRs. This number of coincidences exceeds roughly seven times what is expected from chance coincidence.

Anderson et al. [131] reported the presence of the 143 ms pulsar PSR J0538+2817 in SNR S 147 (G180.0-1.7), whose age is 6×10^5 yr, stating that this age is compatible with that of S 147 estimated to be 0.8-1.6 kpc.

There is no mention of the possibility that there may be another system – such as A 0535+26/HDE 245770 – that may be associated with S 147, as previously published by Giovannelli et al. [132,115,127].

Reich, Zhang & Fürst [133] report the radio map of S 147, shown in Fig. 45, in which the positions of PSR J0538+2817 and A 0535+26/HDE 245770 are reported with a violet cross and a red star, respectively. My personal impression is that there is a sensible discrepancy in the ages of

PoS(FRAPWS2024)035

X-Ray Pulsar	Spin Period (s)	SNR	SNR Diameter (arcmin)@1 GHz
4U 0115+634	3.6	G126.2+1.6	70
4U 0142+614	8.69	G127.1+0.5	45
RX J 0146.9+6121	1413	G132.7+1.3	80
RX J 0440.9+4431	220.5	G160.9+2.6	140x120
A 0535+262	104	G180.0-1.7	180
GS 0834-430	12.3	G260.4-3.4	60x50
1E 1048.1-5937	6.44	G289.7-0.3	18x14
A 1118-616	405	G294.1-0.0	40
4U 1145.1-6141*	297	G296.1-0.5	37x25
4U 1145-619 *	292	G296.1-0.5	37x25
4U 1258-61	272	G302.3+0.7	17
1SAXJ 1324.4-6200	170.84	G308.1-0.1	20x30(?)
2S 1417-624	17.6	G312.4-0.4	38
1SAXJ 1452.8-5949	437.4	G317.3-0.2	11
1M 1516-569	+	G321.9-0.3	31x23
2S 1553-54	9.26	G327.4+0.4	21
AXS J 161730-505505	0.069	G332.4-0.4	10
OAO 1657-415	38	G344.7-0.1	10
1RXSJ 170849.0-400910	10.997	G346.6-0.2	8
GPS 1722-363	414	G351.2+0.1	7
4U 1728-247	120	G5.4-1.2	35
XRE J 1739-302	¿300	G357.7+0.3	24
GRO J 1744-28	0.467	G0.9+0.1	8
GRO 1750-27	4.45	G4.2-3.5	28
AX J 1749.1-2725	220	G1.4-0.1	10
AX J 1820.5-1434	152.26	G16.8-1.1	30x24
X 1833-076	111	G24.7+0.6	30x15
RX 1838.4-0301 (?)	5.45	G28.8+1.5	100(?)
1E 1841-045	11.76	G27.4+0.0	4
GS 1843-024	94.9	G29.7-0.3	3
AX J 1844.8-0258	6.97	G29.6+0.1	4.5x5.0
AX J 1845.0-0433	7	G27.8+0.6	50x30
XTE J 1855-026	361	G30.7-2.0	16
XTE J 1858+034	221	G36.6-07	25(?)
XTE J 1906+09	437	G42.8+0.6	24
4U 1909+05	+	G39.7-2.0	120x60
J 1946+274	15.8	G63.7+1.1	8
J 1948+32	18.7	G69.0+2.7	80(?)
1WGAJ 1958.2+3232	721	G69.7+1.0	16
1SAXJ 2103.5+4545	358.61	G82.2+5.3(?)	95x65
1E 2259+586	6.98	G109.1-1.0	5.4

Figure 44: The X-ray pulsars associated with SNRs. The two pulsars marked with $*$ are positionally associated with the same SNR. The absence of spin period is marked with +; the two relative objects are black hole candidates. Symbol (?) means doubt in the association or uncertainty in the size of the SNR (adopted from [122]).

PoS(FRAPWS2024)035

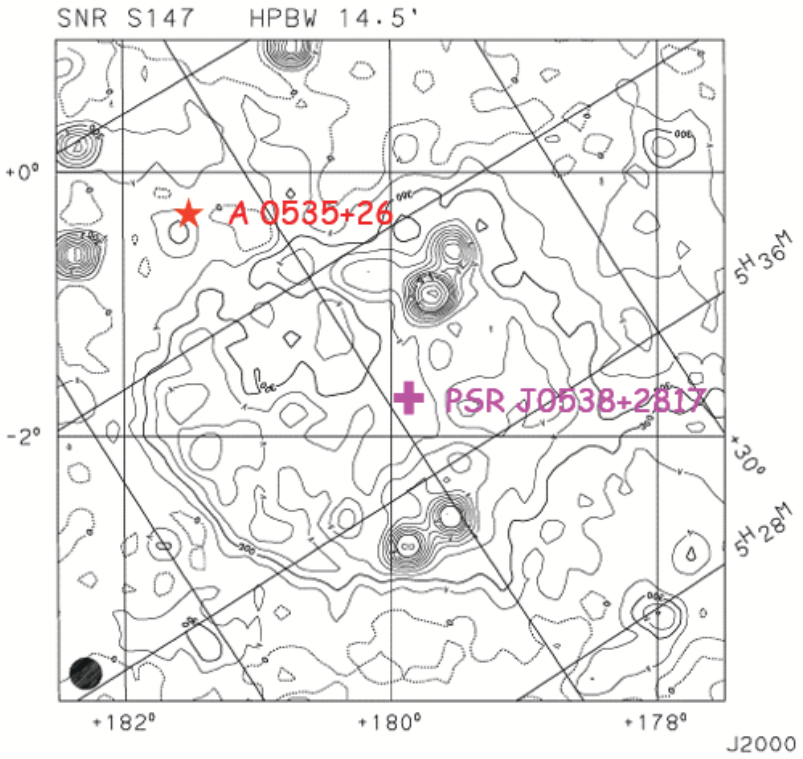

Figure 45: Contour plot of S147 at 863 MHz. Violet cross and red star shown the positions of PSR J0538+2817 and A 0535+26/HDE 245770, respectively (adapted from [133]).

the radio pulsar and the SNR: 6×10^5 yr and 2×10^5 yr, respectively, while the $P_{spin} \sim 104$ s of A 0535+26 is exactly compatible with the age of S 147 see Fig. 42.

Ng et al. [134] report on Very Long Baseline Array (VLBA) astrometry and Chandra imaging of PSR J0538+2817 in the SNR S147. They measure a parallax distance of $1.47^{0.42}_{-0.27}$ kpc. The neutron star is hot, consistent with the young ~ 40 kyr kinematic age. The pulsar progenitor is likely a runaway from a nearby cluster, with NGC 1960 (M36) a leading candidate.

Khabibullin et al. [135] present studies of X-ray emission from the S 147 nebula using the data of SRG/eROSITA All-Sky Survey observations. They argue that new X-ray data of SRG/eROSITA lends support for S 147 being a type II SN exploded in a low-density cavity. Figure 46 shows the broad-band (0.5-1.0 keV) image obtained by SRG/eROSITA in the S147 (left panel), and the multifrequency view of S 147: a combined map of the radio (CGPS data at 1.4GHz, red), H_α (IGAPS data, green) and broad-band X-ray (0.5-1.1 keV, SRG/eROSITA data) emission (right panel). The white cross and yellow star show the positions of PSR J0538+2817 and A 0535+26, respectively.

Dinçel et al. [136] present first results of a long-term study: Searching for OB-type runaway stars inside supernova remnants (SNRs). They identified spectral types and measured radial velocities by optical spectroscopic observations and they found an early type runaway star inside SNR S147. HD 37424 is a B0.5V-type star with a peculiar velocity of 74 ± 8 km s^{-1}. Tracing back the past trajectories via Monte Carlo simulations, they found that HD 37424 was located at the same position as the central compact object, PSR J0538+2817, 30 ± 4 kyr ago. This position is only $\sim$

PoS(FRAPWS2024)035

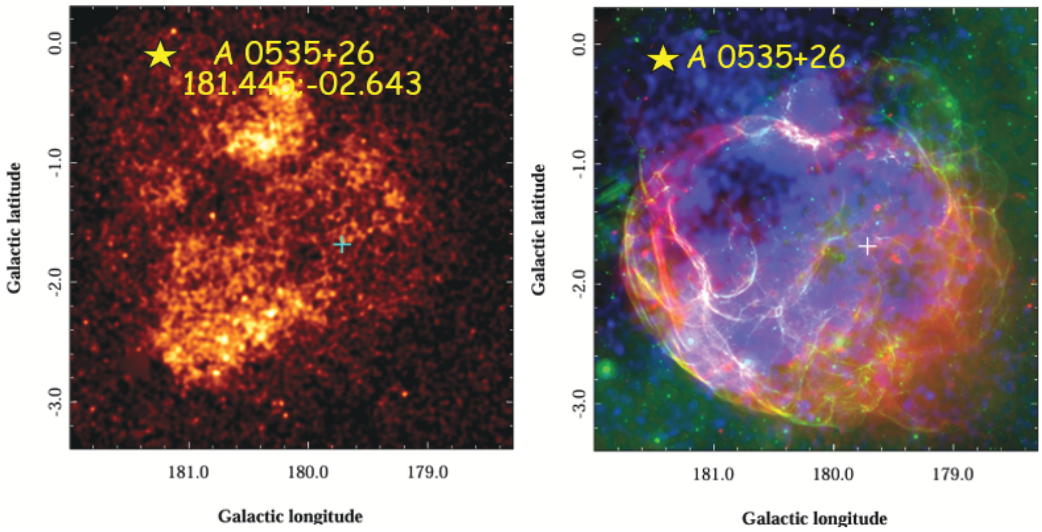

Figure 46: Left panel: the broad-band (0.5-1.0 keV) image obtained by SRG/eROSITA in the S147. Right panel: the multifrequency view of S 147: a combined map of the radio (CGPS data at 1.4GHz, red), H_α (IGAPS data, green) and broad-band X-ray (0.5-1.1 keV, SRG/eROSITA data) emission. The white cross and yellow star show the positions of PSR J0538+2817 and A 0535+26, respectively (adapted from [135]).

4 arcmin away from the geometrical centre of the SNR. So, they suggest that HD 37424 was the pre-supernova binary companion to the progenitor of the pulsar and the SNR. The progenitor was a massive star with a zero-age main sequence mass greater than 13 $M_\odot$. They found a distance of 1333^{+103}_{-112} pc to the SNR. For 1.3 kpc distance and 1.3 mag extinction, the SN which had an apparent brightness of -2.1 to -9.1 mag happened 30 ± 4 kyr ago.

So, taking into account all the conclusions of the articles mentioned so far, a discrepancy in the age of SNR S 147 appears evident. This discrepancy, in my opinion, is overcome if we take into account the origin of SNR S 147 from the explosion of SN in a binary system without its destruction which gave rise to the pulsar X A0535+26, with a kick velocity of 160 km s^{-1} which in 2×10^5 years brought the system to about 33 pc from the center.

2.12 Compton Gamma-Ray Observatory (CGRO)

The Compton Gamma-Ray Observatory (CGRO) was launched on April 5, 1991 having on-board four instruments: BATSE, OSSE, Comptel, EGRET that allowed to measure in a very large energy range: from 30 kev to 30 GeV.

Figure 47 shows its main characteristics (https://heasarc.gsfc.nasa.gov/docs/cgro/cgro.html).

It is very difficult to summarize the contributions that CGRO has provided to astrophysics. I will try to attempt such a summary.

2.12.1 The Burst And Transient Source Experiment (BATSE)

The Burst And Transient Source Experiment (BATSE) (https://heasarc.gsfc.nasa.gov/docs/cgro/batse/) – sensitive from ~ 20-600 keV – detected 2704 Gamma-Ray Bursts (GRBs) whose distribution in galactic coordinates is reported in Fig. 48. This usually is considered the main result of BATSE.

PoS(FRAPWS2024)035

Compton Gamma-Ray Observatory (CGRO)

The Compton Gamma-Ray Observatory (CGRO) was launched on April 5, 1991. The second of NASA's great observatories, CGRO has four instruments that cover an unprecedented six orders of magnitude in energy, from 30 keV to 30 GeV. Over this energy range CGRO has an improved sensitivity over previous missions of a full order of magnitude. It operated for almost 9 years and the mission ended on June 4 2000. Unlikely most satellites, CGRO was too large to burn up entirely in the atmosphere during re-entry. To ensure safety on the Earth's surface, NASA redirected the spacecraft into Earth's atmosphere with a controlled re-entry.

Mission Characteristics

- Lifetime : 5 April 1991 - 4 June 2000
- Energy Range : 30 keV - 30 GeV
- Special Features : First Great Gamma-Ray observatory
- Payload :
  - The Burst and Transient Source Experiment (BATSE)
    an all sky monitor 20-1000 keV
  - The Oriented Scintillation Spectrometer Experiment (OSSE)
    0.05-10 MeV energy range
  - The Compton Telescope (Comptel)
    0.8-30 MeV capable of imaging 1 steradian
  - Energetic Gamma Ray Experiment Telescope (EGRET)
    30 MeV-10 GeV
- Science Hightlight:
  - The Discovery of an isotropic distribution of the Gamma-ray burst events
  - Mapping the Milky Way using the 26 Al Gamma-ray line
  - Discovery of Blazar Active Galactic Nuclei as primary source of the highest energy cosmic Gamma-rays
  - Discovery of the "Bursting Pulsar"
- Archive : HEASARC hosts Catalogs, Other products soon available

Figure 47: The main characteristics of the Compton Gamma-Ray Observatory (CGRO) (https://heasarc.gsfc.nasa.gov/docs/cgro/cgro.html).

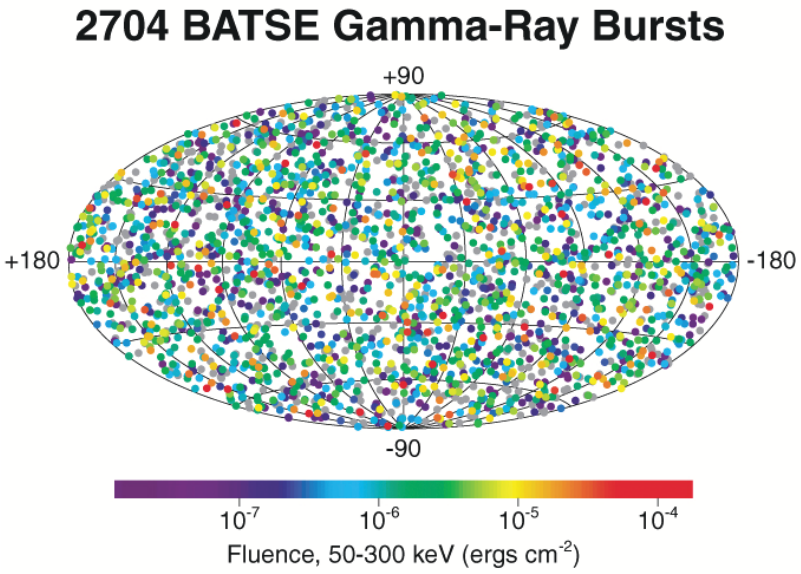

Figure 48: Distribution of 2704 GRBs (https://heasarc.gsfc.nasa.gov/docs/cgro/batse/).

PoS(FRAPWS2024)035

However, BATSE provided other many important results (https://heasarc.gsfc.nasa.gov/docs/journal/cgro7.html) on:

- isotropic and radially non-uniform distribution of gamma-ray bursts on the sky;
- enormous statistical diversity of GRB time profiles;
- bursting pulsar GR0 J1744-28;
- X-ray transient in Scorpius (GRO J1655-40) and correlations between X-rays and radio jets;
- discovery of several new X-ray pulsars and black hole X-ray;
- long term frequency histories of X-ray pulsars;
- terrestrial Gamma-ray flashess.

2.12.2 The Oriented Scintillation Spectrometer Experiment (OSSE)

The Oriented Scintillation Spectrometer Experiment (OSSE) consists of four NaI scintillation detectors, sensitive to energies from 50 keV to 10 MeV. Each of these detectors can be individually pointed. This allows observations of a gamma-ray source to be alternated with observations of nearby background regions. An accurate subtraction of background contamination can then be made (https://heasarc.gsfc.nasa.gov/docs/cgro/osse/). The OSSE instrument has produced many observations that provided the following results:

- maps of electron-positron annihilation radiation from the center of the Galaxy;
- spectra of blazar and Seyfert active galaxies;
- spectral break at 100-200 keV in Seyfert Active Galaxies;
- ^{57}Co emission from supernova 1987A;
- limits on ^{44}Ti and ^{56}Co emissions from Cas A and SN 1991T, respectively;
- hard X-ray continuum in SN 1993J;
- thermal and non-thermal spectral states in black hole candidates;
- nuclear gamma ray emission from solar flares.

Figure 49 shows the map of the Galactic 511 keV positron annihilation line (adapted from https://heasarc.gsfc.nasa.gov/docs/cgro/osse/ after [137]).

PoS(FRAPWS2024)035

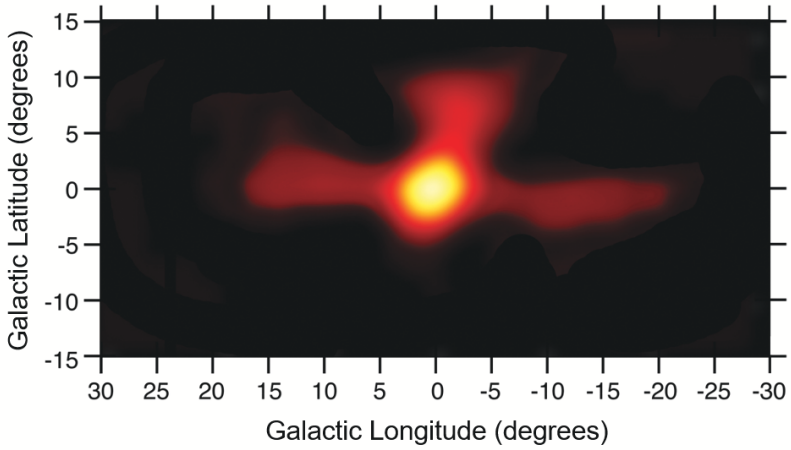

Figure 49: The map of the Galactic 511 keV positron annihilation line (adapted from https://heasarc.gsfc.nasa.gov/docs/cgro/osse/ after [137]).

2.12.3 The Imaging Compton Telescope (COMPTEL)

The Compton Telescope was capable of imaging 1 steradian of the sky in the 0.8-30 MeV range (https://heasarc.gsfc.nasa.gov/docs/cgro/comptel/).

A detailed description of the COMPTEL experiment and its operating characteristics can be found in the report "Instrument Description and Performance of the Imaging Gamma-Ray Telescope COMPTEL aboard NASA's Compton Gamma Ray Observatory" [138].

The main results obtained with the COMPTEL are listed below.

- fundamental insight into the high-energy physics of solar flares. For example, temporal variations as fast as 0.1 s are observed at energies above 10 MeV constraining acceleration models;
- detection of ^{57}Co emission from SN 1987A;
- limits on ^{22}Na emission from ONeMg novae, tightly constraining nova models;
- first all-sky map of Galactic ^{26}Al, tracing sites of recent stellar nucleosynthesis;
- results on the extragalactic diffuse gamma-ray emission compatible with power-law extrapolations and showing no evidence for an MeV excess.

Figure 50 shows the COMPTEL 1 to 30 MeV all-sky map in continuum gamma radiation which represents the results of the first-ever survey of the sky at these energies. The concentration of the emission along the Galactic plane is the most striking aspect of the map. The plane stands out clearly against the rest of the sky indicating that most of the measured gamma-ray fluxes come from regions or objects inside the Galaxy. The dominant Galactic continuum emission seems to come from interstellar space and is visible as diffuse Galactic radiation. Superimposed on the large-scale Galactic emission are point-like sources (like Crab, Vela, Cyg X-1), but many of the Galactic point sources remain unidentified at this time. A significant contribution of unresolved point sources

PoS(FRAPWS2024)035

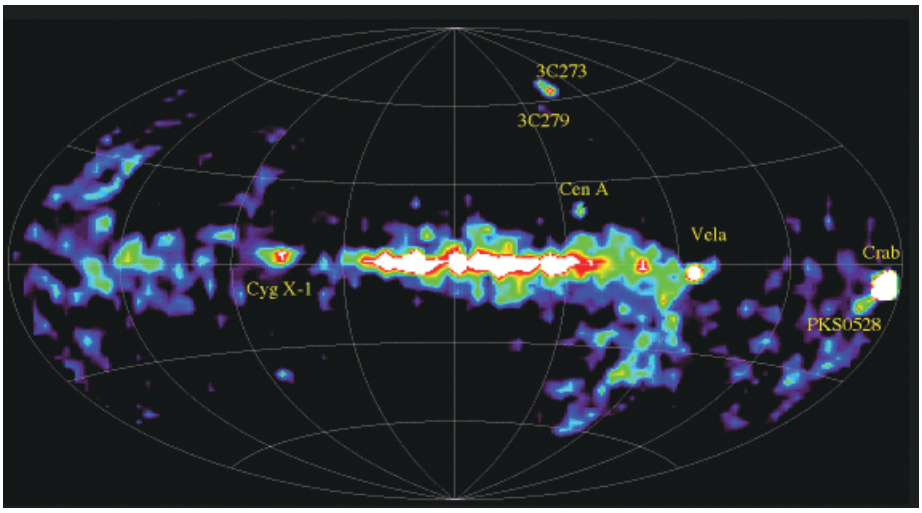

Figure 50: The COMPTEL 1 to 30 MeV all-sky map in continuum gamma radiation (adopted from https://heasarc.gsfc.nasa.gov/docs/cgro/epo/news/catalog.html).

to the apparently diffuse Galactic emission cannot be excluded. At medium and high Galactic latitudes, a few of the gamma-ray blazars, discovered by EGRET, are visible in the COMPTEL map as well. Examples are 3C 273, 3C 279, and PKS 0528+134. The radio galaxy Cen A is also visible at MeV gamma rays. Some of the extragalactic objects detected by COMPTEL are not visible in this map, because they flare up only occasionally: on average they are too weak to be visible in this time-averaged all-sky map (https://heasarc.gsfc.nasa.gov/docs/cgro/epo/news/catalog.html).

2.12.4 The Energetic Gamma Ray Experiment Telescope (EGRET)

EGRET, the Energetic Gamma-Ray Experiment Telescope on CGRO (https://heasarc.gsfc.nasa.gov/docs/cgro/egret/, and [139]), detected gamma rays in the 20 MeV-30 GeV range. It had a very large field of view, approximately 80° in diameter, although the instrument point-spread function and the effective area degrade signficantly beyond 30° off-axis. The effective area on-axis was more than 1000 cm^2 between 100 MeV and 3 GeV. The angular resolution was strongly energy dependent, with a 67% confinement angle of 5.5° at 100 MeV, falling to 0.5° at 5 GeV on axis; bright gamma-ray sources can be localized with approximately 10' accuracy. The energy resolution of EGRET was 20-25% over most of its range of sensitivity. Absolute arrival times for photons were recorded with approximately 50 μs accuracy.

The main results obtained by EGRET are listed below.

- blazars as prodigious gamma-ray emitters;
- high energy tails of gamma-ray bursts and delayed emission;
- Galactic origins of cosmic rays;
- radio-quiet pulsar nature of the source Geminga;
- sensitive map of the diffuse gamma-ray emission of the Milky Way;

PoS(FRAPWS2024)035

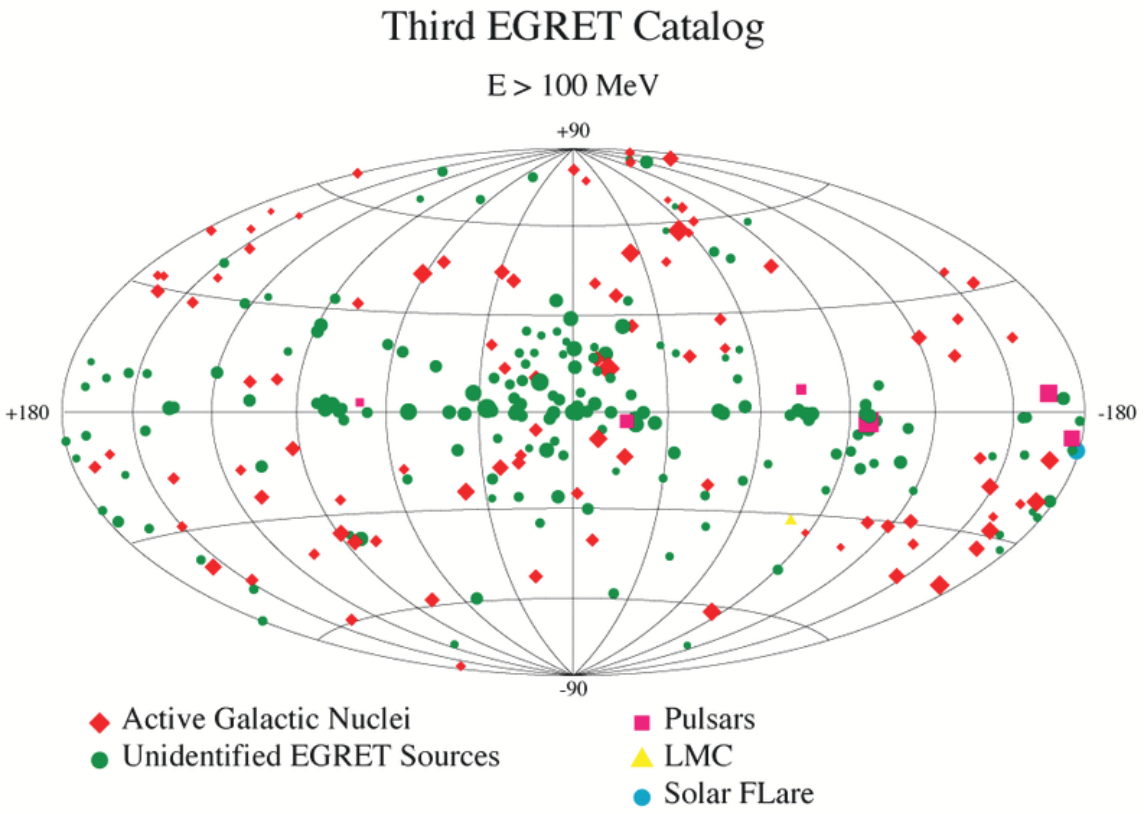

Figure 51: The Third EGRET Catalog (adopted from https://heasarc.gsfc.nasa.gov/docs/cgro/egret/).

- spectrum and map of the of extra-galactic, isotropic diffuse emission.

Figure 51 shows the Third EGRET Catalog (https://heasarc.gsfc.nasa.gov/docs/cgro/egret/, and [140]), which is the most relevant result obtained.

2.13 BeppoSAX

The acronym SAX stands for "Satellite per Astronomia X", italian for "X-Ray Astronomy Satellite". SAX was launched on April 30 1996 and renamed BeppoSAX in honor of Giuseppe "Beppo" Occhialini. BeppoSAX was a major program of the Italian Space Agency with participation of the Netherlands Agency for Aereospace Programs. It was launched on April 30 1996 from Cape Canaveral and operated for 6 years. It was the first X-ray mission with a scientific payload covering more than three decades of energy - from 0.1 to 300 keV - with a relatively large effective area, medium energy resolution and imaging capabilities in the range of 0.1-10 keV (https://heasarc.gsfc.nasa.gov/docs/sax/sax.html). Figure 52 shows the main characteristics of the BeppoSAX.

Among the many important results obtained by BeppoSAX, the discovery of the X-ray afterglow of GRB 970228 [141] stands out, which revolutionised the history of GRBs, giving rise to the search for afterglows along the entire electromagnetic spectrum. Figure 53 shows the discovery of the X-ray afterglow of the GRB 970228.

PoS(FRAPWS2024)035

BeppoSAX

BeppoSAX was a major program of the Italian Space Agency with participation of the Netherlands Agency for Aereospace Programs. It was launched on April 30 1996 from Cape Canaveral and operated for 6 years. It was the first X-ray mission with a scientific payload covering more than three decades of energy - from 0.1 to 300 keV - with a relatively large effective area, medium energy resolution and imaging capabilities in the range of 0.1-10 keV.

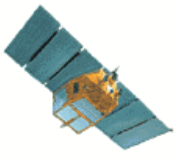

Mission Characteristics

- **Lifetime** : 30 April 1996 - 30 April 2002
- **Energy Range** : 0.1 - 300 keV
- **Special Features** : Broad-band energy
- **Payload** :
  - The Narrow field Instruments (NFI):
    - Four Xray telescopes working in conjnction with one of the following detectors:
      - Low Energy Concentrator Spectrometer (LECS)
        (one unit) 0.1-10 keV, eff area 22 cm^2 @ 0.28 keV, FOV 37′ diameter, angular resolution 9.7′ FWHM @ 0.28 keV.
      - Medium Energy Concentrator Spectrometer (MECS)
        (three units) 1.3-10 keV, eff area total 150 cm^2 @ 6 keV, FOV 56′ diameter, angular resolution for 50% total signal radius 75" @ 6 keV.
    - High pressure Gas Scintillator Proportional Counter (HPGSPC)
      4-120 keV, eff area 240 cm^2 @ 30 keV
    - Phoswich Detection System (PDS)
      15-300 keV. The lateral shields of the PDS are used as gamma-ray burst monitor in the range of 60-600 keV. Eff area 600 cm^2 @ 80 keV
  - Wide Field Camera
    (2 units) 2-30 keV with a field of view 20 deg X 20 deg. The WFC are perpendicular to the axis of the NFI and point in opposite directions to each other. Eff area 140 cm^2.
- **Science Highlight**:
  - First arc-minutes position of GRBs. Position determination on rapid time scale
  - First X-ray follow-up observations and monitoring of the GRB
  - Broad band spectroscopy of different classes of X-ray sources
- **Archive** : HEASARC hosts Spectra, Lightcurves, Images and Raw data for the MECS, LECS and PDS.

Figure 52: The main characteristics of the BeppoSAX (adopted from https://heasarc.gsfc.nasa.gov/docs/sax/sax.html).

Hundreds of researchers are chasing the quest for an explanation of the physics governing GRBs, producing a myriad of published papers. Giovannelli [12] recently published the review "*Gamma-Ray Bursts: The Energy Monsters of the Universe*" on the history of GRBs, where a lot of fundamental papers are cited.

Another important result achieved by BeppoSAX was the detection of "*Hard X-ray Radiation in the Coma Cluster Spectrum*" [142]. This hard X-ray emission had been advocated since 1975 by Auriemma et al. [143] with a "*Proposal for a high angular resolution experiment for observing extragalactic sources in the range 20-100 keV*" by using their "Position Sensitive X-ray Detectors with the Coded Masks", 24 years earlier than Beppo-SAX Detection.

The proposal was rejected by the Italian Extragalactic Astrophysical Community!

BeppoSAX was not only a great success in the past but also paved the way for the future of the sector in Italy and worldwide. The model implemented for gamma-ray burst observations was immediately copied and improved by NASA with the SWIFT mission, in which the Italian community made a fundamental contribution. The BeppoSAX scientific data center has evolved into an ASI (Agenzia Spaziale Italiana) multi-mission center.

PoS(FRAPWS2024)035

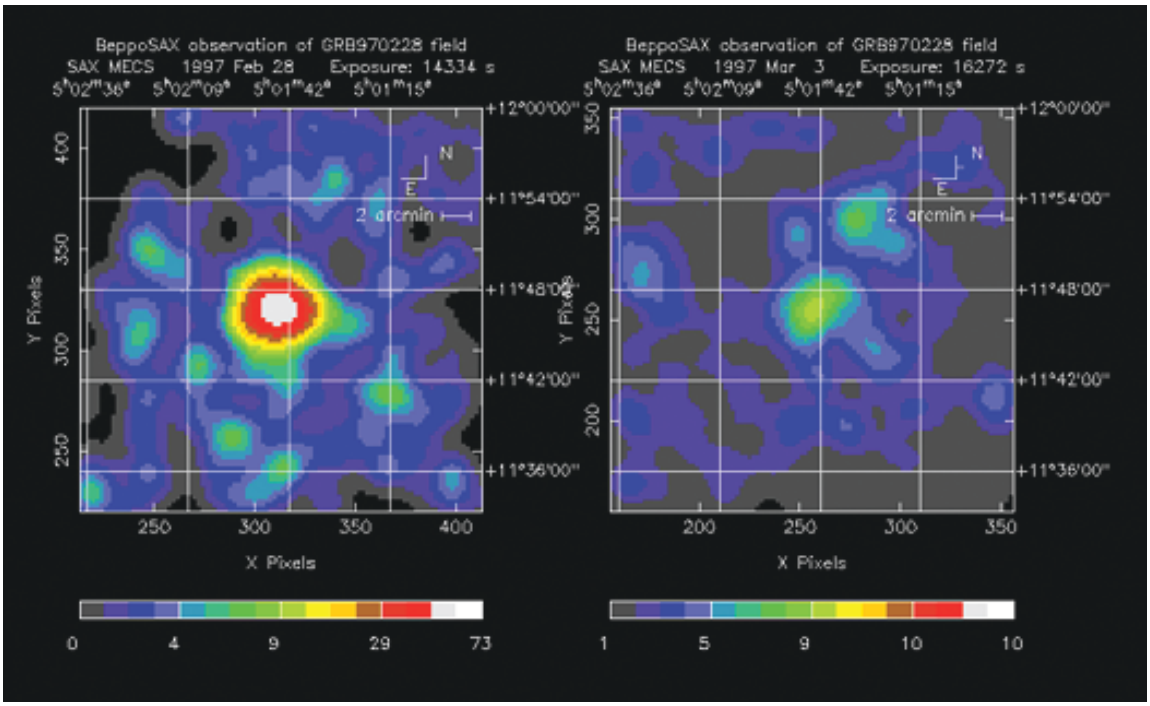

Figure 53: BeppoSAX observations of GRB 970228 field: 1997 Feb 28 (left panel) and 1997 Mar 3 (right panel) (adopted from [141]).

2.14 The International Gamma-Ray Astrophysics Laboratory (INTEGRAL)

INTEGRAL (INTErnational Gamma-Ray Astrophysics Laboratory) was a European mission, in collaboration with Russia and the USA, for the observation from space of some of the most energetic radiation in the Universe. The INTEGRAL was the first space observatory to simultaneously observe objects in X-rays, γ-rays (3 keV - 10 MeV), and visible light. It was launched by a Proton rocket from the Baikonur Cosmodrome in Kazakhstan on 17 October 2002.

Key science areas of INTEGRAL, thanks to its four instruments, are [144]:

- Studies of nucleosynthesis through gamma-ray lines from elements formed in supernovae,
- Studies of positron production and annihilation,
- Studies of the physics of emission mechanisms of white dwarfs, neutron stars, and black holes and associated transient phenomena
- Deep surveys for supermassive black holes in Active Galactic Nuclei,
- Gamma-ray burst studies.

Figure 54 shows the main characteristics of the INTEGRAL (https://heasarc.gsfc.nasa.gov/docs/integral/integral.html).

PoS(FRAPWS2024)035

INTEGRAL

The International Gamma-Ray Astrophysics Laboratory (INTEGRAL) of the European Space Agency was successfully launched on October 17, 2002. It was lifted off from Baikonur in Kazakhstan on a Russian Proton launcher and is now on a 72-hour elliptical orbit, ranging from 9,000 km up to 155,000 km from Earth. INTEGRAL is the successor of the ESA gamma-ray observatory Cos-B and the NASA gamma-ray Observatory CGRO. It is producing a complete map of the sky in the soft gamma-ray waveband and it is capable of performing high spectral and spatial observations in gamma rays. The observatory is also equipped with X-ray and optical detectors to provide simultaneous observations in these wavebands.

Mission Characteristics

- Lifetime : October 2002 - (nominal 2 year mission, extended through June 2023)
- Energy Range : 3 keV - 10 MeV and Optical V-band
- Special Features : High spectral and spatial resolution.
Simultaneous Gamma-ray, X-ray and Optical observations.
- Payload :

  - 2 Gamma-ray instruments
    - Spectrometer (SPI; 20 keV - 8 MeV)
      Coded aperature mask. FOV 16°, detector area. 500 cm^2 (Germanium array) spectral resolution (E/dE) 500 @ 1 MeV, spatial resolution 2°.
    - Imager (IBIS; 15 keV - 10 MeV)
      Coded aperature mask. FOV 9° X 9°, detector area. 2600 cm^2 (CdTe array) & 3100 cm^2 (CsI array), spatial resolution 12 ´.
  - Joint European X-ray Monitor (JEM-X; 3- 35 keV)
    Coded aperature mask with 2 high pressure microstrip gas chambers.
    FOV 4.8°, detector area. each 500 cm^2, spatial resolution 3´.
  - Optical Monitoring Camera (OMC; 500-850 nm). 50mm lens with CCD.
    FOV 5° X 5°.

* INTEGRAL artist's view courtesy of ESA.

- Archive: HEASARC hosts the INTEGRAL data and catalogs.

Figure 54: The main characteristics of the International Gamma-Ray Astrophysics Laboratory (INTEGRAL) adopted from https://heasarc.gsfc.nasa.gov/docs/integral/integral.html).

2.14.1 Spectrometer on INTEGRAL (SPI)

The spectrometer SPI (SPectrometer on INTEGRAL) performed spectral analysis of γ-ray point sources and extended regions in the 18 keV - 8 MeV energy range with an energy resolution of 2.2 keV (FWHM) at 1.33 MeV. This is accomplished using an array of 19 hexagonal high purity Germanium detectors cooled by a Stirling cooler system to an operating temperature of 85 K (15 are currently operational). A hexagonal coded aperture mask is located 1.7 m above the detection plane in order to image large regions of the sky (fully coded field of view = 16°) with an angular resolution of 2.5°. In order to reduce background radiation, the detector assembly is shielded by a veto (anticoincidence) system which extends around the bottom and side of the detector almost completely up to the coded mask. The aperture (and hence contribution by cosmic diffuse radiation) is limited to $\sim 30°$. A plastic veto is provided below the mask to further reduce the 511 keV background (https://www.cosmos.esa.int/web/integral/instruments-spi). A complete description of SPI can be found in [145].

The SPI telescope aboard INTEGRAL allowed for the first time the simultaneous imaging of diffuse and point-like emission in the soft gamma-ray regime.

PoS(FRAPWS2024)035

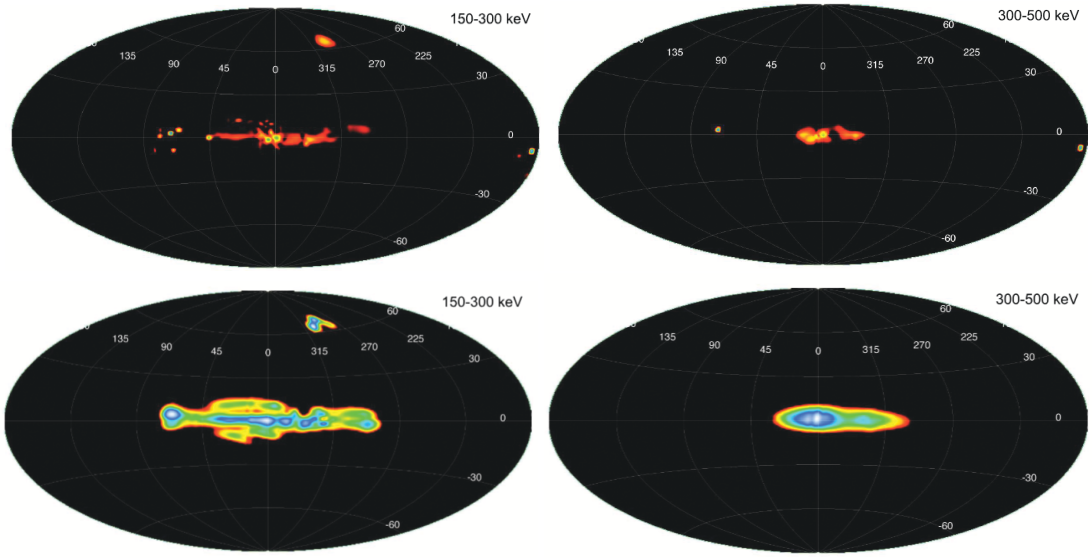

Figure 55: INTEGRAL/SPI multiresolution maps in the energy bands 150-300 keV (upper left panel) and 300-500 keV (upper right panel). Point-source subtracted INTEGRAL/SPI multiresolution maps in the energy bands 150-300 keV (lower left panel) and 300-500 keV (lower right panel) (adopted from [146]).

The skymaps generated from INTEGRAL/SPI data constitute an important result for understanding the emission of the Galaxy. A full set of maps can be seen at http://integral.esac.esa.int/POM Nov2006.html. Figure 55 shows the INTEGRAL/SPI multiresolution maps in the energy bands 150-300 keV (upper panel left) and 300-500 keV (upper panel right), and the point-source subtracted INTEGRAL/SPI multiresolution maps in the energy bands 150-300 keV (lower panel left) and 300-500 keV (lower panel right) [146].

Upper panels of Fig. 55 clearly reveal the presence of diffuse emission in both energy bands. While in the 150-300 keV band still a number of point-sources are seen, they gradually fade away at higher energies. Note that diffuse emission in this context does not necessarily mean that the underlying emission mechanismis indeed diffuse. The apparent morphology may also be explained by a number of faint and unresolved point sources.

Lower panels of Fig. 55 shows the point-source subtracted maps for the energy bands 150-300 keV and 300-500 keV. In the 150- 300 keV band an extended and narrow Galactic ridge emission is seen, reaching from the Cygnus region (at longitude $\sim 80°$) to the Carina region (at longitude $\sim 280°$). Some of the structure seen in the map may be related to source variability, that has explicitly only be taken into account for the strongest known point-sources sources. We therefore caution not to over interpret morphology details, and we are currently working on an improved treatment of source variability in the analysis. In the 300-500 keV band the emission appears much more concentrated towards the inner Galaxy. This concentration can be understood from the increasing contribution of Positronium continuum emission which amounts to roughly half of the Galactic emission seen in the image [146].

One of the most important results of INTEGRAL/SPI was the discovery of the flash of gamma rays linked to the gravitational waves released by the collision of two neutron stars. On 17 August, a burst of gamma rays lit up in space for almost two seconds. It was promptly recorded by ESA's

PoS(FRAPWS2024)035

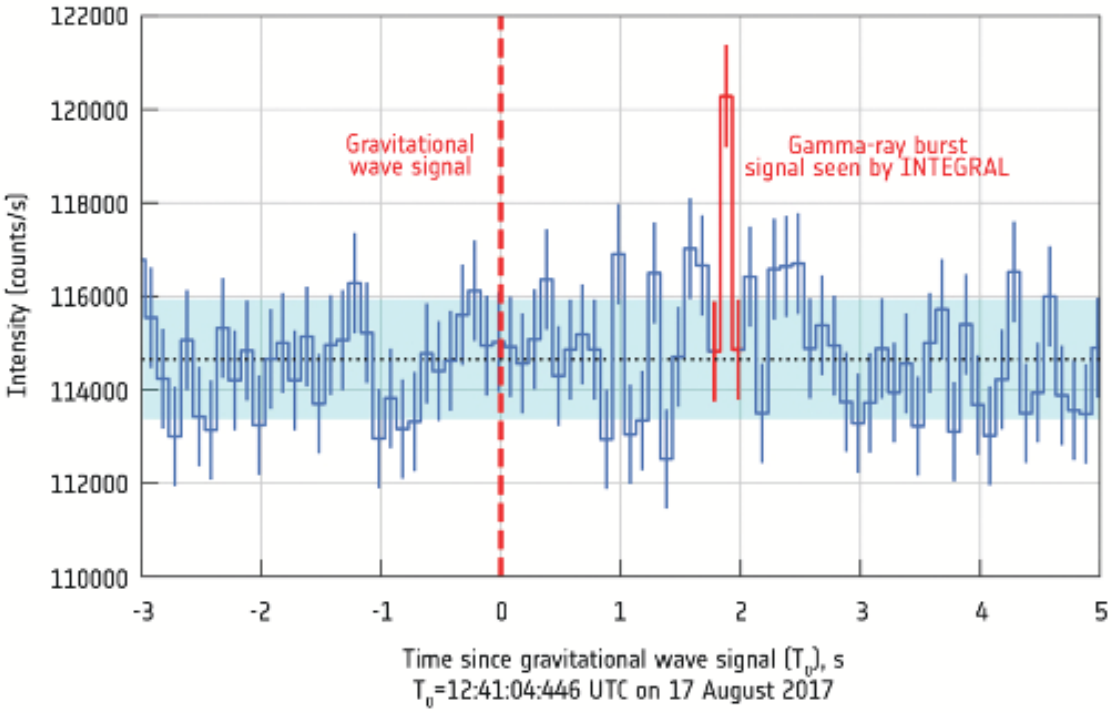

Figure 56: Gamma-ray burst after gravitational waves. Credit: ESA/INTEGRAL/SPI/ISDC (adopted from [147]).

INTEGRAL and NASA's Fermi satellite [147].

Such short gamma-ray bursts are not uncommon: INTEGRAL catches about 20 every year. But this one was special: just seconds before the two satellites saw the blast, an entirely different instrument was triggered on Earth.

One of the two detectors of the Laser Interferometer Gravitational-wave Observatory (LIGO) experiment, in the USA, recorded the passage of gravitational waves – fluctuations in the fabric of spacetime caused by powerful cosmic events [148].

Figure 56 shows the SPI-ACS light curve of GRB 170817A (100 ms time resolution), detected 2 s after GW170817. The red line highlights the 100 ms pulse, which has an S/N of 4.6 in SPI-ACS. The blue shaded region corresponds to a range of one standard deviation of the background [147].

2.14.2 Imager on Board the Integral Satellite (IBIS)

IBIS, the Imager on Board the INTEGRAL Satellite [149], is a coded-aperture instrument that provides fine imaging (12' FWHM), source identification and spectral sensitivity to both continuum and broad lines between 15 keV and 10 MeV. The total field of view (down to zero response) is 29.1° x 29.4°, and the fully coded field of view is 8.3° x 8°. The tungsten coded-aperture mask, optimised for high angular resolution, is located at 3.2 m above the detection plane. As diffraction is negligible at gamma-ray wavelengths, the angular resolution of a coded mask telescope is defined by the size of the mask element as seen from the detector plane, (assuming that the size of a detector pixel is smaller or equal to that of the mask element).

PoS(FRAPWS2024)035

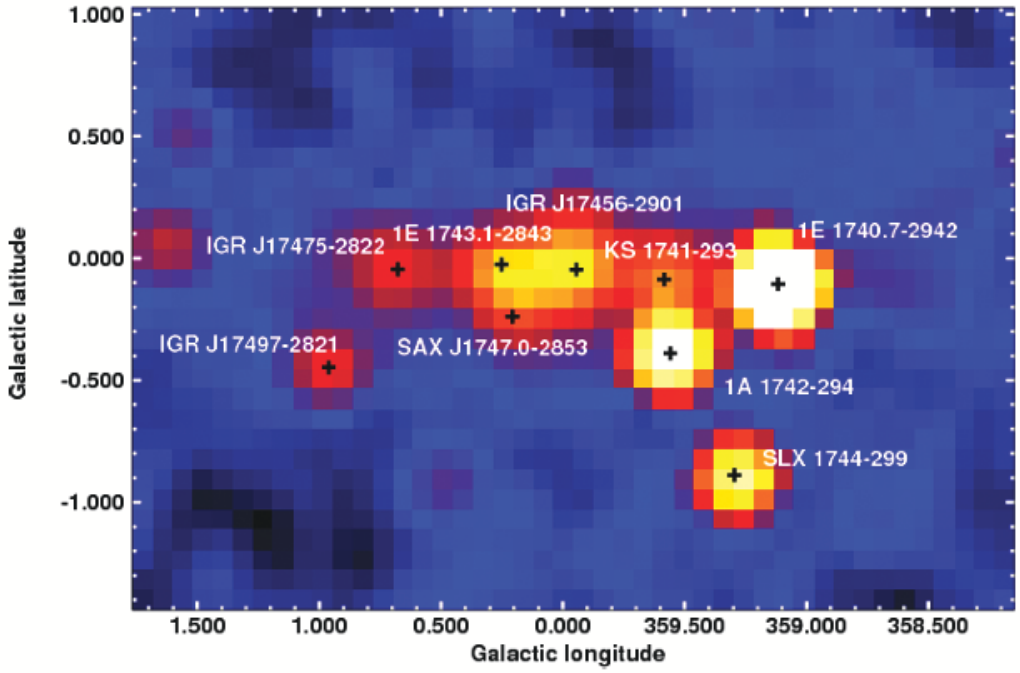

Figure 57: INTEGRAL view of the Galactic Centre in the 20-40 keV energy range, obtained from all IBIS observations of this region between 2003 and 2009, for a total exposure of 20 Ms. The main sources are indicated by black crosses. Most of them are X-ray binaries powered by accretion on neutron stars or stellar-mass black holes. The central source IGR J17456-2901 coincides with the position of Sgr A*. The position of IGR J17475-2822 is compatible with that of the Sgr B2 molecular cloud (adopted from [152]).

IBIS is composed of two detector planes: ISGRI [150] and PICsIT [151] separated by 90 mm. ISGRI, the top layer, has a collecting area of 2600 cm2, is sensitive between 15 and 1000 keV with maximum effective area between 20 and 100 keV. It consists of 8 modules of 64x32 CdTe pixels (128x128) for a total of 16384 pixels, each measuring 4x4 mm (2 mm thick), and spaced by 0.6 mm. Each module has 64x32 pixels and the space between modules is of 2 pixels. There are 2 modules horizontally, and 4 vertically. Therefore, the detector image or shadowgramme has a size of 130x134 pixels (2*64 + 2 = 130 and 4*32 + 3*2 = 134). PICsIT, the bottom layer, has a collecting area of 3000 cm^2, is sensitive between 100 keV and 10 MeV, with maximum effective area between 200 and 400 keV for single events, and a rather uniform sensitivity for multiple events between 500 keV and 10 MeV. It consist of the same 8 modules configuration as ISGRI, but with 32x16 CsI pixels (64x64) for a total of 4096 pixels, each measuring 9x9 mm (30 mm thick). Having two separate detectors permits the reconstruction of the angle of incidence of photons when they interact in both layers. This allows for what is referred to as the Compton mode of operation (https://www.cosmos.esa.int/web/integral/instruments-ibis).

Many important contributions to the knowledge of our universe have been derived from the measurements of IBIS. A few of them are listed below.

- INTEGRAL/IBIS view of the Galactic Centre in the 20-40 keV energy range [144].

  Figure 57 shows the INTEGRAL view of the Galactic Centre in the 20-40 keV energy range,

PoS(FRAPWS2024)035

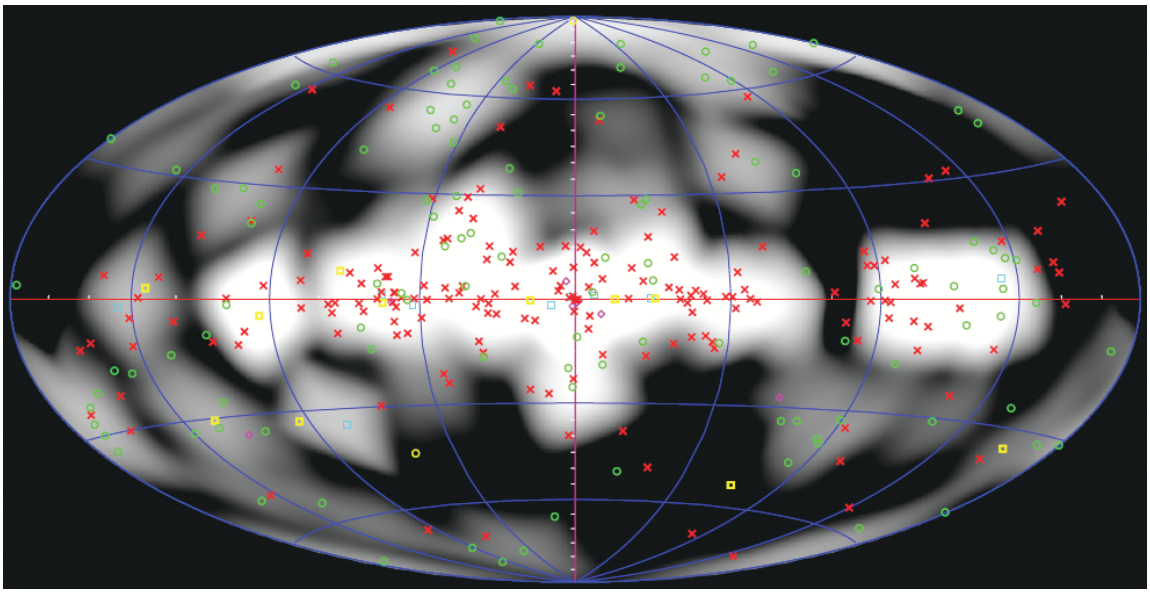

Figure 58: Map of incremental exposure since the third catalog, showing the locations of the new sources found. Key: green circles = AGN; cyan squares = HMXB; magenta diamonds = LMXB; yellow boxes = CVs; red crosses = unknown (adopted from [153]).

obtained from all IBIS observations of this region between 2003 and 2009, for a total exposure of 20 Ms. The main sources are indicated by black crosses. Most of them are X-ray binaries powered by accretion on neutron stars or stellar-mass black holes. The central source IGR J17456-2901 coincides with the position of Sgr A*. The position of IGR J17475-2822 is compatible with that of the Sgr B2 molecular cloud [152].

- The Fourth IBIS/ISGRI catalog [153].

  Figure 58 shows the Fourth IBIS/ISGRI catalog.

- INTEGRAL/IBIS catalog of AGNs [154].

  Figure 59 shows the INTEGRAL/IBIS catalog of AGNs.

2.14.3 Joint European X-ray Monitor JEM-X

The Joint European X-Ray Monitor JEM-X supplements the main Integral instruments (Spectrometer and Imager) and plays a crucial role in the detection and identification of the gamma-ray sources and in the analysis and scientific interpretation of Integral gamma-ray data. JEM-X will make observations simultaneously with the main gamma-ray instruments and provides images with arcminute angular resolution in the 3 - 35 keV prime energy band. The baseline photon detection system consists of two identical high pressure imaging microstrip gas chambers (1.5 bar, 90% Xenon + 10% Methane), at nominal gas gain of 1500. Each detector unit views the sky through its coded aperture mask located at a distance of $\sim$ 3.2 m above the detection plane (https://www.cosmos.esa.int/web/integral/instruments-jemx, and [158]).

Among the many results obtained with the JEM-X, it is relevant a measure of the outbursting stellar-mass black hole binary V404 Cyg which originated together with the data coming from

PoS(FRAPWS2024)035

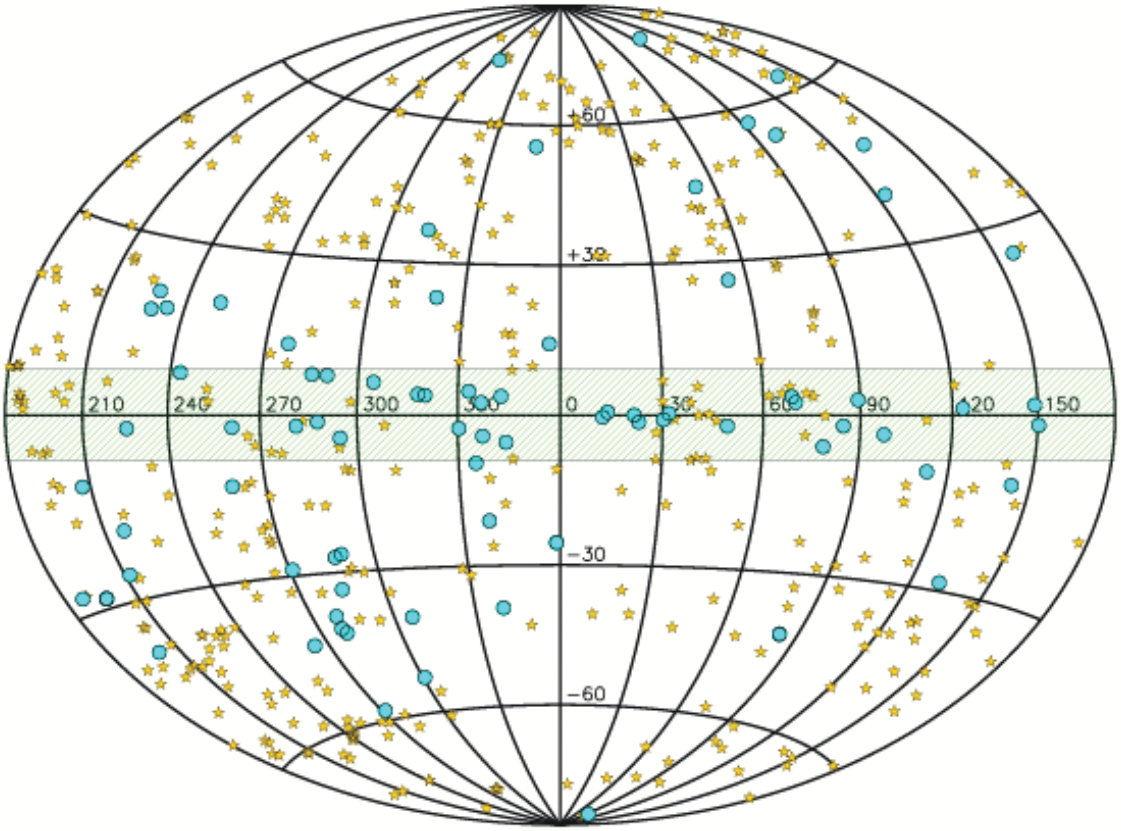

Figure 59: All the AGN detected so far by INTEGRAL/IBIS plotted on the sky. The circles represent the 83 new active galaxies studied in [152], while the stars are the AGN detected in previous surveys and reported in [155-157] (adopted from [154]).

Swift XRT and IBIS/ISGRI the composite spectrum reported in Fig. 60 [159]. The hard tail is not affected by obscuration and poses important constraints on the global understanding of the complex geometry hosting emission, absorption, and scattering. In this case rather atypical behaviour is seen, rather reminiscent of an obscured/absorbed active galactic nucleus (AGN) where the low-flux states might not (solely) be related to a decrease in the intrinsic luminosity, but could instead be caused by an almost complete obscuration of the inner accretion flow.

2.14.4 Optical Monitor Camera OMC

The Optical Monitoring Camera OMC consists of a passively cooled CCD (2055 x 1056 pixels, imaging area: 1024 x 1024 pixels) working in frame transfer mode. The CCD is located in the focal plane of a 50 mm (diameter) lens including a Johnson V-filter to cover the 500 - 600 nm (CCD: 850 nm) wavelength range. The OMC is mounted close to the top of the payload module structure. The OMC observes the optical emission from the prime targets of the INTEGRAL main gamma-ray instruments with the support of the X-Ray Monitor JEM-X. The OMC offers the first opportunity to make long observations in the optical band simultaneously with those at X-rays and gamma-rays. This capability provides invaluable diagnostic information on the nature and the physics of the

PoS(FRAPWS2024)035

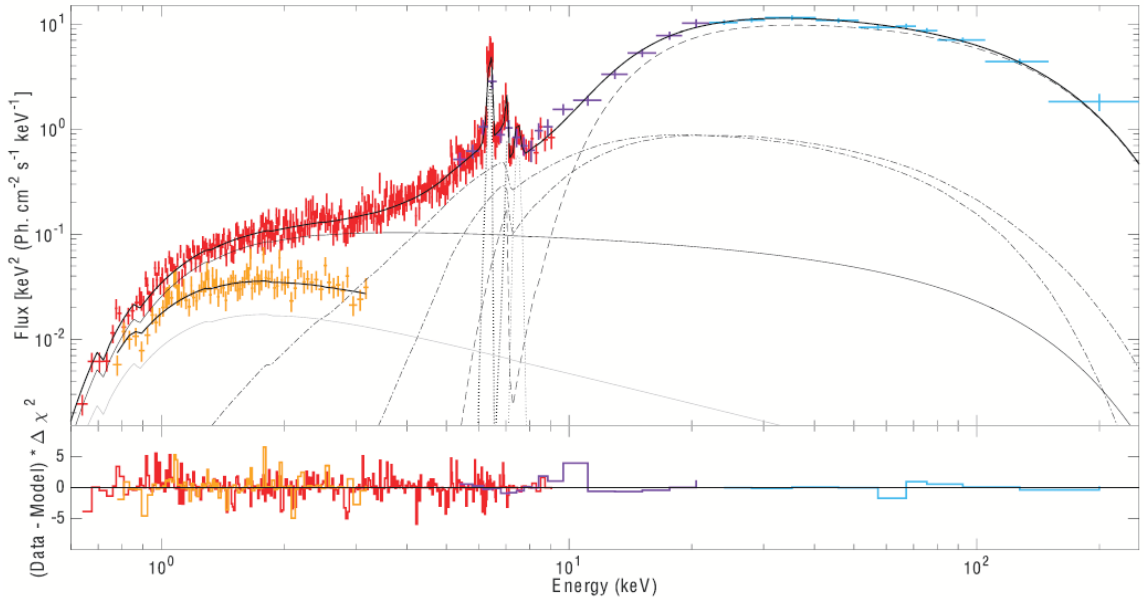

Figure 60: Swift/XRT+INTEGRAL/JEM-X+INTEGRAL/ISGRI spectrum of V404 Cyg. Swift XRT (red and orange: without and with obscuration, respectively) and INTEGRAL JEM-X (purple) plus IBIS/ISGRI (light blue) (adopted from [159]).

sources over a broad wavelength range (https://www.cosmos.esa.int/web/integral/instruments-omc, and [160]).

It is interesting to remark the importance of the OMC. For instance, after almost 6-years of operations, OMC has monitored more than 100,000 sources of scientific interest. In this contribution [161] the authors present the OMC Scientific Archive (http://sdc.laeff.inta.es/omc/) which has been developed to provide the astronomical community with a quick access to the light curves generated by this instrument. For the access to OMC updated catalog see https://sdc.cab.inta-csic.es/omc/.

2.14.5 How INTEGRAL interacted with my work

I would like to report a couple of my lucubrations below.

- As shown in Fig. 28, in the list of magnetic cataclysmic variables detected by INTEGRAL [68], only SS Cyg is attributed a non-magnetic nature. This fact contradicts the evidence that leads to consider SS Cyg an intermediate polar like all the other CVs in the list. In fact, if SS Cyg were non-magnetic, why does INTEGRAL not detect other non-magnetic CVs? (see [76]).

- Looking at the graph of "*Observed hard X-ray (20–100 keV) luminosity versus redshift* for the whole INTEGRAL AGN sample [154], it is clear that the trend is similar to that of the maximum X-ray luminosity versus redshift in the Giovannelli-Polcaro 86 (GP86) diagram [52]. Figure 61 shows the graph of Observed hard X-ray (20–100 keV) luminosity versus redshift for the whole INTEGRAL AGN sample [154] with the points of the GP86 diagram (red stars) superimposed on it. Although the X-ray luminosity in GP86 is 2 keV equivalent monochromatic luminosity – used, as suggested by Zamorani et al. [162] for rendering

PoS(FRAPWS2024)035

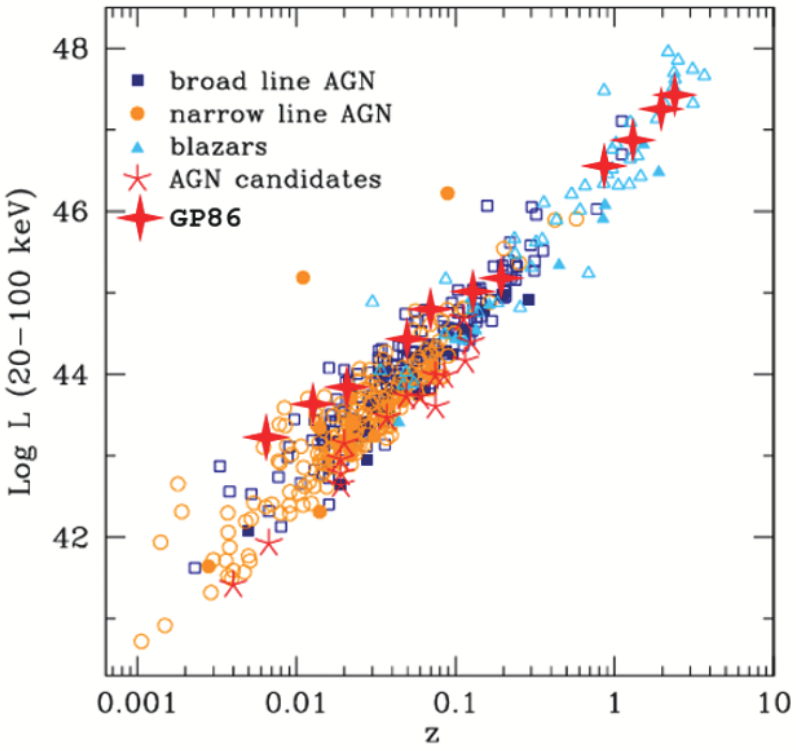

Figure 61: Observed hard X-ray (20–100 keV) luminosity versus redshift for whole INTEGRAL AGN sample. Blue squares are broad-line AGN, gold circles are narrow line AGN, and light blue triangles are blazars. Red stars are AGN candidates still unclassified for which a measure of redshift is available [157]. The filled symbols refer to the new AGN added in [154] (adapted from [154]). Four-pointed red stars refer to GP86 diagram.

comparable the sub-samples used, the most relevant of them coming from the Einstein satellite –, while that of Malizia et al. [154] is 20–100 keV, the coincidence is striking. This means that at z > 0.01, where only AGNs are present, it matches with a straight line, with a slope equal to 1.6. This suggests that such a smooth function implies a physical continuity of these objects, as argued in [52].

2.15 The Astro-rivelatore Gamma a Immagini Leggero (AGILE)

The Astro-rivelatore Gamma a Immagini Leggero (AGILE) is a gamma-ray astronomy mission operated by ASI (Italian Space Agency). It was launched on April 23, 2007 from Satish Dhawan Space Centre in India. The original plan called for a three year mission, but the satellite operated for 17 years and ceased the scientific observations on Jan 18, 2024. It was launched into a near-equatorial orbit, giving it a good observational vantage on terrestrial gamma-ray flashes from thunderstorms and intense atmospheric electrical activity, in addition to its astrophysics observations.

Figure 62 shows the main characteristics of the Astro-rivelatore Gamma a Immagini Leggero (AGILE) (https://heasarc.gsfc.nasa.gov/docs/heasarc/missions/agile.html).

The main scientific results obtained by AGILE can be summarized in the following [163,164].

- Discovery of Crab Nebula fast variability in gamma-rays,

PoS(FRAPWS2024)035

AGILE

The ***Astro-rivelatore Gamma a Immagini Leggero*** **(AGILE)** is a gamma-ray astronomy mission operated by ASI (Italian Space Agency). It was launched on April 23, 2007 from Satish Dhawan Space Centre in India. The original plan called for a three year mission, but the satellite operated for 17 years and ceased the scientific observations on Jan 18, 2024. It was launched into a near-equatorial orbit, giving it a good observational vantage on terrestrial gamma-ray flashes from thunderstorms and intense atmospheric electrical activity, in addition to its astrophysics observations.

Mission Characteristics

- **Lifetime** : April 23, 2007 – Jan 18,2024
- **Energy Range** : 15 keV – 50 GeV
- **Special Features** : Extremely rapid gamma-ray burst alerts, with initial estimated events announced within an hour of observation, and a refined alert within 3 to 3.5 hours. The rapid trigger systems have also proven useful for detecting terrestrial gamma-ray sources from thunderstorms, which are more common in the equatorial region over which the satellite orbits.
- **Payload** :

  - SuperAGILE, a coded mask imager hard X-ray detector with silicon microstrip detectors, sensitive to 15–45 keV with a wide field of view and 6 arcminute one dimensional resolution: microstrips mounted perpendicularly provide two-dimensional source placement. Because celestial gamma-ray sources frequently have small photon counts and considerable angular confusion, a co-observing hard X-ray detector such as SuperAGILE is often vital to source identification.
  - The Gamma-Ray Imaging Detector (GRID) which contains a silicon-tungten tracker, anticoincidence system, and a cesium iodide calorimeter (see below). The tracker consists of a set of two-layer silicon microstrip detectors, interleaved with tungsten foil: gamma rays strike the tungsten, converting into electron/positron pairs which are followed by the microstrips to reconstruct the incident gamma ray's direction. It is sensitive to 30 MeV–50 GeV.
  - The MiniCalorimeter, which is part of the GRID instrument, but can operate independently as need. It contains perpendicular pairs of CsI scintillating bars and operates in the energy range 350 keV–100 MeV.

Figure 62: The main characteristics of the Astro-rivelatore Gamma a Immagini Leggero (AGILE) (https://heasarc.gsfc.nasa.gov/docs/heasarc/missions/agile.html).

- First evidence of cosmic-ray acceleration from supernova remnants,
- Detection of transient gamma-ray emission from microquasars,
- AGILE GRB and other transients: Gravitational Wave (GW) events, neutrinos, Fast Radio Bursts (FRBs), Terrestrial Gamma-ray Flashes (TGFs) and Solar flares

In the next two figures I want to show a couple of AGILE results that I think are excellent.

Figure 63 shows the sky count map above 100 MeV in galactic coordinates of the AGILE-GRID γ-ray detector during the time interval [T_0, T_0 + 48 hr]. The γ-ray source associated with GRB 221009A is shown inside the green circle. The darkened sky regions are due to seasonal lack of exposure of the AGILE-GRID detector due to solar panel constraints [163]. More details about the GRB 221009A are reported in [165].

Figure 64 shows the AGILE-GRID count map (E > 100 MeV) centered on the Cygnus region. The positions of the three PSRs and of the three microquasars are marked with black and white crosses, respectively [163].

2.16 The Spectr-Roengten-Gamma (SRG)

The scientific spacecraft "Spectrum-Roentgen-Gamma" (Spectr-RG or SRG) is an X-ray observatory. SRG's main scientific goal is to chart an unprecedented map of the Universe in X-rays

PoS(FRAPWS2024)035

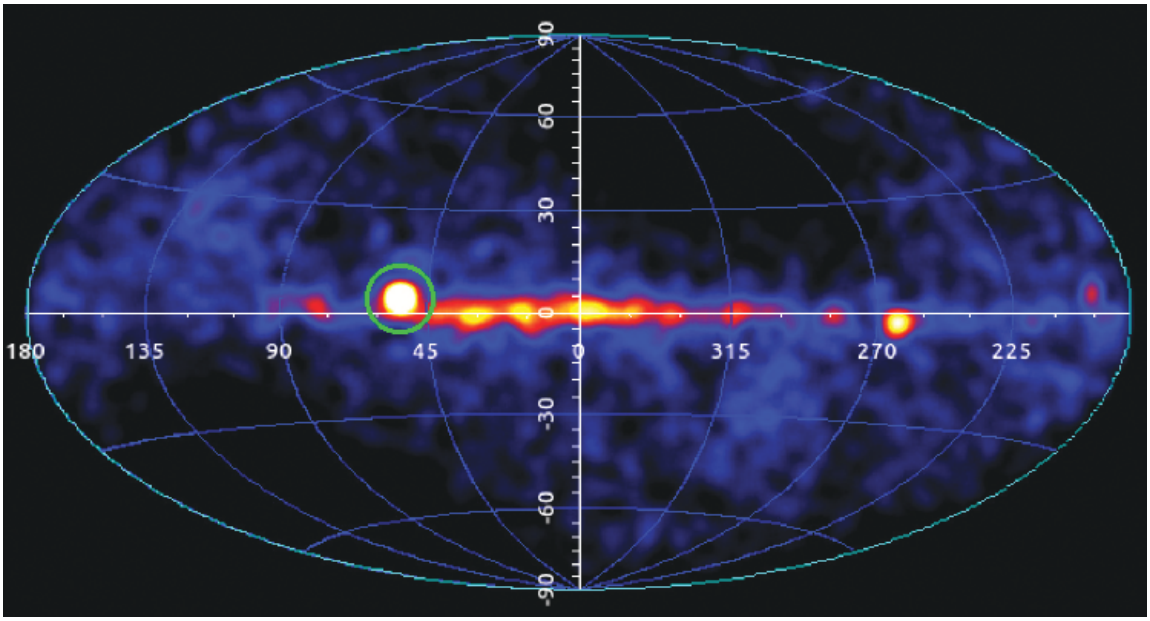

Figure 63: Sky count map above 100 MeV in galactic coordinates of the AGILE-GRID γ-ray detector (adopted from [163]).

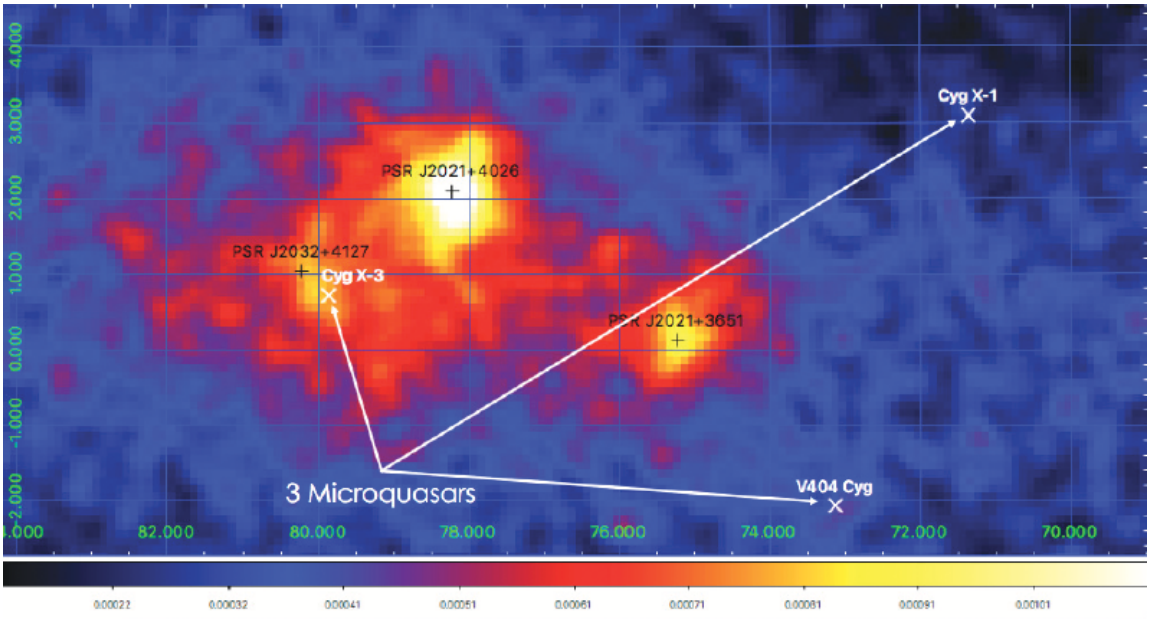

Figure 64: The AGILE-GRID count map (E > 100 MeV) centered on the Cygnus region. The positions of the three PSRs and of the three microquasars are marked with black and white crosses, respectively (adopted from [163]).

PoS(FRAPWS2024)035

The Spectr-Roentgen-Gamma (SRG)

The ***Spectr-Roentgen-Gamma (SRG)*** is a Russian-German high energy astrophysics mission launched on July 13, 2019 from the Baikonur Cosmodrome. After travelling to the Earth-Sun L2 Lagrange point, the instruments began the first of eight planned sky surveys in December 2019. Mission plans call for four years of operations in scanning mode, building all-sky maps over the course of six months. Once completed, the observatory with shift to pointed observations at specific targets of interest. The original mission calls for seven years of operations.

The mission occasionally appears as "Spectrum X-Gamma" (SXG) in English. X-rays are often refered to as Röntgen or Roentgen rays in other countries (and in the case of this mission specifically, in Russia and Germany) named after their discoverer Wilhelm Conrad Röntgen.

Despite the "Gamma" appelation in the mission name, the satellite carries no gamma-ray instrument. The reference was retained for historical reasons, as the mission's earlier proposals called for additional gamma-ray detectors.

Mission Characteristics

- **Lifetime** : December 8, 2019–present
- **Energy Range** : 0.2–30 keV
- **Special Features** : X-ray mirror optics combine moderate resolution imaging with a very wide field of view, with all-sky maps to be produced over a wide range in the soft to hard X-ray range.
- **Payload** :
  - The Extended Roentgen Survey with an Imaging Telescope Array (eROSITA) instrument consists of seven telescopes with 54 nested mirror segments to focus X-rays onto a CCD detector (0.2-10 keV) with an on-axis 18 arcsec HEW. The Filed of view is 0.81 sq deg and the energy resolution is 138 eV at 6 keV. The instrument and mirrors were built by the Max Planck Institute of Extraterrestrial Physics, using a CCD design based on the successful XMM-Newton CCD detectors. They are active cooled to -90° C for improved sensitivity.
  - The Astronomical Roentgen Telescope - X-ray Concentrator (ART-XC) is also an array of seven telescopes in a nested shell design, though with fewer mirror segments (28 per telescope) and a 45 arcsecond resolution in a 36 arcminute field of view spanning 5–30 keV. The detector unit in each telescope is a CdTe crystal with double-side strip detectors with an effective area of 400 cm^2 and 1.2 keV @ 14 keV spectral resolution and a timing resolution of about 1 ms. The instrument was build at the Russian State Nuclear Center and the iridium-coated mirror system was developed and calibrated at NASA's Marshall Space Flight Center.
- **Science Highlights**:
  First all-sky imaging in the X-ray hard band
- **Archive**: The HEASARC hosts the eROSITA data.

Figure 65: The main characteristics of the Spectr-Roengten-Gamma (SRG) (https://heasarc.gsfc.nasa.gov/docs/heasarc/missions/srg.html).

on which all large clusters of galaxies will be marked. The scientific payload consists of two independent telescopes:

- eROSITA (extended ROentgen Survey with an Imaging Telescope Array), a soft-X-ray survey instrument, being provided by Germany [166],
- ART-XC (Astronomical Roentgen Telescope- X-ray Concentrator), a medium-X-ray-energy survey instrument, being developed by Russia [167].

The HEASARC currently serves part of the eROSITA data archive. The ART-XC archive has been published in [168].

Figure 65 shows the main characteristics of the Spectr-Roengten-Gamma (SRG) (https://heasarc.gsfc.nasa.gov/docs/heasarc/missions/srg.html).

With about 900,000 distinct sources, the first eROSITA All-Sky Survey (eRASS1) [169] has yielded the largest X-ray catalogue ever published. Based on just the first six months of observations,

PoS(FRAPWS2024)035

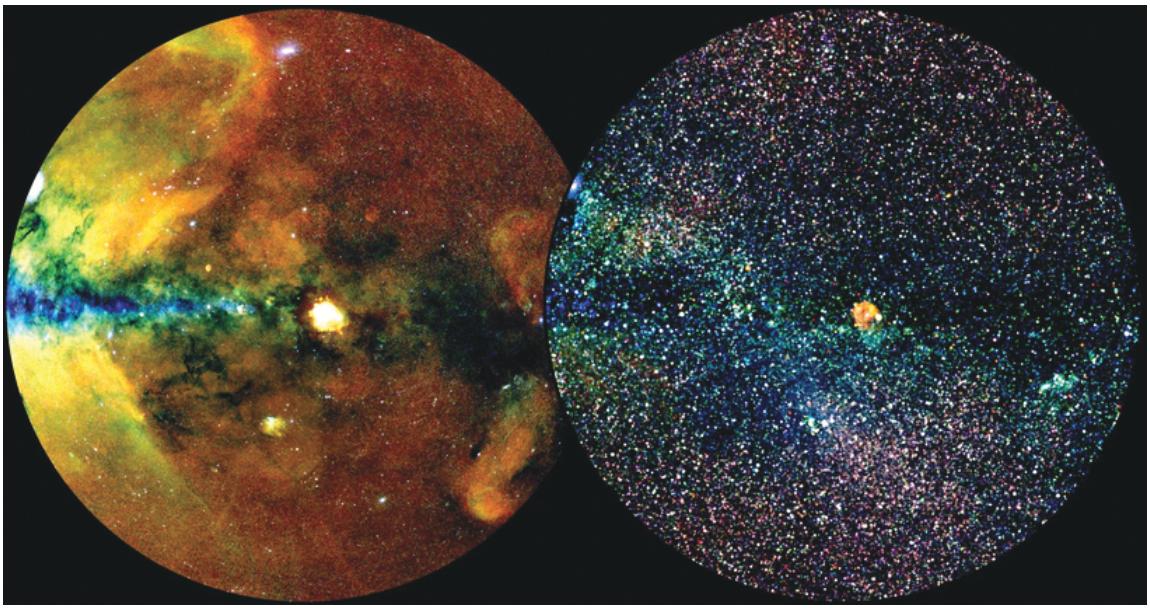

Figure 66: eRosita: half of the X-ray sky, projected onto a circle (so-called Zenithal Equal Area projection) with the centre of the Milky Way on the left and the galactic plane running horizontally. Photons have been colour-coded according to their energy (red for energies 0.3-0.6 keV, green for 0.6-1 keV, blue for 1-2.3 keV). A special image processing algorithm has been used to separate extended features (left) from point sources (right) (Credit: MPE, J. Sanders for the eROSITA consortium).

eROSITA has already detected more sources than had previously been known in the 60-year history of X-ray astronomy. Now available to the worldwide science community, the data will revolutionise our knowledge of the Universe at high energies (https://www.mpe.mpg.de/7989698/news20240131).

Figure 66 (left) shows half of the X-ray sky, projected onto a circle (so-called Zenithal Equal Area projection) with the centre of the Milky Way on the left and the galactic plane running horizontally. Photons have been colour-coded according to their energy (red for energies 0.3-0.6 keV, green for 0.6-1 keV, blue for 1-2.3 keV). A special image processing algorithm has been used to separate extended features (left) from point sources (right) (https://www.mpe.mpg.de/7989698/news20240131).

The curious reader, wishing to better understand the fundamental contribution made by eRosita to the knowledge of our universe, can connect to the link https://erosita.mpe.mpg.de/publications/ where all the scientific works produced by the eRosita consortium are listed in NASA-ADS.

Figure 67 shows the positions in Galactic coordinates of the X-ray sources detected by ART-XC in the 4–12 keV energy band during ARTSS1-5. The size of the symbol reflects the X-ray brightness of a source [168].

Figure 68 shows the image of a $25^\circ \times 25^\circ$ region of the sky near the Galactic center in the 4–12 keV energy band, obtained by convolving the raw photon images with the optimal matched filter, in Galactic coordinates. Some bright sources are labeled.The faintest sources in this region that have been included in the ARTSS1-5 catalog have fluxes $\sim 3 \times 10^{-12}$ erg s^{-1} cm^{-2}.

PoS(FRAPWS2024)035

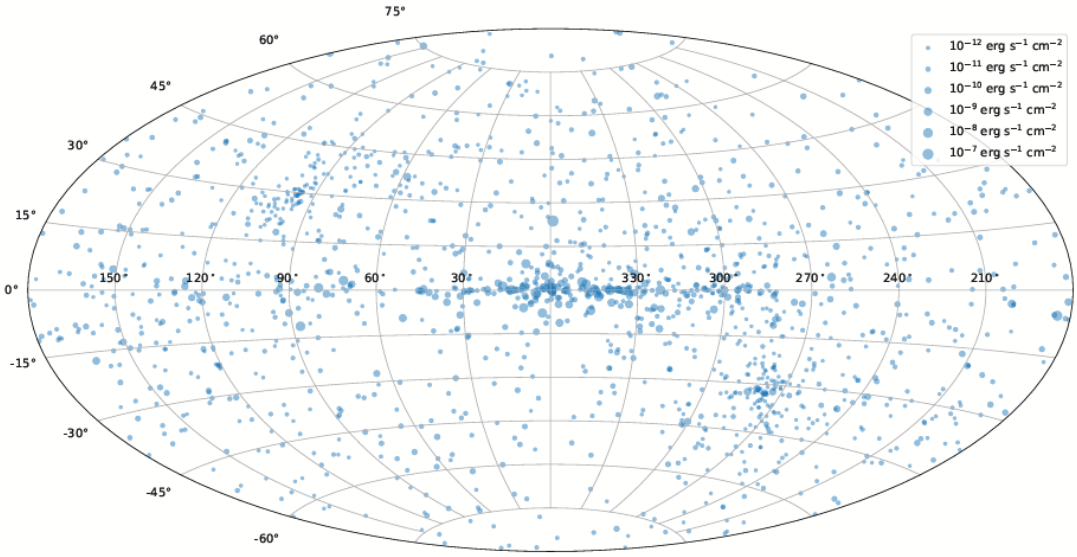

Figure 67: The positions in Galactic coordinates of the X-ray sources detected by ART-XC in the 4–12 keV energy band during ARTSS1-5. The size of the symbol reflects the X-ray brightness of a source, as indicated in the legend (adopted from [168]).

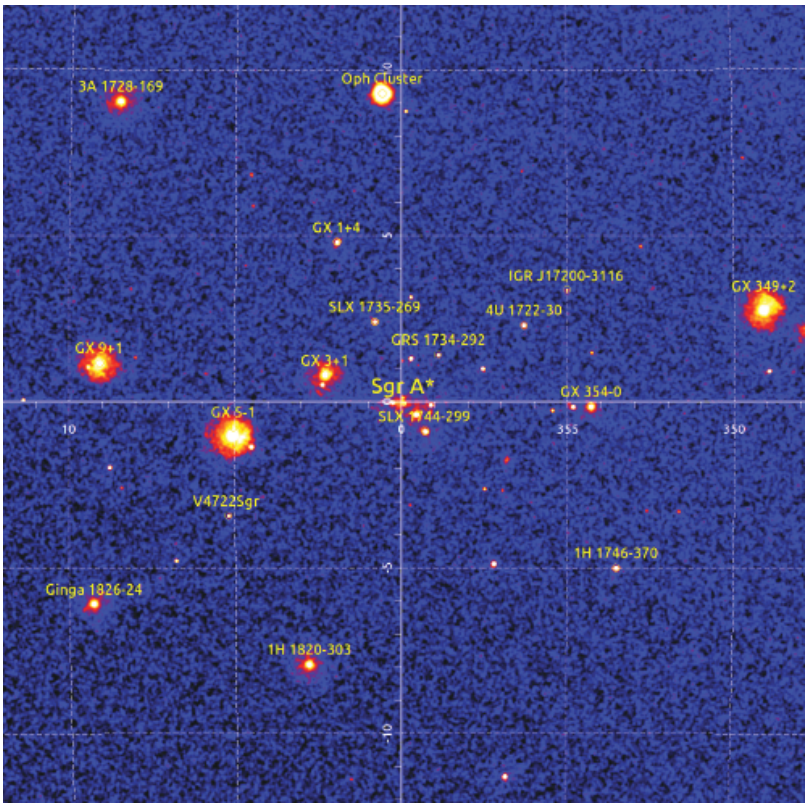

Figure 68: The image of a 25° × 25° region of the sky near the Galactic center in the 4–12 keV energy band, obtained by convolving the raw photon images with the optimal matched filter, in Galactic coordinates. Some bright sources are labeled.The faintest sources in this region that have been included in the ARTSS1-5 catalog have fluxes $\sim 3 \times 10^{-12}$ erg s^{-1} cm^{-2} (adopted from [168]).

PoS(FRAPWS2024)035

2.17 The Imaging X-ray Polarimetry Explorer (IXPE)

The Imaging X-ray Polarimetry Explorer (IXPE) [170-173] exploits the polarization state of light from astrophysical sources to provide insight into our understanding of X-ray production in objects such as neutron stars and pulsar wind nebulae, as well as stellar and supermassive black holes. Technical and science objectives include (https://ixpe.msfc.nasa.gov/):

The Imaging X-ray Polarimetry Explorer (IXPE)

The Imaging X-ray Polarimetry Explorer (IXPE) mission was launched on December 9, 2021 on a SpaceX Falcon 9 rocket from NASA's Kennedy Space Center in Florida into an equatorial orbit of 600 km altitude. The payload consists of three identical grazing incidence telescopes, each comprised of a mirror module assembly, developed at NASA/MSFC, with an X-ray-polarization-sensitive detector, provided by the Italian Space Agency (Agenzia Spaziale Italiana; ASI), at its focus. The payload sits atop a spacecraft bus provided by Ball Aerospace.

The observatory operates in pointing mode observing known targets for multiple (but not necessarily consecutive) orbits. Data are sent to a ground station in Malindi, Kenya, approximately 8 times per day and then are transmitted, via gateways in Italy and the US, to the mission operations center in Boulder, Colorado. From there, science data flows to the science operation center in Huntsville Alabama.

Mission Characteristics

- **Lifetime** : 9 Dec 2021– (operating)
- **Energy Range** : 2–8 keV
- **Angular resolution:** : 30 arcsec HPD (system)
- **Special Features** : Provide simultaneous spectral, spatial and timing polarimetry measuraments
- **Payload** :

  - The Mirror Module Assemblies (MMA) consist of three grazing-incidence mirror modules of Wolter-I type each with 24 concentrically-nested mirror shells with diameters ranging from 162 to 272 mm. The MMAs are mounted on an extendable boom which deployed on orbit to give the appropriate 4 m focal length. A tip/tilt/rotate mechanism provides alignment adjustment.
    Field-of-View (FoV) of a square, 12.9 arcmin on a side (detector limited);
    Angular resolution (HEW) ~ 20-25 arcsec (MMA only);
    Effective area per module at 167 cm^2 at 2.3 keV and 197 cm^2 at 4.5 keV.
  - The Detector Units (DUs) are three Gas Pixel Detectors (GPDs) each located at the focus of an x-ray mirror module. Each GPD provides the position, energy, time and polarization information for every absorbed event. The GPD images the photoelectron tracks produced by the x-rays absorbed in a special fill gas and from its initial emission direction the polarization of the source is determined. The initial interaction point and the total charge in the track provide the location and energy of the absorbed x-ray, respectively.
    Detector sensitive area 15 mm x 15 mm
    Spatial resolution (FWHM) ≤ 123 μm (6.4 arcsec) @ 2 keV
    Energy resolution (FWHM) 0.57 keV @ 2 keV (∝ √E)

- **Science Goals**:

  - Enhance our understanding of the physical processes that produce X-rays from and near compact objects such as neutron stars and black holes.
  - Explore the physics of gravity, energy, and electric and magnetic fields.
  - **Archive**: The HEASARC hosts the IXPE archive.

Figure 69: The main characteristics of the Imaging X-ray Polarimetry Explorer (IXPE) (https://heasarc.gsfc.nasa.gov/docs/heasarc/missions/ixpe.html).

- improving polarization sensitivity by two orders of magnitude over the X-ray polarimeter aboard the Orbiting Solar Observatory OSO-8,
- providing simultaneous spectral, spatial, and temporal measurements,
- determining the geometry and the emission mechanism of Active Galactic Nuclei and micro-quasars,

PoS(FRAPWS2024)035

- finding the magnetic field configuration in magnetars and determining the magnitude of the field,
- finding the mechanism for X ray production in pulsars (both isolated and accreting) and the geometry,
- determining how particles are accelerated in Pulsar-Wind Nebulae.

Figure 69 shows the main characteristics of the Imaging X-ray Polarimetry Explorer (IXPE) (https://heasarc.gsfc.nasa.gov/docs/heasarc/missions/ixpe.html).

The impact of IXPE on advancing our knowledge of our Universe has been recognized by The High Energy Astrophysics Division (HEAD) of the American Astronomical Society, which awarded the 2024 Bruno Rossi Prize to Martin Weisskopf, Paolo Soffitta, and the IXPE team for their development of the Imaging X-ray Polarimetry Explorer, whose novel measurements advance our understanding of particle acceleration and emission from astrophysical shocks, black holes, and neutron stars.

It is very difficult to chose IXPE highlights among the many results obtained. More that 70 discovery papers have been published by the IXPE Science Team. However, Soffitta & Costa [174] review IXPE's results after nearly three years of successful operation, focusing on their implications for key questions in Fundamental Physics.

A special issue of Galaxies (ISSN 2075-4434) "*X-Ray Polarimetry: A New Era Begins with the Imaging X-Ray Polarimetry Explorer* contains 10 papers, which demonstrate the impact of IXPE on the advancement of our knowledge of the Universe.

Also a special session on IXPE has been reserved in the program of this Mondello Worskhop 2024 on *Frontier Research in Astrophysics - IV*, for which the refereed proceedings will be available within 2025.

3. Conclusions

At the end of this overview of the experiments described in this review, I would like to emphasize the importance of each in providing crucial information to increase the knowledge of our Universe. Obviously, the choice of experiments described was dictated by my direct experience, which allowed me to contribute with my papers to the advancement of our understanding of the physics of high-energy cosmic sources.

I believe my choices have helped to illustrate the experiments that I consider the milestones of the years:

- 1970s: UHURU, SAS-2, COS-B, HEXE-1, HXR-76, HEAO-1, Ariel V, HEAO-2 (Einstein).
- 1980s: IUE, ASTRON, CORSA-B (Hakucho).
- 1990s: ROSAT, CGRO, BeppoSAX.
- 2000s: INTEGRAL, AGILE.
- 2010s: SRG (eRosita & ART-XC).

PoS(FRAPWS2024)035

- 2020s: IXPE.

A more complete description of *A Chronological History of X-Ray Astronomy Missions* has been published by Santangelo, Madonia & Piraino [4].

My hope is to have been useful to young people so that they learn a way of doing research that is apparently anomalous, but effective.

Acknowledgments This research has made use of the NASA's Astrophysics Data System.

References

[1] Giacconi, R., Gursky, H., Paolini, F.R., Rossi, B.: 1962, Phys. Rev. Lett. 9, 439.

[2] Giovannelli, F., Sabau-Graziati, L.: 2004, SSR, 112, 1-443 (GSG2004).

[3] Lena, P.: 1988, *Observational Astrophysics*, Springer–Verlag Berlin–Heidelberg, Germany.

[4] Santangelo, A., Madonia, R., Piraino, S.: 2023, in *Handbook of X-ray and Gamma-ray Astrophysics*. Edited by Cosimo Bambi and Andrea Santangelo, Springer Living Reference Work, ISBN: 978-981-16-4544-0, id. 124, 68 pp.

[5] Landau, L.D.: 1932, Phys. Zs. Sowjet. 1, 285.

[6] Baade, W., Zwicky, F.: 1934, Phys. Rev. 45, 138.

[7] Zwicky, F.: 1938, ApJ 88, 522-525.

[8] Zwicky, F.: 1939, PhRv 55, Issue 8, 726-743.

[9] Brecher, K.: 1999, American Astronomical Society, 195th AAS Meeting, id. 130.05; Bulletin of the American Astronomical Society, Vol. 31, p. 1560.

[10] Zel'dovich, Ya,B., Guseinov, O.Kh.: 1965, Soviet Physics Doklady 10, 524.

[11] Guseinov, O.Kh., Zel'dovich, Ya.B.: 1966, Soviet Astronomy 10, 251-253.

[12] Giovannelli, F.: 2025, Galaxies 13, id. 16, 49 pp.

[13] Klebesadel, R.W., Strong, I.B., Olson, R.A.: 1973, ApJL 182, L85-L88.

[14] Mazets, E.P., Golenetskii, S.V., Il'inskii, V.N.: 1974, Pis'ma v ZhurnEhTF 19, 126-128.

[15] Mazets, E.P., Golenetskii, S.V., Il'inskii, V.N., Gurian, Iu.A., Kharitonova, T.V.: 1974, JETP Letters 20, 32-34.

[16] Mazets, E.P., Golenetskii, S.V., Il'inskii, V.N., Gurian, Iu.A., Kharitonova, T.V.: 1975, Ap&SS 33, Issue 2, 347-357.

[17] Paczyński, B.: 1986, ApJL 308, L43-L46.

PoS(FRAPWS2024)035

[18] Sacahui, J.R., Penacchioni, A.V., Braga, J., Castro, M.A., D'Amico, F.: 2016, JHEAp 9-10, 16-24.

[19] Tsvetkova, A., Svinkin, D., Karpov, S., Frederiks, D.: 2022, Universe 8, 373, 51 pp.

[20] Zhang, B.: 2013, talk at the *Multi-Messenger Transient Workshop*, KIAA, China.

[21] Zhang, B.: 2013 in *Gamma-ray Bursts: 15 Years of GRB Afterglows*, A.J. Castro-Tirado, J.Gorosabel & I.H. Park (Eds.), EAS Publications Series 61, 285-293.

[22] Forman, W., Jones, C., Cominsky, L., Julien, P., Murray, S., Peters, G., Tananbaum, H., Giacconi, R.: 1978, ApJS 38, 357-412.

[23] Hartman, R. C., Fichtel, C.E., Kniffen, D.A., Lamb, R.C., Thompson, D.J. et al.: 1977, in *The Structure and Content of the Galaxy and Galactic Gamma Rays*, NASCP 2, 15-26 (SEE N77-20977 11-88).

[24] Strong, A.W., Worrall, D.M.: 1976, J. Phys. A: Mathematical and General 9, Issue 5, 823-827.

[25] Fichtel, C.E., Hartman, R.C., Kniffen, D.A., Thompson, D.J., Bignami, G.F. et al.: 1975, ApJ 198, 163-182.

[26] Giovannelli, F.: 1997, in *Frontier Objects in Astrophysics and Particle Physics*, F. Giovannelli & G. Mannocchi (Eds.), Italian Physical Society, Editrice Compositori, Bologna, Vol. 57, 337-345.

[27] Turner, D.G., Forbes, D.: 192, PASP 94, 789-801.

[28] Polcaro, V.F., Rossi, C., Norci, L., Giovannelli, F.: 1989, AcA 39, 323-332.

[29] Janes, K.A.: 1992, in *The Astronomy and Astrophysics Encyclopedia*, S.P. Maran (Ed.), Cambridge University Press, Cambridge, UK, p. 692.

[30] Manchanda, R.K., Polcaro, V.F., Norci, L., Giovannelli, F., Brinkmann, W., Radecke, H.D. et al.: 1996, A&A 305, 457-467.

[31] Taylor, J.H., Manchester, R.N., Lyne, A.G.: 1993, ApJS 88, 529-568.

[32] Thompson, D.J.: 2004, in *Cosmic Gamma-Ray Sources*. K.S. Cheng & G.E. Romero (Eds.), ASTROPHYSICS AND SPACE SCIENCE LIBRARY Vol. 304. Kluwer Academic Publishers, Dordrecht, The Netherlands, p. 149-168.

[33] Bignami, G.F., Caraveo, P.A.: 1996, ARA&A 34, 331-382.

[34] Fierro, J.M., Arzoumanian, Z., Bailes, M., Bell, J.F., Bertsch, D.L. et al.: 1995, ApJ 447, 807-812.

[35] Lipunov, V.M.: 1995, in *Frontier Objects in Astrophysics and Particle Physics*, F. Giovannelli & G. Mannocchi (Eds.), Italian Physical Society, Editrice Compositori, Bologna, Vol. 47, 61-76.

PoS(FRAPWS2024)035

[36] Giovannelli, F. Karakuła, S., Tkaczyk, W.: 1981, in *Origin of Cosmic Rays*, Dordrecht, D. Reidel Publishing Co., Proc. IAU Symp. 94, 335-336.

[37] Giovannelli, F. Karakuła, S., Tkaczyk, W.: 1982, AcA 32, no. 1-2, 121-130.

[38] Lipunov, V.M., Postnov, K.A.: 1988, Ap&SS 145, Issue 1, 1-45.

[39] Swanenburg, B.N., Bennett, K., Bignami, G.F., Buccheri, R., Caraveo, P. et al.: 1981, ApJL 243, L69-L73.

[40] Ubertini, P.: 2008, Mem. SAIt 79, 783-791.

[41] Trümper, J.: 2012, talk at conference *X-Ray Astronomy: Towards the next 50 Years*, Milano, 1-5 October 2012.

[42] Trümper, J., Pietsch, W., Reppin, C., Voges, W., Staubert, R., Kendziorra, E.: 1978, ApJL 219, L105-L110.

[43] Cortiglioni, S., Mandolesi, N., Morigi, G., Ciapi, A., Inzani, P., Sironi, G.: 1981, Ap&SS 75, Issue 1, 153-161.

[44] Auriemma, G., Angeloni, L., Belli, B.M., Bernardi, A., Cardini, D., Costa, E., Emanuele, A., Giovannelli, F., Ubertini, P.: 1978, ApJL 221, L7-L11.

[45] Wood, K.S., Meekins, J.F., Yentis, D.J., Smathers, H.W., McNutt, D.P. et al.: 1984, ApJS 56, 507-649.

[46] Margon, B., Nelson, J., Chanan, G., Thorstensen, J.R., Bowyer, S.: 1977, ApJ 216, 811-818.

[47] Giovannelli, F.: 2005, *The Impact of Multifreuency Observations in High Energy Astrophysics*, PhD Thesis, Faculty of Physics, Department of Astronomy and Meteorology, University of Barcelona, Spain.

[48] Bartolini, C., Guarnieri, A., Piccioni, A., Giangrande, A., Giovannelli, F.: 1978, IAU Circ., No. 3167.

[49] Chartres, M., Li, F.: 1977, IAU Circ., No. 3154.

[50] Giangrande, A., Giovannelli, F., Bartolini, C., Guarnieri, A., Piccioni, A.: 1980, A&AS 40, 289-294.

[51] Bunner, A.N., Cline, T.L., Gerald J. Fishman, G.J., Rye, Jr., G.M. et al.: 1988, in *Gamma Ray Astrophysics to the Year 2000*, Report of the NASA Gamma Ray Program Working Group.

[52] Giovannelli, F., Polcaro, V.F.: 1986, MNRAS 222, 619-627.

[53] Hasinger, G., Lehmann, I., Giacconi, R., Schmidt, M., Trümper, J., Zamorani, G.: 1999, in *Highlights in X-ray Astronomy: International Symposium in honour of Joachim Trümper's 65th birthday*, B. Aschenbach & M.J. Freyberg (eds.), Max-Planck-Institut für extraterrestrische Physik, Garching, Germany, MPE report No. 272, 199.

PoS(FRAPWS2024)035

[54] Hasinger, G., Miyaji, T., Schmidt, J.H.M.M.: 2000, MPE-Report No. 273, 83.

[55] Becker, G.D. Sargent, W.L.W., Rauch, M., Simcoe, R.A.: 2006, ApJ 640, Issue 1, 69-80.

[56] Mineo, S., Gilfanov, M., Lehmer, B.D., Morrison, G.E., Sunyaev, R.: 2014, MNRAS 437, Issue 2, 1698-1707.

[57] Yuan, Q., Wang, Q.D.: 2016, MNRAS 456, Issue 2, 1438-1450.

[58] Giovannelli, F., Ferrari-Toniolo, M., Bartolini, C. Guarnieri, A., Rucinski, S.M. et al.: 1980, in *The second European International Ultraviolet Explorer (IUE) Conference*, B. Battrick & J. Mort (Eds.), ESA SP-157, 159-164.

[59] Giovannelli, F., Ferrari-Toniolo, M., Giangrande, A., Persi, P., Bartolini, C. et al.: 1981, SSRv 30, Issue 1-4, 407-414.

[60] Giovannelli, F., De Loore, C., Bartolini, C., Burger, M., Ferrari-Toniolo, M. et al.: 1982, in *ESA 3rd European IUE Conference*, ESA SP-176, 233-239.

[61] Giovannelli, F., Bernabei, S., Rossi, C., Sabau-Graziati, L.: 2007, A&A 475, Issue 2, 651-657.

[62] De Loore, C., Giovannelli, F., van Dessel, E.L., Bartolini, C., Burger, M. et al.: 1984, A&A 141, 279-296.

[63] de Martino, D., Waters, L.B.F M., Giovannelli, F., Persi, P.: 1989, in *ESA, The 23rd ESLAB Symposium on Two Topics in X Ray Astronomy*, Volume 1: X Ray Binaries, 519-520.

[64] Giovannelli, F., Gaudenzi, S., Lombardi, R., Bartolini, C., Guarnieri, A., Piccioni, A.: 1985, in *Multifrequency Behaviour of Galactic Accreting Sources*, Franco Giovannelli (Ed.), Edizioni Scientifiche SIDEREA, Roma, pp. 37-49.

[65] Gaudenzi, S., Giovannelli, F., Mandalari, M., Corradini, M., Lombardi, R.: 2011, A&A 525, id. A147, 11 pp.

[66] Lombardi, R., Giovannelli, F., Gaudenzi, S.: 1987, Ap&SS 130, Issue 1-2, 275-278.

[67] Martinez-Pais, I.G., Giovannelli, F., Rossi, C., Gaudenzi, S.: 1994, A&A 291, 455-467.

[68] Scaringi, S., Bird, A.J., Norton, A.J., Knigge, C., Hill, A.B. et al.: 2010, MNRAS 401, Issue 4, 2207-2218.

[69] Harrison, T.E., McNamara, B.J., Szkody, P., McArthur, B.E., Benedict, G.F., Klemola, A.R., Gilliland, R.L.: 1999, ApJ 515, Issue 2, L93-L96.

[70] Miller-Jones, J.C.A., Sivakoff, G.R., Knigge, C., Körding, E.G., Templeton, M., Waagen, E.O.: 2013, Science 340, Issue 6135, 950-952.

[71] Pala, A.F., Gänsicke, B.T., Breedt, E., Knigge, C., Hermes, J.J. et al.: 2020, MNRAS 494, Issue 3, 3799-3827.

PoS(FRAPWS2024)035

[72] Howell, S.B., Cash, J., Mason, K.O., Herzog, A.E.: 1999, AJ 117, Issue 2, 1014-1022.

[73] Gaudenzi, S., Claudi, R.U., Giovannelli, F., Lombardi, R., Pelosi, M., Strappolini, M.: 2002, Mem. SAIt 73, 213-222.

[74] Körding, E., Rupen, M., Knigge, C., Fender, R., Dhawan, V., Templeton, M., Muxlow, T.: 2008, Sci 320, Issue 5881, 1318-1320.

[75] Dubus, G., Campbell, R., Kern, B., Taam, R.E., Spruit, H.C.: 2004, MNRAS 349, Issue 3, 869-881.

[76] Giovannelli, F., Sabau-Graziati, M.D., Claudi, R.U., Gaudenzi, S., Rossi, C.: 2024, in *The Golden Age of Cataclysmic Variables and Related Objects - VI*. Online at https://pos.sissa.it/cgi-bin/reader/conf.cgi?confid=460, id. 28.

[77] Bisnovatyi-Kogan, G.S., Lamzin, S.A.: 1980, SvAL 6, 17-20. Translation from Pisma v Astronomicheskii Zhurnal, vol. 6, Jan. 1980, p. 34-38.

[78] Sheffer, E.K., Kopaeva, I.F., Averintsev, M.B., Bisnovatyi-Kogan, G.S., Golynskaya, I.M., Gurin, L.S., Dyachkov, A.V., Zenchenko, V.M., Kurt, V.G., Mizyakina, T.A., Mironova, E.N., Sklyankin, V.A., Smirnov, A.S., Titarchuk, L.G., Shamolin, V.M., Shafer, E.Y., Shmelkin, A.A., Giovannelli, F.: 1992, SvA 36, NO.1, 41-52. Or 1992, AZh 69, no. 1, 82-105 (in Russian).

[79] Giovannelli, F., Vittone, A.A., Rossi, C., Errico, L., Bisnovatyi-Kogan, G.S., Kurt, V.G., Lamzin, S.A., Larionov, M., Sheffer, E.K., Sidorenkov, V.N.: 1995, A&A Suppl. 114, 341-361.

[80] Lamzin, S.A., Bisnovatyi-Kogan, G.S., Errico, L., Giovannelli, F., Katysheva, N.A., Rossi, C., Vittone, A.A.: 1996, A&A 306, 877-891.

[81] Giovannelli, F.: 1994, SSRv 69, 1-138.

[82] Bouvier, J.: 1990, AJ 99, 946-964.

[83] Giovannelli, F., Errico, L., Vittone, A.A., Rossi, C.: 1991, A&AS 87, 89-95.

[84] Giovannelli, F., Bisnovatyj-Kogan, G.S., Golynskaya, I.M., Kurt, V.G., Lamzin, S.A. et al.: 1985, in *X-ray astronomy '84*, M. Oda & R. Giacconi (Eds.), Institute of Space and Astronautical Science, Tokyo, Japan, pp. 77-80.

[85] Bartolini, C., Bianco, G., Guarnieri, A., Piccioni, A., Giovannelli, F.: 1983, in *Rapid Variability of Early-Type Stars*, Hvar Observatory, Bulletin (ISSN 0351-2651), vol. 7, no. 1, 159-166.

[86] Priedhorsky, W.C., Terrell, J.: 1983, Nature 303, Issue 5919, 681-683.

[87] Chartres, M., Li, F.: 1977, IAU Circ., No. 3154.

PoS(FRAPWS2024)035

[88] Guarnieri, A., Bartolini, C., Piccioni, A., Giovannelli, F.: 1985, in *Multifrequency Behaviour of Galactic Accreting Sources*, Franco Giovannelli (Ed.), Edizioni Scientifiche SIDEREA, Roma, pp. 310-317.

[89] de Martino, D., Vittone, A., Giovannelli, F., Ciatti, F., Margoni, R. et al.: 1985, in *Multifrequency Behaviour of Galactic Accreting Sources*, Franco Giovannelli (Ed.), Edizioni Scientifiche SIDEREA, Roma, pp. 326-331.

[90] Giovannelli, F., Bartolini, C., Guarnieri, A., Piccioni, A., Burger, M. et al.: 1990, Ap&SS 169, Issue 1-2, 139-145.

[91] Rosenberg, F.D., Eyles, C.J., Skinner, G.K., Willmore, A.P.: 1975, Nature 256, 628-630.

[92] Giovannelli, F., Ferrari Toniolo, M., Persi, P., Golinskaya, I.M., Kurt, V.G. et al.: 1985, in *X-ray astronomy '84*, M. Oda & R. Giacconi (Eds.), Institute of Space and Astronautical Science, Tokyo, Japan, pp. 205-208.

[93] Giovannelli, F., van Dessel, E.L., Burger, M., De Loore, C., Bartolini, C. et al.: 1986, in *New Insights in Astrophysics: 8 Years of UV Astronomy with IUE*. Compiled by E.J. Rolfe, ESA SP-263, 459-461.

[94] Violes, F., Niel, M., Bui-van, A., Vedrenne, G., Chambon, G., Estulin, I.V., Rakhamimov, Sh.Iu.: 1982, ApJ 263, 320-324.

[95] Rössiger, S.: 1978, IBVS, 1395.

[96] Nagase, F., Hayakawa, S., Kunieda, H., Makino, F., Masai, K. et al.: 1982, ApJ 263, 814-822.

[97] Giovannelli, F., Sabau-Graziati, L.: 2011, Acta Polytechnica Vol. 51, No. 2., p. 21.

[98] Guarnieri, A., Bartolini, C., Piccioni, A., Giovannelli, F., van Dessel, E.L. et al.: 1985, in *Multifrequency Behaviour of Galactic Accreting Sources*, Franco Giovannelli (Ed.), Edizioni Scientifiche SIDEREA, Roma, pp. 318-325.

[99] Giovannelli, F., Bisnovatyi-Kogan, G.S., Klepnev, A.S.: 2013, A&A 560, id.A 1, 11 pp.

[100] Nandra, K., Clavel, J., Edelson, R.A., George, I.M., Malkan, M.A. et al.: 1998, ApJ 505, Issue 2, 594-606.

[101] Maoz, D ., Edelson, R., Nandra, K.: 2000, AJ 119, Issue 1, 119-125.

[102] Marshall, K., Ryle, W.T., Miller, H.R.: 2008, ApJ 677, Issue 2, 880-883.

[103] Doroshenko, V.T., Sergeev, S.G., Efimov, Yu.S., Klimanov, S.A., Nazarov, S.V.: 2009, AstL 35, Issue 6, 361-374.

[104] Giovannelli, F., Bisnovatyi-Kogan, G.S., Bruni, I., Corfini, G., Martinelli, F., Rossi, C.: 2015, AcA 65, 107-116.

PoS(FRAPWS2024)035

[105] Giovannelli, F., Bisnovatyi-Kogan, G.S., Bruni, I., Martinelli, F., Monaci, M., Rossi, C.: 2014, ATel, No. 6528.

[106] Giovannelli, F., Bisnovatyi-Kogan, G.S., Bruni, I., Martinelli, F., Monaci, M., Rossi, C.: 2014, ATel, No. 6585.

[107] Nakajima, M., Sakamoto, T., Mihara, T., Ueda, Y., Ueno, S.: 2014, ATel, No. 6569.

[108] Smak, J.: 1984, PASP 96, 5-18.

[109] Lasota, J.-P.: 2001, New Astron. Rev. 45, Issue 7, 449-508.

[110] Bisnovatyi-Kogan, G.S., Giovannelli, F.: 2017, A&A 599, id. A55, 7 pp.

[111] Wheatley, P.J., Mauche, C.W., Mattei, J.A.: 2003, MNRAS 345, Issue 1, 49-61.

[112] Shahbaz, T., Bandyopadhyay, R.M., Charles, P.A., Wagner, R.M., Muhli, P., et al.: 1998, MNRAS 300, Issue 4, 1035-1040.

[113] Orosz, J.A., Remillard, R.A., Bailyn, C.D., McClintock, J.E.: 1997, ApJL 478, Issue 2, L83-L86.

[114] Giovannelli, F., Sabau-Graziati, L., Norci, L., Polcaro, V.F.: 1993, in *23rd International Cosmic Ray Conference*, D.A. Leahy, R.B. Hicks & D. Venkatesan (Eds.). Invited, Rapporteur, and Highlight Papers. Singapore: World Scientific, Vol. 1, 33-36.

[115] Giovannelli, F., Polcaro, V.F., Sabau-Graziati, L., Norci, L.: 1993, in *Frontier Objects in Astrophysics and Particle Physics*, F. Giovannelli & G. Mannocchi (Eds.), Italian Physical Society, Editrice Compositori, Bologna, Vol. 40, 323-332.

[116] Minkowski, R.: 1958, RvMP 30, Issue 3, 1048-1052.

[117] Kirshner, R.P., Arnold, C.N.: 1979, ApJ 229, 147-152.

[118] Savonije, G.J., van den Heuvel, E.P.J.: 1977, ApJL 214, L19-L22.

[119] van den Heuvel, E.P.J.: 1981, SSRv 30, 623-642.

[120] Kundu, M.R., Angerhofer, P.E., Fuerst, E., Hirth, W.: 1980, A&A 92, 225-229.

[121] Sofue, Y., Fürst, E., Hirth, W.: 1980, PASJ 32, 1-10.

[122] Giovannelli, F., Sabau-Graziati, L.: 2001, in *Frontier Objects in Astrophysics and Particle Physics*, F. Giovannelli & G. Mannocchi (Eds.), Italian Physical Society, Editrice Compositori, Bologna, Vol. 73, 251-261.

[123] Dewey, R.J., Cordes, J.M.: 1987, ApJ 321, 780-798.

[124] Brandt, N., Podsiadlowski, P.: 1995, MNRAS 274, Issue 2, 461-484.

PoS(FRAPWS2024)035

[125] Vanbeveren, D.: 2000, in *The Evolution of the Milky Way: stars versus clusters*, Francesca Matteucci & Franco Giovannelli (Eds.), Kluwer Academic Publishers, pp. 139-150.

[126] Motch, C., Stella, L., Janot-Pacheco, E., Mouchet, M.: 1991, ApJ 369, 490-505.

[127] Giovannelli, F., Polcaro, V.F., Sabau-Graziati, L., Norci, L.: 1994, in *Evolutionary links in the zoo of interacting binaries*, D'Antona, F., Caloi, V., Maceroni, C., Giovannelli, F. (Eds.), Mem. SAIt 65, 373-378.

[128] van Paradijs, J.: 1989, in *Timing Neutron Stars*, H. Ögelman & E.P.J. van den Heuvel (Eds.), Kluwer Academic/Plenum Publishers, New York, NY USA, pp. 191-207.

[129] Green, D.A.: 1998, *A Catalog of Galactic Supernova Remnants*, Mullard Radio Astronomy Observatory, Cambridge, UK.

[130] Green, D.A.: 1991, PASP 103, 209-220.

[131] Anderson, S.B.; Cadwell, B. J.; Jacoby, B. A.; Wolszczan, A.; Foster, R. S.; Kramer, M.

[132] Giovannelli, F., Sabau-Graziati, L., Norci, L., Polcaro, V.F.: 1993, in *23rd International Cosmic Ray Conference*, D.A. Leahy, R.B. Hicks, & D. Venkatesan (Eds.), Invited, Rapporteur, and Highlight Papers. Singapore: World Scientific, Vol 1, pp. 33-36.

[133] Reich, W., Zhang, X., Fürst, E.: 2003, A&A 408, 961-969.

[134] Ng, C.-Y., Romani, R.W., Brisken, W.F., Chatterjee, S., Kramer, M.: 2007, ApJ 654, Issue 1, 487-493.

[135] Khabibullin, I.I., Churazov, E.M., Chugai, N.N., Bykov, A.M., Sunyaev, R.A. et al.: 2024, A&A 689, id. A 278, 12 pp.

[136] Dinçel, Neuhäuser, B.R., Yerli, K., Ankay, A., Tetzlaff, N., Torres, G., Mugrauer, M.: 2015, MNRAS 448, 3196-3205.

[137] Purcell, W.R., Cheng, L.-X., Dixon, D.D., Kinzer, R.L., Kurfess, J.D. et al.: 1997, ApJ 491, Issue 2, 725-748.

[138] Schönfelder, V., Aarts, H., Bennett, K., de Boer, H., Clear, J. et al.: 1993, ApJS 86, 657-692.

[139] Kanbach, G., Bertsch, D.L., Fichtel, C.E., Hartman, R.C., Hunter, S.D. et al.: 1989, SSRv 49, Issue 1-2, 69-84.

[140] Hartman, R.C., Bertsch, D.L., Bloom, S.D., Chen, A.W., Deines-Jones, P. et al.: 1999, ApJS 123, Issue 1, 79-202.

[141] Costa, E., Frontera, F., Heise, J., Feroci, M., in't Zand, J. et al.: 1997, Nature 387, Issue 6635, 783-785.

[142] Fusco-Femiano, R., Dal Fiume, D., Feretti, L., Giovannini, G., Grandi, P. et al.: 1999, ApJL 513, Issue 1, L21-L24.

PoS(FRAPWS2024)035

[143] Auriemma, G., Costa, E., Giovannelli, F., Medici, G., Ubertini, P.: 1975, *Communication at the Italian Extragalactic Astronomy, 1975, April 3*, Internal Report of the CNR - Laboratorio di Astrofisica Spaziale, LAS-75-26, July 1975.

[144] Winkler, C., Diehl, R., Ubertini, P., Wilms, J.: 2011, SSRv 161, Issue 1-4, 149-177.

[145] Vedrenne, G., Roques, J.-P., Schönfelder, V., Mandrou, P., Lichti, G.G. et al.: 2003, A&A 411, L63-L70.

[146] Knödlseder, J., Lonjou, V., Weidenspointner, G., Jean, P., Strong, A. et al.: 2007, in *The first GLAST Symposium*, AIP Conf. Proc. 921, 130-134.

[147] Savchenko, V., Ferrigno, C., Kuulkers, E., Bazzano, A., Bozzo, E. et al.: 2017, ApJ 848, Issue 2, article id. L15, 8 pp.

[148] Abbott, B.P., Abbott, R., Abbott, T.D., Acernese, F., Ackley, K. et al.: 2017, PhRvL 119, Issue 16, id. 161101, 18 pp.

[149] Ubertini, P., Lebrun, F., Di Cocco, G., Bazzano, A., Bird, A.J. et al.: 2003, A&A 411, L131-L139.

[150] Lebrun, F., Leray, J.P., Lavocat, P., Crétolle, J., Arquès, M.: 2003, A&A 411, L141-L148.

[151] Labanti, C., Di Cocco, G., Ferro, G., Gianotti, F., Mauri, A. et al.: 2003, A&A 411, L149-L152.

[152] Terrier, R., Ponti, G., Bélanger, G., Decourchelle, A., Tatischeff, V. et al.: 2010, ApJ 719, Issue 1, 143-150.

[153] Bird, A.J., Bazzano, A., Bassani, L., Capitanio, F., Fiocchi, M. et al.: 2010, ApJS 186, Issue 1, 1-9.

[154] Malizia, A., Bassani, L., Landi, R., Molina, M., Masetti, N. et al.: 2023, A&A 671, id. A152, 15 pp.

[155] Malizia, A., Bassani, L., Bazzano, A., Bird, A.J., Masetti, N. et al.: 2012, MNRAS 426, Issue 3, 1750-1766.

[156] Malizia, A., Landi, R., Molina, M., Bassani, L., Bazzano, A. et al.: 2016, MNRAS 460, Issue 1, 19-29.

[157] Malizia, A., Bassani, L., Stephen, J.B., Bazzano, A., Ubertini, P.: 2020, A&A 639, id. A5, 10 pp.

[158] Lund, N., Budtz-Jørgensen, C., Westergaard, N.J., Brandt, S., Rasmussen, I.L. et al.: 2003, A&A 411, L231-L238.

[159] Motta, S.E., Kajava, J.J.E., Sánchez-Fernández, C., Giustini, M., Kuulkers, E.: 2017, MNRAS 468, Issue 1, 981-993.

PoS(FRAPWS2024)035

[160] Mas-Hesse, J.M., Giménez, A., Culhane, J.L., Jamar, C., McBreen, B. et al.: 2003, A&A 411, L261-L268.

[161] Domingo, A., Gutiérrez-Sánchez, R., Rísquez, D., Caballero-García, M.D., Mas-Hesse, J.M., Solano, E.: 2010, in *Highlights of Spanish Astrophysics V*, Ap&SS Proc., ISBN 978-3-642-11249-2. Springer-Verlag Berlin Heidelberg, p. 493.

[162] Zamorani, G., Henry, J.P., Maccacaro, T., Tananbaum, H.,; Soltan, A. et al.: 1981, ApJ 245, 357-374.

[163] Vercellone, S., Pittori, C., Tavani, M.: 2024, Universe 10, Issue 4, id. 153, 29 pp.

[164] Pittori, C., Tavani, M., Argan, A., Bulgarelli, A., Barbiellini, G. et al.: 2025, arXiv:2501.12970.

[165] Tavani, M., Piano, G., Bulgarelli, A., Foffano, L., Ursi, A. et al.: 2023, ApJL 956, Issue 1, id. L23, 11 pp.

[166] Predehl, P., Andritschke, R., Arefiev, V., Babyshkin, V., Batanov, O. et al.: 2021, A&A 647, id. A1, 16 pp.

[167] Pavlinsky, M., Tkachenko, A., Levin, V., Alexandrovich, N., Arefiev, V. et al.: 2021, A&A 650, id. A42, 18 pp.

[168] Sazonov, S., Burenin, R., Filippova, E., Krivonos, R., Arefiev, V. et al.: 2024, A&A 687, id. A183, 12 pp.

[169] Merloni, A., Lamer, G., Liu, T., Ramos-Ceja, M.E., Brunner, H.: 2024, A&A 682, id. A34, 38 pp.

[170] Weisskopf, M.C., Ramsey, B., O'Dell, S., Tennant, A., Elsner, R., Soffitta, P. et al.: 2016, Proc. of the SPIE, 9905, id. 990517, 10 pp.

[171] Soffitta, P.: 2017, Proc. of the SPIE, 10397, id. 103970I, 9 pp.

[172] Weisskopf, M.C., Soffitta, P., Ramsey, B.D., Baldini, L.: 2022, in *Handbook of X-ray and Gamma-ray Astrophysics*. Cosimo Bambi & Andrea Santangelo (Eds.), Springer Living Reference Work, ISBN: 978-981-16-4544-0, id. 43, pp 1-46.

[173] Soffitta, P.: 2024, Instruments 8, Issue 2, 25-42.

[174] Soffitta, P., Costa, E.: 2024, in *Proc. 42nd International Conference on High Energy Physics (ICHEP2024)*, arXiv:2412.17214.

PoS(FRAPWS2024)035